Impedance-Based Affinity Micro and Nanosensors for Continuous Glucose Monitoring

Zhixing Zhang

Submitted in partial fulfillment of the
requirements for the degree of
Doctor of Philosophy
under the Executive Committee
of the Graduate School of Arts and Sciences

COLUMBIA UNIVERSITY

2022

Abstract

Impedance-Based Affinity Micro and Nanosensors for Continuous Glucose Monitoring

Zhixing Zhang

Diabetes mellitus is a metabolic disease with abnormally high concentration of glucose in blood in patients. Continuous glucose monitoring, which involves measuring glucose concentration in the patient throughout the day and night, can significantly reduce the risk of diabetes-related complications. Commercially available CGM sensors are not yet suited for long-term applications due to reliability and accuracy issues associated with the irreversible, consumptive nature of the underlying electrochemical reactions.

Affinity sensing methods, which are based on reversible affinity binding between glucose and a recognition molecule, hold the potential to address these challenges in CGM applications. These methods do not involve the consumption of glucose and can offer improved stability and accuracy for CGM. When combined with impedance-based transduction methods, affinity sensors can also offer a high level of miniaturization, allow low-cost instrumentation, and are amenable to physical and functional integration. The affinity sensors investigated in this thesis include hydrogel-based affinity microsensors and graphene-based affinity nanosensors.

We first present a dielectric affinity microsensor that consists of a pair of coplanar electrodes functionalized *in situ* with a glucose-responsive hydrogel for dielectrically based affinity measurement of glucose in subcutaneous tissue. We present a study of the effects of the choice of hydrogel compositional parameters on the characteristics of the hydrogel-based microsensor, allowing the identification of the optimal hydrogel composition for the microsensor to sensitively and rapidly respond to changes in glucose concentration. A differential design is then demonstrated, both *in vitro* and *in vivo*, to effectively minimize the influence of fluctuations in the environmental conditions, thereby allowing the hydrogel-based microsensor to function appropriately as a subcutaneously implanted device.

In addition, we present a preliminary study on affinity nanosensors for non-invasive monitoring of glucose concentrations in physiological media such as tears. The affinity nanosensor is based on a chemically modified graphene field-effect transistor for the electrical measurement of glucose concentrations. The study explores the sensing mechanism of the nanosensors and demonstrates a device with high sensitivity and low limit of detection, which satisfies the requirement for monitoring glucose concentrations in tears.

Experimental results demonstrate that these affinity micros and nanosensors are capable of measuring glucose concentrations with a suitable sensitivity and dynamic range for the intended physiological media, with potential applications to minimally invasive or non-invasive continuous glucose monitoring in diabetes care.

Keywords: affinity sensing, continuous glucose monitoring, field-effect transistor sensors, graphene, hydrogels, impedimetric sensors, phenylboronic acids

Table of Contents

List of Figures

List of Tables

List of Abbreviations

AAPBA	3-acrylamidophenylboronic acid
AAPH	2,2'-Azobis (2-methylpropionamidine) dihydrochloride
AC	alternating current
BAC	*N*, *N′*-bis(acryloyl)cysteine
CDC	Centers for Disease Control and Prevention
CGM	continuous glucose monitoring
Con A	concanavalin A
DC	direct current
DMAPAA	dimethylaminopropyl acrylamide
FET	field effect transistor
GFET	graphene field effect transistors
HEAA	acryl *N*-Hydroxyethyl acrylamide
IDE	interdigitated electrodes
ISF	interstitial fluid
MEMS	microelectromechanical systems
NAPH-1-BA	naphthalene-1-boronic acid
PBA	phenylboronic acid
PDMS	polydimethylsiloxane
PHEAA	poly(*N*-hydroxyethyl acrylamide)
PHEAA-*ran*-PAAPBA	poly(*N*-hydroxyethyl acrylamide-*ran*-3-acrylamidophenylboronic acid)

RF	radio frequency
SAM	self-assembly layer
TEGDA	tetraethyleneglycol diacrylate
2APBA	2-acrylamidophenylboronic acid
3-QBA	3-quinolinylboronic acid
4-NPBA	4-nitrophenylboronic acid
8-QBA	8-quinolinylboronic acid

Acknowledgments

Throughout the course of this thesis research, I have been fortunate to receive a great deal of help from many individuals. Their constant support and encouragement have been tremendously valuable for me to complete the thesis.

Foremost, I would like to express my sincerest gratitude to my advisor, Professor Qiao Lin, for his invaluable, never-ending support, encouragement, and guidance during my entire doctoral studies. I will forever be grateful to him for offering me an opportunity to work in his lab, and for introducing me to microelectromechanical systems (MEMS) technology and micro/nanosensors and guiding me in conducting research in these exciting fields.

I wish to thank Professor Rudolph L. Leibel and his associates Drs. Charles A. LeDuc and Alicja A. Skowronski at the Columbia University Medical Center, and Professor Qian Wang and his lab members Dr. Yok Maturavongsadit and Dr. Monchupa Kingsak at the University of South Carolina, for their help, advice and enlightenment through fruitful collaborations on in vivo studies of glucose microsensors and chemical synthesis of glucose sensing materials, respectively.

I am also grateful to the members of my thesis committee, Professors Jeffrey W. Kysar, Qiao Lin, P. James Schuck, Qian Wang, and Yuan Yang, for their insightful questions, comments and suggestions on this thesis.

Additionally, I would like to thank the other members of the Lin lab, including Shulei Chen, Dr. Yaofei Chen, Wenting Dai, Dr. Chuanyu Han, Dr. Zhuang Hao, Dr. Yuan Jia, Dr. Yijun Li, Xin Meng, Dr. Timothy Olsen, Dr. Bing Song, Dr. Hao Sun, Dr. Junyi Shang, Kechun Wen, Dr. Xuejun Wang, Dr. Shifeng Yu, Dr. Jaeyoung Yang, Dr. Jing Zhu, and Dr. Yibo Zhu. I am also grateful for the constant support and encouragement from Yuyun Yang.

Finally, I am indebted to my parents, Aihong Zhang and Yaonan Zhang. Their unconditional love, support, and encouragement always give me the strength to overcome any obstacles, big or small, in my pursuit of scientific research.

Dedication

To my parents

Chapter 1: Introduction

1.1 Background

Diabetes mellitus is a group of metabolic diseases characterized by hyperglycemia resulting from defects in insulin secretion, insulin action, or both. In the US, diabetes is the leading cause of kidney failure, nontraumatic lower-limb amputations and new cases of blindness, and a common cause of stroke and heart disease[1,2]. According to CDC National Diabetes Statistics Report, 2020, 34.2 million people, or 10.5% of the US population had diabetes[3].

To help minimize the progression of diabetes and the potential complications, strict glucose control and monitoring is recommended for patients. Conventional finger prick-based glucometers can provide sparsely discrete glucose measurements of a patient[4]. While effective for self-monitoring, this process can be uncomfortable for patients and can lead to non-compliance, thus limiting the potential benefits.

Continuous glucose monitoring (CGM), which automatically tracks the glucose concentration of patients in real-time through day and night, can provide a reliable basis for patients to guide their insulin injections and can alarm patients if detection of abnormal blood glucose concentration events[5–8]. CGM is demonstrated to reduce the risk of complications caused by hypoglycemia or hyperglycemia[5,8–10]. Current available commercial continuous glucose monitoring devices, such as FreeStyle Libre[11], Dexcom G6[12], and Medtronic Guardian Connect[13] are minimally invasive systems, containing a needle-type sensor that penetrated the skin and is embedded underneath the interstitial tissue. The sensors measure the glucose concentration in interstitial fluid (ISF), which correlates with blood glucose concentration with a temporal lag of

5-15 min due to the diffusive glucose exchange between blood and ISF[7]. These sensors are predominantly based on the electrochemical measurement method which relies on using glucose enzyme to react with glucose to produce an electric current proportional to glucose concentration[14–17]. While electrochemical CGM sensors are well established, the irreversible consumption of glucose during the electrochemical reactions can potentially induce changes in the local equilibrium glucose concentration, causing significant inaccuracies[18]. In addition, since electrochemical reaction rates are diffusion-dependent, the accuracy and stability of the device are further compromised by the hampered diffusion rate caused by biofouling (e.g., accumulation of cells and proteins on the sensor surface)[19,20]. Moreover, degradation of the functional enzymes involved in electrochemical sensors further affects the device's accuracy, reliability, and longevity[18,21–23].

1.2 Affinity Glucose Sensing Methods

To enable more reliable, stable and accurate monitoring of glucose, affinity sensing methods, which are based on reversible binding of analytes with receptors to realize specific detection, have been under active investigation[24–26]. The affinity sensing method utilizes a biological recognition element such as an antibody, receptor protein, or DNA which can reversibly and specifically bind to the target analyte without the need for enzyme[27–29]. The primary advantage of such sensors lies in the equilibrium-driven nature of affinity binding, resulting in unaffected steady-state sensor readings by changes in glucose diffusion rate[28]. Furthermore, affinity sensing is considerably more tolerant of biofouling as additional diffusion barriers may prolong the time of the sensor signal to reach an equilibrium state, but the magnitude of the signal at a steady state is usually not affected, thereby not affecting the accuracy of the readings[30].

For affinity measurement of glucose, a variety of transduction methods have been used. These methods use optical[31–35], mass-based[30,36,37], amperometric[38–41], impedimetric and potentiometric[42–45] platforms to convert the affinity binding event between glucose and sensing material into detectable signals to determine glucose concentration. Optical methods measure the glucose-binding-induced changes in color[35], light absorption (optical absorption spectroscopy), transmission, emission, fluorescence[46–48], and diffraction wavelength[49–51] in the sensing material. Glucose responsive hydrogel integrated optical fibers[52,53] and CMOS imaging sensors[54] have been developed for CGM applications. In mass-based methods, affinity glucose sensing is realized with QCM[55], piezoelectric[37,56,57], and microcantilever[30,58,59] based transducers to correlate the measurement of the glucose-induced changes in the mass, osmotic pressure, or viscosity of the sensing material with glucose concentrations. Electrochemical methods including voltammetry or amperometry have been used for signal transduction. Voltammetric sensors using boronic acid-modified electrodes require the addition of redox markers, such as potassium ferro/ferri cyanide ($Fe(CN)_6^{3-/4-}$), to sample solutions because boronic acid itself does not produce a redox signal[60], which limits its practical use in CGM applications. Amperometry glucose sensors based on redox-active moieties modified boronic acid, such as ferroceneboronic acid (FcBA), have been developed to achieve reagentless electrochemical-based affinity glucose sensors[61–63].

Among these transduction methods for affinity glucose sensing, optical transduction methods have demonstrated their accuracy and reliability in glucose measurement, but typically require sophisticated, expensive, and bulky instrumentation. This poses challenges to reaching the level of miniaturization suitable for personalized CGM systems. Mass-based biosensors, such as the most commonly used quartz crystal microbalance or piezoelectric-based biosensors, can allow glucose measurement with high sensitivity under *in vitro* characterization[64,65], however, their suitability for *in vivo* application is hampered by biomass accumulation induced by biofouling and non-specific adsorption. While FcBA offers an electrochemical approach to realize affinity glucose sensors, its low-level specificity and low affinity to glucose when immobilized on electrode surface hinder its application in glucose sensing[62]. In addition, electrochemical-based transduction methods are also susceptible to interferences from electroactive species, such as uric acid and ascorbic acid, in the measurement media[66].

In contrast, impedimetric and field-effect transduction methods can effectively address these limitations and are discussed below.

1.3 Impedimetric and Field-Effect Transduction Methods for Affinity Glucose Sensing

Impedimetric and field-effect transistor-based affinity sensors transduce affinity bindings into detectable signals by inducing changes in the electrical properties or charge distributions of sensing materials.

Impedimetric affinity sensors. Impedimetric biosensor is based on the concept of impedance spectroscopy, which is a powerful method of analyzing the frequency-dependent electrical impedance of a system and is sensitive to surface phenomena and changes in bulk properties[67,68]. An impedimetric transducer consists of a pair of electrodes in either parallel-plate[42,69] or coplanar configuration[45,70] on a support substrate. By applying an AC perturbation voltage with a small amplitude at a particular frequency on one electrode and detecting the current response from the other, the complex impedance Z of a system can be determined. The impedance Z is the quotient of the voltage-time function $V(t)$ and the resulting current-time function $I(t)$[68].

$$Z = \frac{V(t)}{I(t)} = \frac{V_0 \sin(2\pi ft)}{I_0 \sin(2\pi t + \phi)} \tag{1}$$

where V_0 and I_0 are the maximum voltage and current signals, f is the frequency, t the time, ϕ the phase shift between the voltage-time and current–time functions. The impedance of the system can be directly interrogated by connecting the two electrodes to an impedance analyzer or interfacing the input and output electrode with a voltage-impedance converter, of which the output is measured by a phase-sensitive detector for interpretation of the device impedance.

In the case of an impedimetric affinity sensor, the receptors are functionalized either on the electrodes or incorporated inside a scaffold structure immobilized between the electrodes, for example, embedded inside a polymer solution or a crosslinked hydrogel matrix that is confined between the electrodes. When the recognition complex between the receptor and the analyte is formed, the electrical properties of the recognition surface or the bulk materials will be altered, which are reflected as impedance change and are monitored by the impedimetric sensor. The change of either resistance or capacitance or overall impedance is used to correlate to a change in analyte concentration. Affinity-based impedimetric sensors have been demonstrated for affinity measurements of different types of analytes, such as proteins[70,71], nucleic acids[72], antibodies, and antigens[73].

Field-effect transistor-based affinity sensors. Since the emergence of the ion-selective field-effect transistor (FET) in 1970[74], FET-based biosensors have attracted extensive attention due to their miniature size and weight, inexpensive mass fabrication, and facile integration with interfacing electronic circuits[75]. A FET sensor comprised three electrodes, namely, a source electrode upon which a DC voltage V_s is applied, a drain electrode to detect the current I_{sd} flowing between the source and drain electrodes, and a gate electrode upon which a DC gate voltage V_g is applied to modulate the conductivity of the semiconductor bridged between the source and drain electrodes[76,77]. The working principle of the FET sensor is based on the field-effect, by which gate voltage (V_g) can influence the semiconductor band structure and therefore alter its conductivity. When this concept is applied with a bio-sensing layer immobilized onto the semiconductor surface, a bio-recognition event that occurs near this surface can induce changes in the charge distribution, resulting in a change in the conductivity of the semiconductor channel[75]. Being sensitive to the charge redistribution often involved in the biorecognition process[76], FET biosensors have achieved success in the sensing of different biomolecular[78–80] and cellular events[81,82].

Impedimetric and FET-based affinity methods offer several advantages over the other transduction methods mentioned above. The fabrication of impedimetric and FET sensors is compatible with standard planar fabrication processes for large-scale circuitry, enabling the low cost of mass fabrication. The planar structure of these sensors is highly amenable for reliable integration of thin layers of sensing material to enable rapid diffusion of the analyte, leading to fast sensing speed. Compared with optical methods which rely on expensive and bulky instrumentation, the impedimetric and FET sensors can readily achieve the miniaturized size as the measurement circuit can be integrated with the device to form a system of high integration level. Impedimetric and FET-based approach does not need redox markers for electrochemical transduction of the signal, which is compatible with real-time monitoring, and are not susceptible to interferences from the electrode active species. Thus, these electrically-based transduction methods offer a high level of miniaturization, allow low-cost instrumentation, and are amenable to physical and functional integration.

1.4 Recognition Ligands and Transduction Materials for Affinity Glucose Sensing

1.4.1 Glucose-Binding Ligands

Different molecules have been functionalized on the bio-transducer interface to generate a measurable response to glucose, including Concanavalin A and boronic acid-based molecules.

Concanavalin A. Concanavalin A **(**Con A) is a protein that can specifically bind to glucose[25]. Con A was the first molecule used to demonstrate the concept of affinity sensor[24]. Extensive studies have been focused on developing Con A-based glucose sensors that measure the glucose-binding induced changes in the fluorescence[24,32,83] and viscosity[30,84] of the sensing materials. Despite the promise to compose long-term CGM systems, Con A has been associated with a variety of toxicological effects, which imposes safety concerns to be used in minimally invasive or implantable CGM sensors[85].

Boronic acid-containing receptors. Another choice for affinity glucose sensors is using synthetic phenylboronic acid (PBA)-based receptors. PBA-derivatives have been reported to interact with glucose rapidly and reversibly to form boronate esters in aqueous media. Being a biocompatible functional group with low cytotoxicity and low immunogenicity, boronic acid derivatives can address the safety concerns with the toxicological properties of Con A[86,87]. In addition, boronic acid is quite stable under physiological conditions and can significantly resolve the instability of Con A due to its denaturation in the physiological environment and electrostatic interaction with charged molecules[88].

1.4.2 Transduction Materials

PBA-containing polymer solutions. Polymer solutions have been used as a hydrophilic matrix to attach phenylboronic acid to increase its binding strength to glucose. The PBA-based fluorescent monomer was polymerized with a hydrophilic monomer to generate a linear polymer solution whose fluorescent is glucose-dependent. PBA-containing polymer solutions, which have glucose-dependent viscosity, were incorporated with MEMS viscometric sensors to construct miniaturized affinity glucose microsensors[26,58]. While demonstrating the potential in sensitive and selective measurements of glucose mostly *in vitro*, these devices required the use of semi-permeable membranes to hold the glucose-sensitive polymer solution, which significantly increased the complexity, limited the miniaturization of the device, and affected the reliability of the microsensor.

PBA-containing hydrogels. Hydrogels are three-dimensionally crosslinked hydrophilic polymer networks and have a modulus similar to subcutaneous tissue, capable of absorbing a large amount of water allowing rapid diffusion of analytes[89]. Possessing these characteristics, hydrogels can limit the biofouling and minimize the foreign body effect and have been used as biocompatible coatings for implantable sensors to serve as a sensor-body interface to promote its performance and biocompatibility[90]. For example, a hydrogel-coated biosensor was functional after 21 days implanted in an animal, while only 13.5% of the controls were still functional[90]. Recently, the ability of hydrogels to sensitively respond to external stimuli (pH, temperature, biological receptors, etc.) has gained considerable attraction in biosensing applications. With a receptor that specifically bind with a target analyte embedded inside, hydrogels are capable to sense binding events and transduce the binding process to detectable signal through alternating their swollen state[91,92]. PBA cross-linked hydrogels can be responsive to glucose concentrations. By integrating these glucose-responsive hydrogels with an appropriate transducer system, hydrogel-based sensors can be developed to measure glucose concentrations while possessing all the benefits endowed by hydrogels. Thus, hydrogel-based biosensors are highly promising in achieving long-term monitoring devices implanted in the body.

Hydrogel-based affinity glucose sensors. Integration of boronic acid-containing hydrogel can potentially lead to the development of long-term CGM sensors by minimizing the bio-fouling, allowing enhanced signal transduction at the body-transducer interface. Glucose-induced changes in diffraction wavelength[33,93,94], osmotic pressure[56,95], or electrical property changes[42,45,96] of PBA containing hydrogels were monitored with optical fibers[31,46], CMOS imaging sensors[54], capacitive or impedimetric transducers[42,45], and field-effect transistors[97] to construct affinity sensors that suit CGM applications. Hydrogels have been integrated within hollow optical fibers made with semi-permeable membrane[31,46], immobilized within the gap between the top and bottom electrode of a microfabricated parallel plate capacitor and immobilized as a thin layer on top of the transducer surface, such as a coplanar-electrode impedimetric transducer[45,98] or a field-effect transistor[97]. Among different integration methods, *in situ* immobilization of the hydrogel layer onto the coplanar surface of the electrode via covalent linkage allow relatively unrestricted volume expansion and shrinkage of the hydrogel in response to glucose while maintaining a reliable attachment of hydrogel to the transducer, which is highly promising to afford a sensor-body interface with long-term reliability. However, the stability, measurement accuracy, response time and biocompatibility of the hydrogel-based glucose affinity sensors need to be further improved.

Nanomaterials. Nanomaterials have attracted considerable research interest in constructing biosensors because they offer the potential for improved biocompatibility, sensitivity, and scalability over conventional silicon-based materials[99–102]. Graphene, a monoatomic layer of carbon atoms distributed in honeycomb lattices[103], possesses extraordinary material properties including high surface-to-volume ratio, excellent electronic properties, and optical transparency, which are attractive in constructing field-effect transistor (FET) sensors. In an electrolyte-gated GFET device, the graphene is bridged between a source electrode and a drain electrode, between which a DC voltage V_{sd} is applied. A gate electrode, upon which a voltage V_g is applied through the electrolyte, is used to set the graphene's electrical potential, modulating its conductivity. When functionalized with a biorecognition element, such as aptamers or antibodies, GFET nanosensors for specific detection of the target can be formed. The signal transduction of the binding activity to a detectable electrical signal using a GFET nanosensor relies on the extreme sensitivity of graphene's electrical property to the change in the charge distribution on its surface. In an affinity glucose nanosensor, glucose binds with the aromatic boronic acids adsorbed on the graphene surface to form a glucose–boronated ester complex, altering the conductivity of the graphene, which are measured to determine the glucose concentration. Graphene-based glucose nanosensors hold the potential to achieve low-cost continuous glucose monitors with high accuracy, low limit of detection and fast time response.

1.5 Contributions of This Thesis

This thesis focuses on developing affinity micro and nanosensors to meet the demands for implantable CGM devices with biocompatibility, fast time response, and high-level miniaturization. we investigate microelectromechanical systems (MEMS)-based, subcutaneously implantable affinity microsensors for measuring glucose concentrations in interstitial fluid, and explore graphene affinity nanosensors for non-invasive monitoring of glucose in physiological media such as tears.

Previously existing affinity glucose microsensors have measured glucose-induced changes in fluorescence intensity, viscosity, or volume of the sensing materials. These measurement methods, while effective, are not well suited for implantable operation due to issues such as requirements of optical access or mechanical moving parts. The first study of this thesis makes an initial demonstration of a hydrogel-based MEMS dielectric affinity glucose microsensor to alleviate these limitations. The microsensor measures glucose concentration by detecting the change in the dielectric properties of a thin layer of glucose affinity hydrogel integrated with an impedimetric transducer. The device eliminates the semipermeable membrane commonly used in the existing affinity sensors by adopting a biocompatible synthetic hydrogel. This leads to a major simplification in the device design and construction as well as improvement in the operational reliability. The microsensor has shown a repeatable and reversible response to glucose concentration changes in a range of 30-500 mg/dL, demonstrating the potential of the dielectrically based affinity sensing approach for continuous glucose monitoring.

In the second study, a systematic investigation is made to understand the effects of the hydrogel composition on dielectrically based affinity glucose sensing. Specifically, we investigate the effects of the compositional parameters, including the glucose-responsive monomer, hydrophilic monomer, and crosslinker, on the glucose-induced changes in swelling and dielectric properties of the hydrogel. This leads to the identification of an optimum hydrogel composition that offers an appropriate tradeoff between the ability of the hydrogel to reliably adhere to the surface and the ability of the device to sensitively measure glucose concentrations. Furthermore, the coplanar-electrode-based microsensor, when functionalized with a ~5-µm-thick hydrogel, exhibits a repeatable and reversible response in a physiologically relevant glucose concentration range of 30–360 mg/dL with a resolution down to 25 µg/dL and a response time < 30 s.

In the third study of this thesis, we build on the results from the first two studies and present a differential hydrogel-based microsensor, which has the capability to reject environmental disturbances (such as variations in the temperature and pH) that can compromise the reliability and accuracy of glucose concentration measurements. The differential microsensor contains two identical measurement units placed in close proximity, each integrated with a thin layer of PBA containing hydrogel or a reference hydrogel (containing no PBA). The difference between signals of the two units is used as the sensor output to more accurately represent the response to glucose concentration changes. This differential measurement scheme, in combination with an optimal transducer design and reliable *in situ* hydrogel integration, allows accurate, rapid, and stable glucose measurements. Preliminary *in vitro* and *in vivo* testing results demonstrate that the differential microsensor is capable of measuring glucose concentrations reversibly and rapidly (time response < 21 s) with a sensitivity of 7.5 pF/(mg/dL), resolution of 0.1 mg/dL and drift of 0.13%/h.

The final study of this thesis is a preliminary investigation of graphene affinity nanosensors for non-invasive monitoring of glucose concentrations in physiological media such as tears. The nanosensor consists of aromatic boronic acid-functionalized graphene in an electrolyte-gated field-effect transistor configuration. The sensing mechanism of the affinity nanosensor for glucose measurement is first investigated through pH-based measurements. The findings reveal that glucose-boronic acid complexes can donate electrons to graphene, resulting in a decrease in the Dirac point. The nanosensors are then applied to glucose measurements. Testing of the devices functionalized with each of four aromatic boronic acids has shown sensitive measurements of glucose concentrations at physiological pH within ranges corresponding to those in human tears. In particular, nanosensors modified with 8-quinolinylboronic acid (8-QBA) exhibits a rapid (<15 s) and reversible response to glucose concentrations in the range 0.18-180 mg/dL with a sensitivity (32 mV/(mg/dL)) and low limit of detection (38 μg/dL) for potential non-invasive, continuous monitoring of glucose in tears.

1.6 Organization of This Thesis

Impedance-based affinity glucose micro and nanosensors. In Chapter 2, we describe an initial demonstration of dielectrically based MEMS sensors that use an integrated glucose-responsive hydrogel to achieve affinity glucose sensing. Chapter 3 presents a systematic study of the effects of hydrogel composition on the glucose-induced swelling and dielectric property changes of the hydrogel in the affinity glucose microsensors. Chapter 4 describes a differential dielectric microsensor for accurate *in vivo* glucose measurement. In Chapter 5, a preliminary study is presented on affinity nanosensors for non-invasive monitoring of glucose concentrations in physiological media such as tears. Finally, a summary of this thesis is given and the opportunities for future work are discussed in Chapter 6.

Chapter 2: Hydrogel-Based Affinity Glucose Sensing: Initial Demonstration

2.1 Introduction

In this chapter, an initial demonstration is presented of a hydrogel-based MEMS dielectric affinity glucose microsensor. Our group has previously explored hydrogel-based affinity glucose microsensors[42], which, while demonstrating the potential of hydrogels for affinity glucose sensing, were limited by a very slow time response (~16 min) due to the use of a thick hydrogel layer (~250 μm) that required long diffusion times between the sensor surface and surroundings. The hydrogel layer also poorly adhered to the sensor surface and led to significant reliability issues. These limitations will be addressed here with a new microsensor design.

The microsensor consists of a coplanar capacitive transducer coated with a thin (~10 μm) hydrogel layer. The binding between the hydrogel and glucose causes a change in the permittivity of the hydrogel, which is measured from the impedance of the transducer to determine the glucose concentration. Key to the rapid responsiveness and robust construction of the device is the adoption of a substantially thinner hydrogel (~10 μm), achieved by the innovative use of *in situ* gelation, to speed up the time response (potentially down to 1.2 seconds). Additionally, the device adopts a coplanar capacitive transducer, which, compared with the parallel-plate-based configuration used in the previous work[42], is considerably more robust and easier to fabricate, is amenable to *in situ* hydrogel preparation, and fully avails the hydrogel layer to glucose exchange. The device has been tested in phosphate-buffered saline (PBS) solution at pH 7.4 and 37 °C. Testing results showed that in a glucose concentration range of 0-500 mg/dL the microsensor exhibited a repeatable and reversible response to glucose with a resolution down to 0.32 mg/dL based on effective capacitance and 0.27 mg/dL based on effective resistance, thereby demonstrating the potential of the device for continuous glucose monitoring.

2.2 Methods

2.2.1 Principle and Design

The hydrogel-based affinity sensor is integrated with a glucose-responsive hydrogel formed by *in situ* radical polymerization by successive addition of 3-acrylamidophenylboronic acid (AAPBA) as free radical glucose-sensitive monomer, acryl *N*-hydroxyethyl acrylamide (HEAA) as the hydrophilic monomer, tetraethyleneglycol diacrylate (TEGDA) as the cross-linker and 2,2'-azobis(2-methylpropionamidine) dihydrochloride (AAPH) as the polymerization initiator. When diffusing into the affinity hydrogel, glucose binds reversibly to phenylboronic acid moieties in the AAPBA segments to form strong cyclic boronate ester bonds, inducing partial crosslinking of the hydrogel matrix and causing a molecular structure change. As electric polarization is strongly influenced by the material's molecular structure changes, the binding process of the glucose to the immobilized affinity hydrogel induces changes in its dielectric properties, which can be detected using an interdigitated-electrode (IDE) sensor (Figure 2.1).

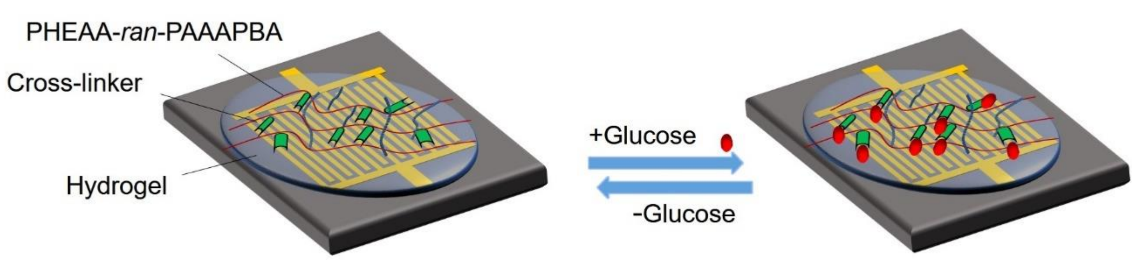

Figure 2.1: Principle of the hydrogel-based MEMS affinity sensor.

The complex permittivity of hydrogel is represented by $\varepsilon^* = \varepsilon' - j\varepsilon''$, where the real permittivity ε' represents the ability of the hydrogel to store electric energy, while the imaginary permittivity ε'' is related to the dissipation of energy[104]. When the hydrogel is integrated into the IDEs, the microsensor can be represented by a capacitor and a resistor connected in series. The complex interaction of hydrogel with glucose can cause changes in the charge distribution, double-layer structure, composition as well as conformation of the hydrogel, which would, in general, induce changes in both the real part and imaginary part of dielectric properties of the hydrogel. Thus, the microsensor's effective capacitance and resistance can be influenced by the interaction of glucose with hydrogel and are measured to determine the glucose concentration.

The MEMS microsensor adopts a coplanar capacitive transducer sensor. The IDEs situated on the silicon dioxide substrate consist of 40 pairs of gold electrodes with a thickness of 50 nm, 1.5 mm length, 20 µm width and interspacing (Figure 2.2a and Figure 2.2b). A thin layer of hydrogel (~ 10 µm) is covalently attached to the sensor surface via *in situ* radical polymerization to substantially speed up the time response. When immersing the sensor in glucose solutions, glucose molecules can rapidly diffuse through the thin layer of hydrogel and reversibly bind with the hydrogel, changing its complex permittivity, which can be interrogated via measurement of the impedance between the IDEs to determine the glucose concentration. An on-chip resistive temperature sensor is integrated for monitoring the surface temperature and providing feedback to a temperature control system (Figure 2.2c).

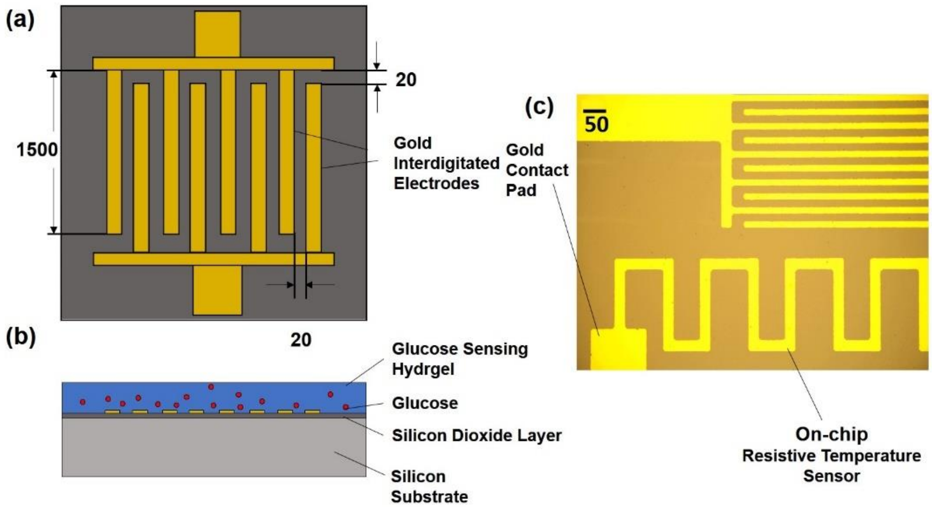

Figure 2.2: Schematic of the MEMS hydrogel-based affinity CGM sensor: (a) top view, and (b) side view. (c) Image of a fabricated microsensor. Unit: μm.

2.2.2 Fabrication

The hydrogel-based microsensor chip was fabricated using the standard MEMS fabrication process. A thin layer of metal (Cr/Au 5/45 nm) was deposited on a silicon dioxide substrate by thermal evaporation and patterned to form the IDEs and on-chip resistive temperature sensor. The hydrogel thin film was integrated on the electrode using *in situ* radical polymerization. Specifically, a mixture of the deoxygenated hydrogel components was first spin coated on the microsensor surface and then heated to 70 °C in nitrogen to initiate *in situ* gelation via radical polymerization from a mixture of monomers, cross-linker, and initiator dissolved in water.

2.2.3 Materials

The hydrogel was synthesized in house via free radical polymerization of the pre-mixed solution of AAPBA (1.1% w/v), HEAA (5.5% v/v), TEGDA (0.08% v/v), and AAPH (0.16%

w/v). D-(+)-glucose and phosphate-buffered saline (PBS, 0.15 M, pH 7.4) were bought from Sigma-Aldrich. A glucose stock solution (500 mg/dL) was prepared by dissolving D-(+)-glucose (2.5 g) in 500 mL PBS. Then glucose solutions (40, 80, 100, 200, and 300 mg/dL) were prepared by further diluting the stock solution with PBS.

2.2.4 Experimental Procedures

During testing, the microsensor was placed in an acrylic flow cell (1.2 mL in volume) filled with the glucose solution to be tested (Figure 2.3a). To minimize thermally induced dielectric property change of the hydrogel and solution, during all experiments the temperature of the test cell was controlled at 37 °C by closed-loop control of a Peltier heater (Melcor, CP14) according to feedback from the integrated resistive temperature sensor. The microsensor was coupled to an impedance/voltage transformation circuit driven by a small sinusoidal input from a function generator (Agilent, 33220A) (Figure 2.3b), which imposes an AC field between the IDEs of the microsensor to induce a glucose concentration-dependent change in the permittivity of the hydrogel. The impedance of the microsensor can be determined by measurements of the amplitude and phase of the system output voltage V_{out} , detected using a lock-in amplifier (Stanford Research Systems, SR830) from a known input voltage V_{in}, via the impedance/voltage transformation circuit. We calculated the effective capacitance and effective resistance of the microsensor based on an equivalent circuit that consists of a serial connection of a capacitor C_{x} and resistor R_{x} representing the microsensor. The microsensor's complex impedance can be determined by $Z_{\mathrm{x}}=R_{\mathrm{x}}+1/(j\omega C_x)=-V_{\mathrm{out}}/(R_{\mathrm{f}}V_{\mathrm{in}})$, where R_{f} is a reference resistance.

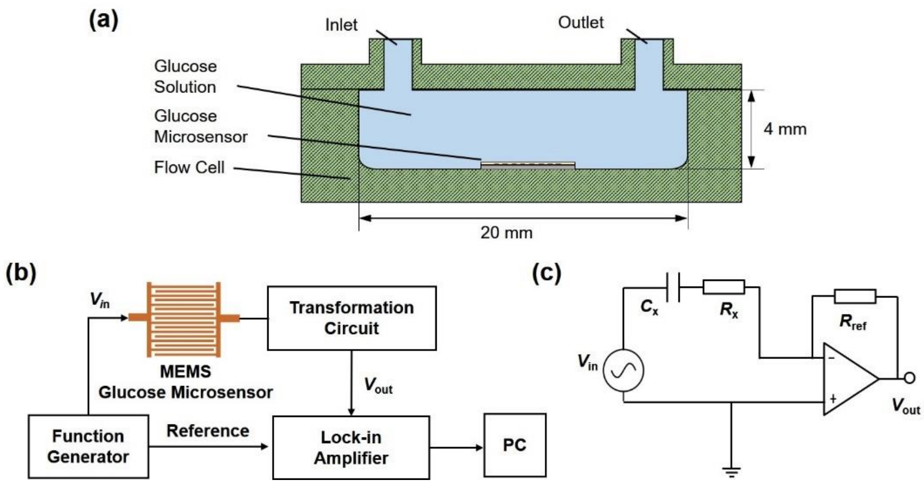

Figure 2.3: Method for microsensor testing. (a) Side view of the test flow cell. (b) Experimental setup. (c) Impedance/voltage transformation circuit.

2.3 Results and Discussion

We first investigated the frequency dependence of the microsensor response to glucose concentrations from 0 to 500 mg/dL over selected frequencies in the range of 1 kHz to 100 kHz. Then we characterized the time-resolved response of the microsensor to a sequence of glucose variations at a specific frequency, to assess its potential applicability to glucose monitoring. Finally, we tested the response of the microsensor to other potential interferents including fructose, galactose, and lactate at their physiological concentrations to compare the sensor’s response to a normal glucose concentration of 100 mg/dL.

2.3.1 Frequency Dependency of Device Response

We first characterized the frequency dependence of the sensor response to glucose concentrations. In the experiment, a series of glucose concentrations (40, 80, 100, 200, 300, and 500 mg/dL) in PBS buffer were tested sequentially. For instance, a PBS buffer was first introduced to the test cell and an AC power source was applied to the microsensor. The microsensor was then allowed to reach equilibrium followed by a frequency sweep from 1 kHz to 100 kHz. The tested frequency range was chosen between 1 kHz and 100 kHz since the unwanted parasitic impedance induced by the electrical double layer becomes more dominant at a frequency less than 1 kHz[105] and the maximum frequency that can be detected using a lock-in amplifier is 100 kHz. Error bars reflect standard errors from triplicates of measurements. The same experiments were repeated for all other concentrations, from which the steady-state effective capacitance and effective resistance of the microsensor, as a function of the excitation frequency, were computed from the output voltage of the measurement circuit and plotted as a function of frequency (Figure 2.4a) and Figure 2.4b). The microsensor's effective resistance and effective capacitance both decreased consistently with the increasing frequency due to the dielectric relaxation of the hydrogel. Several polarization mechanisms (i.e., the shift of electric charges from their equilibrium positions under the influence of an electric field)[104], such as dipole reorientation, counterion diffusion, and interfacial polarization, contributed to the measured response of the microsensor.

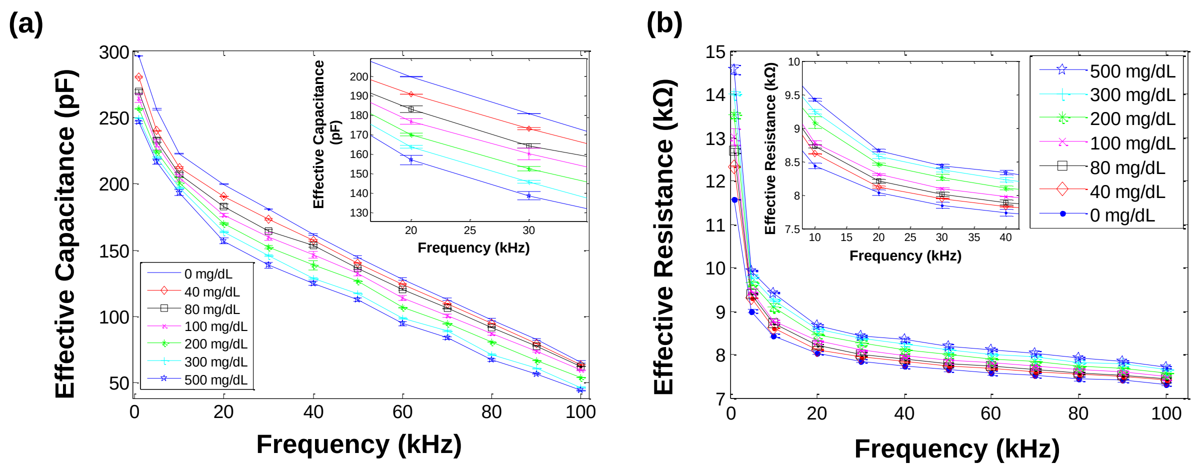

Figure 2.4: Effective capacitance and resistance of the microsensor. (a) Dependence of effective capacitance on measurement frequency. (b) Dependence of effective resistance on measurement frequency.

At the same time, the effective capacitance and the effective resistance were recorded as a function of glucose concentration at three chosen frequencies (1 kHz, 2 kHz, 5 kHz) (Figure 2.5a and Figure 2.5b). At a specific frequency, the microsensor's effective capacitance decreased monotonically with glucose concentration in the entire range tested (0–500 mg/dL), while the effective resistance of the microsensor increased monotonically with the entire tested glucose concentration. Specifically, at 1 kHz, the effective capacitance decreased from 297.2 pF to 246.6 pF and the effective resistance increased from 11.58 kΩ to 14.57 kΩ as the glucose concentration increased from 0 mg/dL to 500 mg/dL. This was reflected in the binding between the hydrogel and glucose, which influenced the polarization of the hydrogel. The AAPBA units appended on the hydrogel backbone could form cyclic boronate esters with glucose molecules at a 1:1 or 2:1 ratio, leading to a change in the net permanent dipole moments of AAPBA units (or their dipole reorientation). In addition, based on our previous observation[87], the binding with glucose can induce partial crosslinking of the hydrogel, which in turn will increase the elastic resistance of the dipole rearrangement in the electric field, leading to a change in the hydrogel complex permittivity. The combination of these effects can contribute to the concentration-dependent sensor response to glucose concentrations.

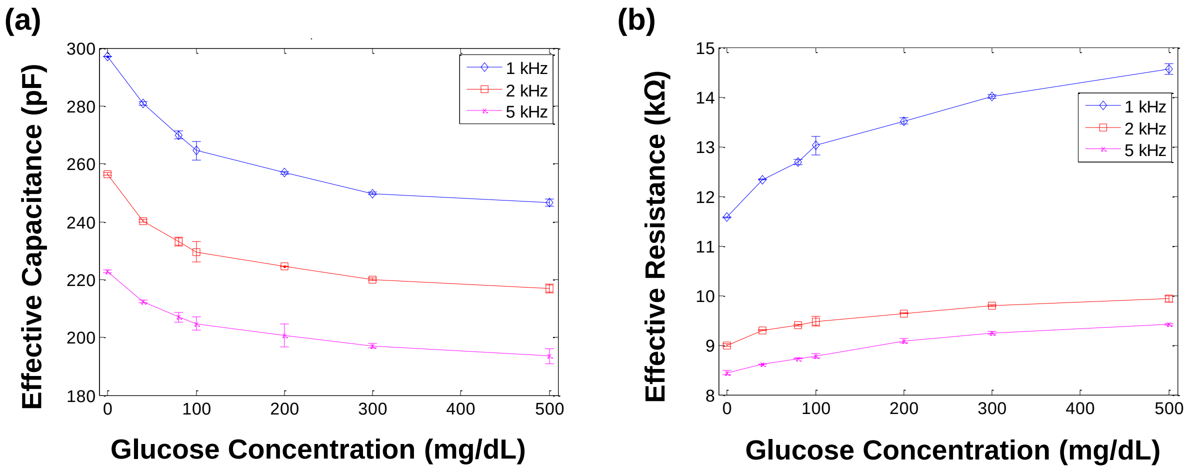

Figure 2.5: Effective capacitance and resistance of the microsensor. (a) Dependence of effective capacitance on glucose concentration. (b) Dependence of effective resistance on glucose concentration.

Next, we characterized the microsensor's sensitivity, i.e., change in effective capacitance or resistance due to glucose concentration change ($\Delta C/\Delta c_{glucose}$, $\Delta R/\Delta c_{glucose}$,). The device characteristics indeed generally varied with the glucose concentration due to the nonlinearity of the sensor response. With the capacitive transducer operating at 1 kHz for glucose concentration ranging from 0 to 500 mg/dL tested, the sensitivity, calculated at a given concentration value, varied from 410 fF(mg/dL)$^{-1}$ to 15.8 fF(mg/dL)$^{-1}$ based on effective capacitance, and from 18.9 Ω(mg/dL)$^{-1}$ to 2.8 Ω(mg/dL)$^{-1}$ based on effective resistance, respectively. Using an estimated noise of 90 μV and 0.085° in the magnitude and phase of the output AC voltage of the measurement circuit and instrumentation, the corresponding resolution in glucose concentration in this range was estimated to be from 0.27 mg/dL to 3.2 mg/dL based on effective capacitance, and from 0.20 mg/dL to 2.5 mg/dL based on effective resistance, respectively. It is interesting to note that the sensor response, while nonlinear in the full range, was quite linear from 40-100 mg/dL, with R^2 = 0.99. In this range, the sensitivity was 270 fF(mg/dL)$^{-1}$ based on effective capacitance and 11.09 Ω(mg/dL)$^{-1}$ based on effective resistance, and the resolution was 0.32 mg/dL based on effective capacitance and 0.27 mg/dL based on effective resistance, respectively.

2.3.2 Device Response to Time-Dependent Glucose Concentration Changes

We then measured the time-resolved response of the sensor to a sequence of glucose variations to assess its potential applicability to glucose monitoring. Noting that as the measurement frequency increased, the sensor response became more diminished because of dielectric relaxation[106]. We performed the measurements at a fixed frequency of 1 kHz, which offered a pronounced sensor response. The test cell was initially filled with PBS buffer and then replaced with PBS solution of glucose, first sequentially at concentrations of 40, 80, and 300 mg/dL, and then sequentially in the reverse order at the same set of concentrations. From the measurement results (Figure 2.6a and Figure 2.6b), both the effective capacitance and resistance were consistent at a given glucose concentration setpoint, regardless of whether that setpoint resulted from an increase or decrease in the glucose concentration used in the preceding test. For example, the effective resistance at a glucose concentration of 80 mg/dL over the two periods, approximately defined by the internals from 30 to 40 min (when the glucose concentration increased from 40 to 80 mg/dL) and defined by the internals from 56 to 66 min (when the glucose concentration decreased from 300 to 80 mg/dL), were respectively 12.85 kΩ and 12.90 kΩ, which agree within 0.4%. Similarly, the reversibility was found to be within 0.6% and 0.8% for the measurement data at 40 and 0 mg/dL glucose concentrations, respectively. This indicates that the device was highly reversible in response to glucose concentration variations.

The time dependence of the measured sensor output could be well represented by an exponential function, and based on a least-square fit, exhibited a time constant of 1.6 min for the effective capacitance, and 1.8 min for the effective resistance. These time constants are a substantial reduction from that (16 min) calculated for our previously reported device[42] and are comparable to those (0.65-1.30 min) estimated for the commercially available electrochemical CGM sensors[107]. To understand the physical significance of these time constants, we consider the transport of glucose molecules to the sensor surface. When there was a change in glucose concentration in the solution fed into the test flow cell, glucose molecules were first transported through the flow cell to the liquid-hydrogel interface, and then diffused through the hydrogel layer and bound to boronic acid moieties (Figure 2.3a). The time constant for glucose transport through the flow cell, estimated via simulation of convective-diffusive mass transfer (under conditions used in the tests and with a glucose diffusivity of 4.5×10^{-11} m^2/s), was approximately 1.5 min and comparable to the time constants of the measurement data. On the other hand, the time constant for glucose diffusion through the hydrogel, estimated via one-dimensional diffusion (under conditions used in the tests and with a glucose diffusivity of 4.5×10^{-11} m^2/s), was approximately 1.2 sec and the glucose-boronic acid-binding was expected to be as fast as milliseconds[108]. These two latter time scales were both substantially smaller than the time constants of the measurement data. Thus, it was concluded that the measured time constants were dominated by those of convective-diffusive transport of glucose in the test flow cell, and did not reflect the true response time (which could be as low as several seconds) of the hydrogel-based sensor. Note that the flow cell was not part of the glucose microsensor and was only used as an *in vitro* testing tool. Measurement of the microsensor's true response time would require a new test setup, to be constructed in future work, capable of generating glucose concentration changes at the sensor surface within a much shorter time duration.

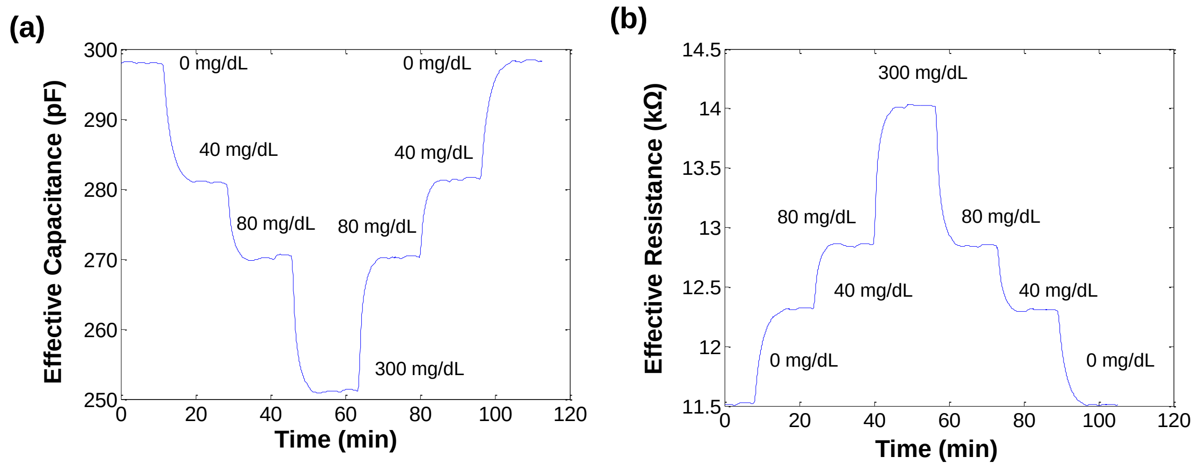

Figure 2.6: Microsensor response at 1 kHz in response to time-varying glucose concentrations: (a) effective capacitance, and (b) effective resistance.

2.3.3 Device Response to Potential Interferents

Boronic acid is known to bind, in addition to glucose, with monosaccharides through boronic acid-diol interactions[109]. Monosaccharides that exist in blood mainly include fructose and galactose. Lactate, which is present in blood at a typical concentration of 11.2 mg/dL[110]), could be the primary interferent in glucose measurement in a physiological sample. Fructose (~1.8 mg/dL) and galactose (~1.8 mg/dL) are present in blood at much lower concentrations. We tested the device on these potential interferents at their physiological concentrations. At 1 kHz, the effective capacitance changes of the device due to lactate (12 mg/dL), fructose (2 mg/dL), and galactose (2 mg/dL) were determined to be respectively 4.3%, 4.7%, and 2.1% of that induced by glucose (100 mg/dL), while the effective resistance change to the interferents at the physiological concentrations above were respectively 3.3%, 4.5%, and 2.2% of that due to glucose (100 mg/dL). The device was hence considered appropriately selective for measurements of physiological glucose concentrations.

2.4 Summary

We have made an initial demonstration of a dielectric affinity microsensor that consists of hydrogels attached to a pair of coplanar electrodes *in situ* for dielectrically based affinity measurement of glucose in subcutaneous tissue. The hydrogel, incorporating 3-acrylamidophenylboronic acid (AAPBA) that recognizes glucose via affinity binding, is synthetically prepared on the electrodes via *in situ* polymerization. When implanted in subcutaneous tissue, glucose molecules in interstitial fluid diffuse rapidly through the hydrogel and bind to the phenylboronic acid moieties. This induces a change in the hydrogel's complex permittivity and hence in the impedance between the electrodes, which can be measured to determine the glucose concentration.

The microsensor offers several distinct advantages. The *in situ* hydrogel preparation allows for a reduced hydrogel thickness (~10 μm) to enable the device to respond rapidly to glucose concentration changes in tissue, as well as covalent electrode attachment of the hydrogel to eliminate the need for semipermeable membranes that would otherwise be required to restrain the sensing material within the device. Meanwhile, the use of coplanar electrodes is amenable to the *in situ* preparation and facilitates glucose accessibility of the hydrogel, and combined with dielectrically based transduction, also eliminates mechanical moving parts often found in existing affinity glucose microsensors that can be fragile and complicated to fabricate.

Experimental results showed that the effective capacitance and effective resistance of the microsensor, in a measurement frequency range of 1–100 kHz, responded consistently to glucose concentration changes ranging from 0 to 500 mg/dL. At a given frequency, the device's effective capacitance decreased, while the effective resistance increased with glucose concentration as the hydrogel likely became less polarizable due to the glucose-hydrogel binding. At a frequency of 1 kHz, the measurement resolution of the microsensor in the glucose range (40-100 mg/dL) was estimated to be 0.32 mg/dL based on effective capacitance measurements and 0.27 mg/dL based on effective resistance measurements. In response to time-varying glucose concentration changes, the device exhibited a highly reversible response. Additionally, the measurement data showed a time constant of 1.6 min based on effective capacitance and 1.8 min based on effective resistance. These time constants were determined to be due to convective-diffusive transport of glucose in the experimental setup, with the actual time response of the device expected to be considerably faster (possibly down to several seconds). These results demonstrate that the device holds the potential to enable reliable and accurate continuous measurement of glucose in subcutaneous tissue for continuous glucose monitoring applications.

Chapter 3: Effects of Hydrogel Composition on Hydrogel-Based Affinity Glucose Sensing

3.1 Introduction

Through the initial demonstration of hydrogel-based affinity glucose microsensors, we explored thin layers of phenylboronic acid-containing hydrogels covalently attached to coplanar electrodes (Chapter 2)[42,45]. These devices offer reliable adherence of hydrogels to the electrodes and are rapidly response to glucose concentration changes. In this chapter, we systematically investigate the behavior of the hydrogels as influenced by their composition, and identify the optimal compositional parameters of the hydrogels for affinity glucose sensing.

We will continue to use the microsensor design in which a thin layer of poly(*N*-hydroxyethyl acrylamide-*ran*-3-acrylamidophenylboronic acid) (PHEAA-*ran*-PAAPBA), a glucose-sensitive hydrogel, is covalently attached to a MEMS impedimetric transducer. The hydrogel is a copolymer of 3-acrylamidophenylboronic acid (AAPBA) monomers (serving as the glucose-sensing component) and hydroxyethyl acrylamide (HEAA) monomers (the hydrophilic component). Reversible affinity binding of glucose with the boronic acid moiety in AAPBA induces changes in the dielectric property of the hydrogel, which can be measured by the MEMS transducer to determine the glucose concentration. Additionally, the MEMS transducer uses coplanar capacitive electrodes, which, compared with more commonly used parallel-plate electrodes, are amenable to *in situ* hydrogel preparation and allow highly efficient access of glucose molecules to the hydrogel while offering ease of fabrication and improved robustness. Furthermore, with covalent immobilization of a uniform thin layer of hydrogel onto the coplanar electrodes, the device offers reliable hydrogel-electrode adhesion that rapidly responds to glucose concentration changes as required in CGM applications. By systematically investigating the effects of the molar ratio of AAPBA to HEAA (i.e., glucose-sensitive to hydrophilic monomer) and the molar ratio of tetra (ethylene glycol) diacrylate (TEGDA) (i.e., the crosslinker for the hydrogel formation) to HEAA on the glucose-induced changes in the hydrogel before and after its integration with the MEMS transducer, the optimal hydrogel composition identified allows the microsensor to sensitively and rapidly respond to changes in glucose concentrations in the measurement media. Testing results showed that the hydrogel with an AAPBA-HEAA molar ratio of 1/5 and a TEGDA-HEAA molar ratio of 1/1000 offered the optimal tradeoff between the device's sensitivity to glucose and reliable functionalization with the hydrogel. Furthermore, the microsensor, with a ~5-μm-thick hydrogel, exhibited a repeatable and reversible response in a glucose concentration range of 0–360 mg/dL with a resolution of 25 μg/dL and a response time < 30 s. The device has potential applications for continuous glucose monitoring in the interstitial fluid within the subcutaneous tissue.

3.2 Methods

3.2.1 Microsensor Design and Fabrication

The PHEAA-*ran*-PAAPBA hydrogel consists of AAPBA, which contains glucose-binding boronic acid moieties, as a glucose-sensing component, and HEAA as the hydrophilic component, which improves the solubility of the hydrogel (Figure 3.1a). TEGDA is used as the crosslinker and 2,2′-Azobis(2-methylpropionamidine) dihydrochloride (AAPH) is used as the initiator to start free radical polymerization, the process of forming the hydrogel from the monomers. Phenylboronic acid (PBA) can bind reversibly to diols to form a cyclic boronic ester in aqueous media. (Figure 3.1b). The boronic acid-glucose interaction alters the charge distribution surrounding the polymer chain, attracting counterions and inducing structural changes in the hydrogel matrix, reflecting the glucose changes with its dielectric properties. During operation, glucose permeates through the hydrogel and reversibly binds to the PBA moieties in the hydrogel. When the hydrogel is interfaced with the coplanar capacitive electrodes, glucose concentration can be determined by measuring the glucose-binding-induced change in hydrogel's dielectric properties via monitoring the impedance between the electrodes.

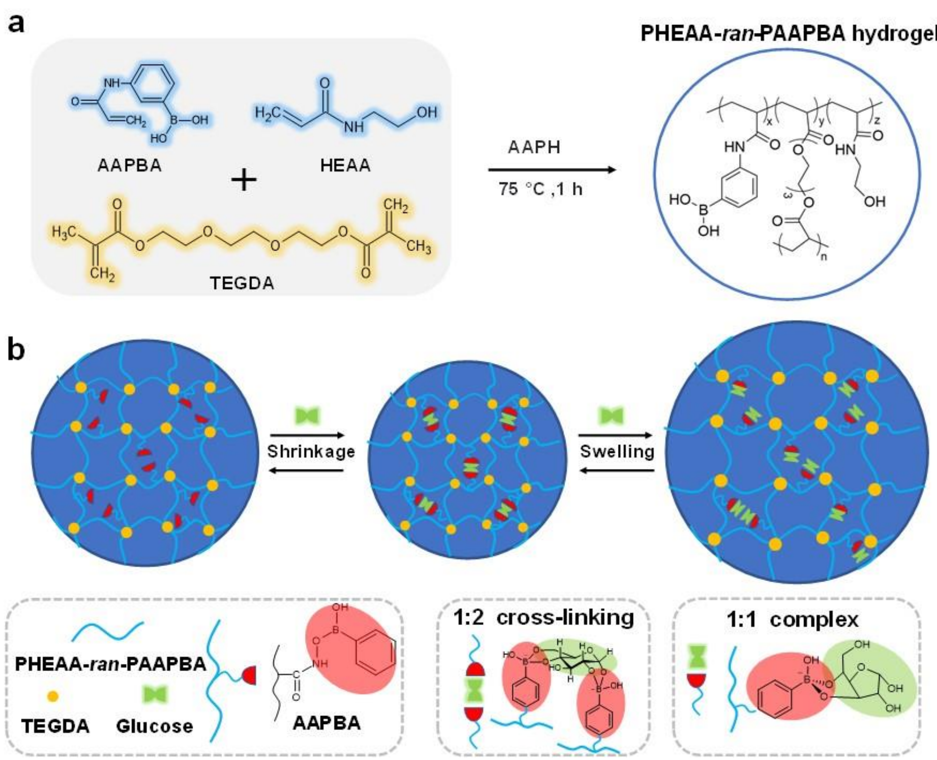

Figure 3.1: Principle for the hydrogel-based microsensor. (a) Components of the PHEAA-*ran*-PAAPBA hydrogel. HEAA and AAPBA monomers are polymerized with TEGDA as the crosslinker. (b) With glucose concentration lower than a critical value, glucose binds with AAPBA moieties at a 1:2 ratio, cross-linking the hydrogel chains and contracting the hydrogel. With an increase in glucose concentration, the 1:2 glucose-AAPBA complex splits to two 1:1 glucose-AAPBA complexes, reducing the crosslinking of the hydrogel and expanding its volume.

The PHEAA-*ran*-PAAPBA hydrogel is integrated with a MEMS impedimetric transducer that includes a pair of coplanar electrodes on a support substrate (Figure 3.2a). The

MEMS transducer has 20 2-mm electrode ‘fingers’ that are spaced 50 µm apart. *In situ* copolymerization covalently links the glucose affinity hydrogel to the surface of the gold electrodes. The thin hydrogel layer enables rapid diffusion of glucose into the hydrogel, reversibly binding with immobilized AAPBA groups and changing the hydrogel’s dielectric properties. This allows the glucose concentration to be determined by monitoring impedance changes of the affinity glucose sensor.

The MEMS transducer was fabricated using standard photolithography as described elsewhere[45]. Briefly, a thin layer of metal (Ti/Au 10/100 nm) was deposited by E-Beam evaporation on a silicon wafer coated with a 300-nm thermally grown insulating silicon dioxide layer and patterned using a lift-off process to form the coplanar electrodes. The MEMS transducer surface was cleaned using a 5:1:1 mixture of deionized (DI) water, ammonia (25%), and hydrogen peroxide (30%) at 75 °C[111], and then modified with an *N*, *N′*-Bis(acryloyl)cystamine (BAC) self-assembled monolayer (SAM) by immersion in 0.5 mM BAC dissolved in methanol for 24 hours[112,113]. The carboxyl groups of BAC molecules undergo free radical polymerization to form the hydrogel by reacting with the carboxyl groups within HEAA or AAPBA, covalently immobilizing the hydrogel on the MEMS transducer surface (Figure 3.2b). The microsensor was sonicated in fresh methanol for 10 minutes and rinsed with DI water to remove the unbound BAC molecules.

The PBA containing hydrogel was prepared *in situ* on the sensor surface using free radical copolymerization, with varying relative amounts of AAPBA, HEAA, TEGDA, and AAPH, as follows. A mixture of deoxygenated hydrogel components was first prepared. The MEMS transducer chip was clamped to a 10-µm deep microfluidic channel. The mixture for hydrogel was introduced to the microfluidic channel via a syringe pump. The transducer-microchannel assembly was then heated at 78 °C for 1 hour to allow *in situ* free radical polymerization. Because of the 10-μm microchannel used during the preparation process, a uniform (~ 5 μm when fully hydrated) layer of hydrogel (Figure 3.2d) formed on the MEMS transducer surface (Figure 3.2c).

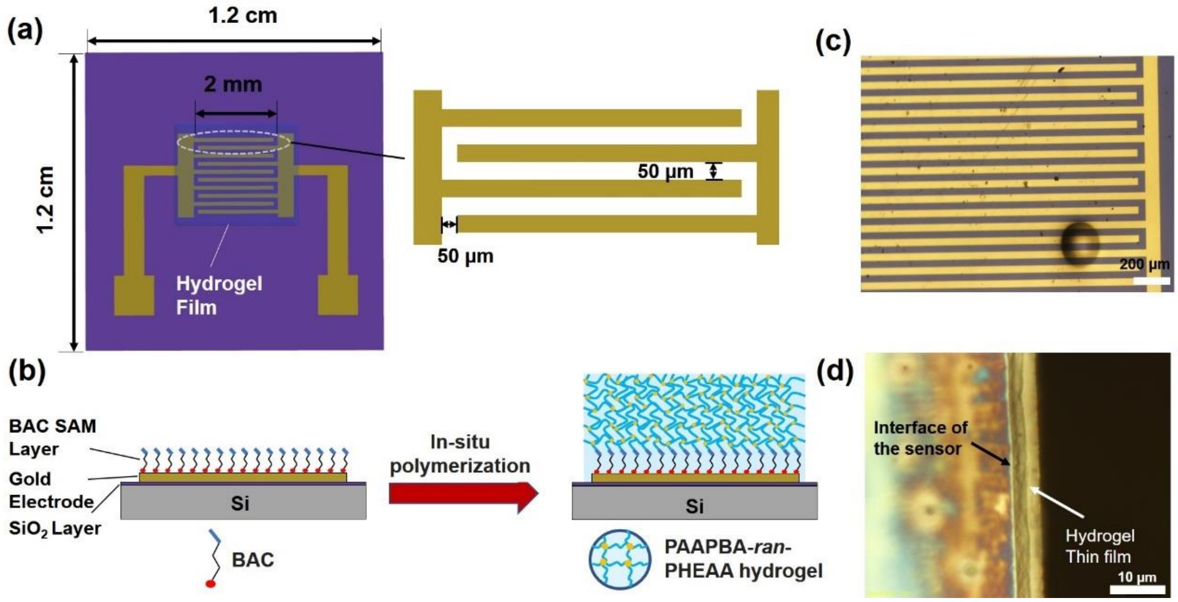

Figure 3.2: Affinity glucose microsensor. (a) Device schematic. (b) Side view of the glucose sensor. Hydrogel is immobilized *in situ* on gold electrodes through synthetic copolymerization. (c) Micrograph of a MEMS transducer coated with a thin layer of hydrogel. (d) Micrograph of the hydrogel thin film of uniform thickness.

3.2.2 Glucose Sensing Principle

As glucose molecules permeate into and out of the hydrogel, they bind reversibly to the PBA moieties in the hydrogel. This binding process causes a change in the complex permittivity of the hydrogel, altering the impedance between the two electrodes, which is then monitored to determine the glucose concentration.

The complex permittivity of the hydrogel can be written in the form $\varepsilon^* = \varepsilon' - j\varepsilon''$, where the real part ε' stands for the ability of the material to store electric energy, while the imaginary part ε'' represents the dielectric loss or dissipation of electromagnetic energy[104]. When subject to an alternating electric field, the hydrogel becomes polarized from short-range transport of positive and negative electric charges in opposite directions. Several polarization mechanisms[114], such as dipole reorientation, counterion diffusion, and interfacial polarization, generally contribute to this dielectric polarization of the hydrogel. In particular, counterion polarization and dipolar polarization reflect the redistribution of ions and reorientation of electrical dipoles within the hydrogel structure, which can be significantly influenced by the binding of boronic acid groups in the hydrogel with glucose molecules. An equivalent circuit model containing a resistor and a capacitor connected in parallel is used to calculate the equivalent resistance (R_x) and equivalent capacitance of the glucose sensor (C_x)[115].

3.2.3 Materials and Testing Procedures

Chemicals and reagents used in the experiments include PHEAA-*ran*-PAAPBA which is synthesized using a previously described method[42,45]. Phosphate-buffered saline solution (PBS, pH 7.4, ionic strength 0.15 M) and D-(+)-glucose were purchased from Thermo Fisher Scientific (Waltham, MA). *N*, *N*'-bis(acryloyl)cystamine (BAC), fructose, galactose, and sodium lactate were purchased from Sigma-Aldrich (St. Louis, MO). All chemicals were used as received. Stock solutions (1800 mg/dL) of glucose were prepared by dissolving glucose powder (0.9 g) into 50 mL PBS buffer. Glucose solutions at varying concentrations (30, 60, 90, 120, 150, 240, and 360-mg/dL) were prepared by diluting the stock solution with the appropriate volume of PBS buffer (0.15 M).

The swelling of PHEAA-*ran*-PAAPBA hydrogels was tested when they were exposed to physiologically relevant glucose concentrations (0-360 mg/dL) in PBS buffer. Hydrogels of different compositions were prepared by mixing the appropriate amount of AAPBA, HEAA, TEGDA, and AAPH, respectively, dissolved in 1 mL water/DMSO solution (v:v, 1:1). The hydrogel mixtures were first degassed by nitrogen gas and then heated to 78 °C for 1 hour in a thermal chamber (Sigma Systems M10) to allow for polymerization of the hydrogel. Small hydrogel cylinders (6 mm diameter, 4 mm thickness) were cut from the formed hydrogel. The hydrogel cylinders were hydrated in PBS buffer or in buffer containing the glucose concentration to be tested for 48 hours at room temperature. To determine the glucose-induced changes in the mass of hydrogels, we removed the hydrogel cylinders from the glucose solutions, blotted the surface using filter paper, and weighted them using an analytical balance. To ensure the accuracy of mass measurements, multiple measurements were performed for each glucose concentration, measurements from each concentration were all within an 8% range.

The affinity microsensor was tested using two experimental configurations. One configuration used an impedance analyzer (SP-200, Biologic, Seyssinet-Pariset, France) to measure the frequency-dependent impedance of the affinity sensor; the other used a custom-built impedance/voltage transformation circuit to measure the kinetic response of the affinity microsensor at a fixed frequency (Figure 3.3). During testing, we coupled the device with a custom-made microfluidic channel. Concentrations of glucose in PBS were introduced into the microfluidic channel using a fluidic injection pump (Figure 3.3). Glucose molecules permeate into and out of the hydrogel reversibly binding to the PBA moieties in the hydrogel resulting in a complex permittivity change of the hydrogel, manifested by the impedance change of the affinity sensor. The resulting change in the frequency-dependent impedance was measured by the impedance analyzer at frequencies ranging from 1 kHz to 1 MHz; the time-transient impedance change at a specific frequency was measured by interfacing the affinity sensor with an impedance/voltage transformation circuit, described elsewhere[42]. Briefly, a 5-mV sinusoidal input from a function generator (33220A, Keysight Technologies, CA) at a constant frequency was imposed on the glucose microsensor. The complex impedance was converted to an AC voltage output via the impedance-voltage transformation circuit, whose amplitude and phase were both detected by a lock-in amplifier (SR830, Stanford Research Systems, CA) (Figure 3.3).

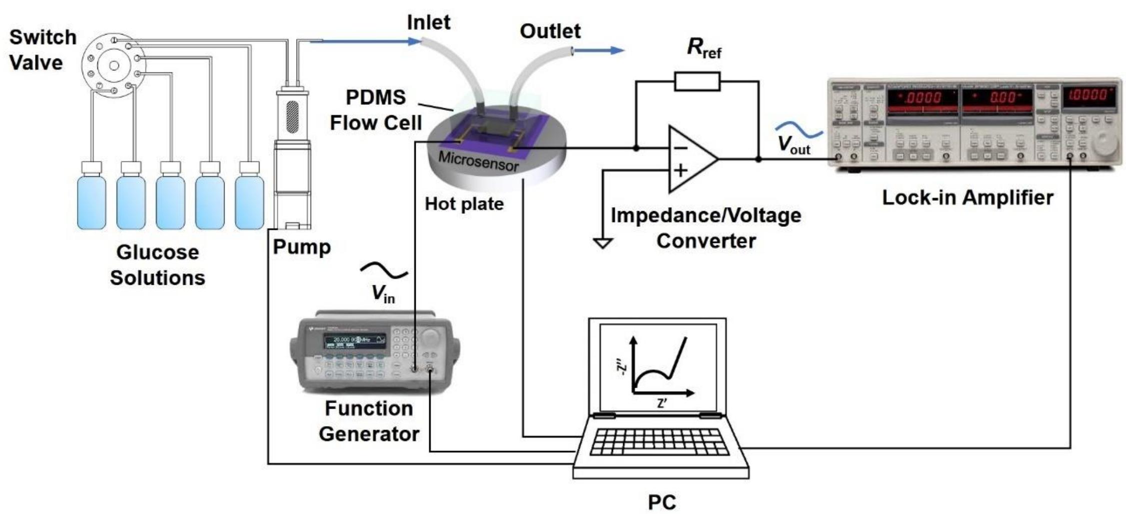

Figure 3.3: Experimental setup for characterization of the transient impedimetric response of the glucose affinity microsensor.

3.3 Results and Discussion

3.3.1 Swelling Behavior of Hydrogel Specimens

In the PBA-containing hydrogel, immobilized PBA moieties can reversibly bind with diols in glucose, forming either a 1:1 complex or a 2:1 cross-linking complex between PBA and glucose[116,117] (Figure 3.1b). When glucose concentration is below a critical level, the 2:1 cross-linking complex is preferentially formed[50,116], inducing additional cross-linking that causes contraction of the hydrogel matrix. As the glucose concentration increases, the 2:1 complex is converted to 1:1 complexes, reducing the cross-linking in hydrogel and increasing the amount of the free anionic 1:1 complex. The reduction in cross-linking density and increase in anionic charge contribute to swelling, i.e., the expansion in the hydrogel volume (Figure 3.1b).

To test such swelling behavior of hydrogels, we measured glucose-binding-induced changes in the mass of hydrogel specimens. These specimens had different content of crosslinker (TEGDA), as represented by the TEGDA-HEAA molar ratio, and different content of the glucose-binding monomer (AAPBA), as represented by the AAPBA-HEAA molar ratio. Here, the molar concentration of the base component HEAA was fixed at 0.96 mol/L for all hydrogels.

Three TEGDA-HEAA molar ratios were used: 1/2000, 1/1000, and 1/100, corresponding to an increasingly higher content of the TEGDA crosslinker. In addition, three AAPBA-HEAA molar ratios were used: 1/30, 1/10, and 1/5, corresponding to an increasingly higher content of the glucose-binding component AAPBA. The highest AAPBA-HEAA molar ratio tested was 1/5, because we found that values higher than 1/5 increased the hydrophobicity of the hydrogel and caused excessive phase separation inside the hydrogel. These hydrogels are named with a two-index scheme given by C*m*-G*n*, where the crosslinker index C*m* = C2000, C1000, or C100 corresponding to a 1/2000, 1/1000, or 1/100 TEGDA-HEAA molar ratio, respectively, and the glucose binding index G*n* = G30, G10 or G05 corresponding to a 1/30, 1/10 or 1/5 AAPBA-HEAA molar ratio, respectively. For example, C1000-G05 corresponds to a hydrogel with a 1/1000 TEGDA-HEAA molar ratio and a 1/5 AAPBA-HEAA molar ratio. In the discussions below, we also refer to hydrogels with the same TEGDA-HEAA molar ratio of 1/2000, 1/1000, or 1/100 but different AAPBA-HEAA molar ratios as “group C2000”, “group C1000” or “group C100” hydrogels, respectively.

The steady-state normalized mass changes of all hydrogels in response to glucose concentrations (0-360 mg/dL) in PBS buffer are summarized in Figure 3.4 and Table 1.

Table 1: Response of PAAPBA-*ran*-PHEAA hydrogels with different compositions to 0-360 mg/dL glucose concentrations in PBS buffer (pH 7.4).

Hydrogel		TEGDA-AAPBA-HEAA molar ratio	$\Delta m_{30}{}^{b}/m_0{}^{a}$ (%)	$\Delta m_{90}{}^{b}/m_0{}^{a}$ (%)	$\Delta m_{360}{}^{b}/m_0{}^{a}$ (%)
High crosslinker density	C100-G05	1/20/100	-5.1	-12.0	-13.7
	C100-G10	1/10/100	-2.8	-5.9	-9.5
	C100-G30	1/3.3/100	2.9	4.8	8.2
Medium crosslinker density	C1000-G05	0.1/20/100	-4.7	-12.7	-29.5
	C1000-G10	0.1/10/100	-1.2	-4	-11.4
	C1000-G30	0.1/3.3/100	2.6	7.1	12.2
Low crosslinker density	C2000-G05	0.05/20/100	-6.3	-14	-20.5
	C2000-G10	0.05/10/100	-1.9	-5.8	-10.4
	C2000-G30	0.05/3.3/100	4.2	9.9	16.5

[a]m_0 is the mass of the hydrogel in pH 7.4 PBS buffer at 37 °C in the absence of glucose. b $\Delta m_c = m_c - m_0$, where m_c is the mass of the hydrogel in pH 7.4 PBS buffer containing glucose concentration of *c* mg/dL.

The group C100 hydrogels (C100-G05, C100-G10, and C100-G30), which had an identically high TEGDA-HEAA molar ratio (1/100) but different AAPBA-HEAA molar ratios (1/5, 1/10, and 1/30), were characterized by measuring their glucose-binding-induced changes in mass (Figure 3.4a). As shown in Figure 3.4a, hydrogels C100-G05 and C100-G10 exhibited a decrease in mass in response to increasing glucose concentrations from 30 to 240 mg/dL. However, when the glucose concentrations exceeded 240 mg/dL, the mass of the hydrogel C100-G05 and C100-G10 began to increase. The non-monotonic changes in the mass of the hydrogel C100-G05 and C100-G10 over a range of glucose concentrations between 30 and 360 mg/dL indicated that the 2:1 complex between PBA and glucose formed below glucose concentrations of 240 mg/dL resulted in the contraction of the hydrogels. Glucose concentrations above 240 mg/dL resulted in the conversion of the 2:1 to 1:1 complexes between PBA and glucose formed in C100-G05 and C100-G10 hydrogels, leading to an expansion in hydrogel volume and thus increasing their mass (Figure 3.2b). Unlike hydrogels C100-G05 and C100-G10, hydrogel C100-G30 exhibited a monotonic increase in mass in response to glucose concentrations between 30-360 mg/dL (Figure 3.4a). We ascribe the glucose-binding-induced increase in mass to the expansion in hydrogel volume caused by the formation of the 1:1 PBA-glucose complex, increasing the negative charge presented in the hydrogel creating an osmotic force that caused swelling of the hydrogel[116].

The glucose-binding-induced mass changes of the group C1000 hydrogels (C1000-G05, C1000-G10, and C1000-G30), with an identically medium TEGDA-HEAA molar ratio (1/1000) but different AAPBA-HEAA molar ratios (1/5, 1/10, and 1/30), were tested next (Figure 3.4b). Unlike the non-monotonic mass changes of some of the group C100 hydrogels (C100-G05 and C100-G10), the masses of the hydrogel C1000-G05 and C1000-G10 specimens monotonically decreased in response to glucose concentration changes in the 30 to 360 mg/dL range. The extension of the monotonic range for glucose-induced mass change could be attributed to the facilitation of the 2:1 complex formation between glucose and PBA groups by using the TEGDA-HEAA molar ratio of 1/1000.

Moreover, we measured glucose-binding-induced mass changes of group C2000 hydrogels (C2000-05, C2000-G10, and C2000-G30) that had an identically low TEGDA-HEAA molar ratio (1/2000) but different AAPBA-HEAA molar ratios (1/5, 1/10, and 1/30) (Figure 3.4c). These hydrogels exhibited larger normalized changes in mass in response to a 240 mg/dL glucose concentration ($\Delta m_{240}/m_0$) compared to C100 hydrogels since highly cross-linked hydrogels have a tighter structure and can induce less volume change compared to loosely cross-linked hydrogels[118]. While hydrogels C100-G05, C100-G10, C2000-G05, and C2000-G10 exhibited a non-monotonic response to physiologically relevant glucose concentrations (0-360 mg/dL), hydrogels C1000-G05 and C1000-G10 showed monotonic changes in mass within this range of glucose concentrations. These results indicate that hydrogel with a TEGDA-HEAA molar ratio of 1/1000 showed optimum performance for glucose measurement.

Another factor that impacts the response of the hydrogel to glucose concentration is the molar ratio of AAPBA to HEAA. We compared the responses of hydrogels with different AAPBA-HEAA molar ratios (1/30, 1/10, and 1/5). All hydrogels with an AAPBA-HEAA molar ratio of 1/5 exhibited higher glucose-induced mass changes than hydrogels made with lower AAPBA-HEAA molar ratios (Figure 3.4). This suggests that among the AAPBA-HEAA molar ratios (1/30, 1/10, and 1/5) tested, the 1/5 ratio most effectively facilitated the formation of 1:2 binding between glucose and PBA groups; higher concentrations of PBA have more available glucose binding sites in the hydrogels. This is consistent with previously reported molar ratios (1/4[118] and 1/5[119]) of PBA-containing monomers to hydrophilic monomers that allowed for the highest glucose-induced responses of affinity holographic glucose sensors.

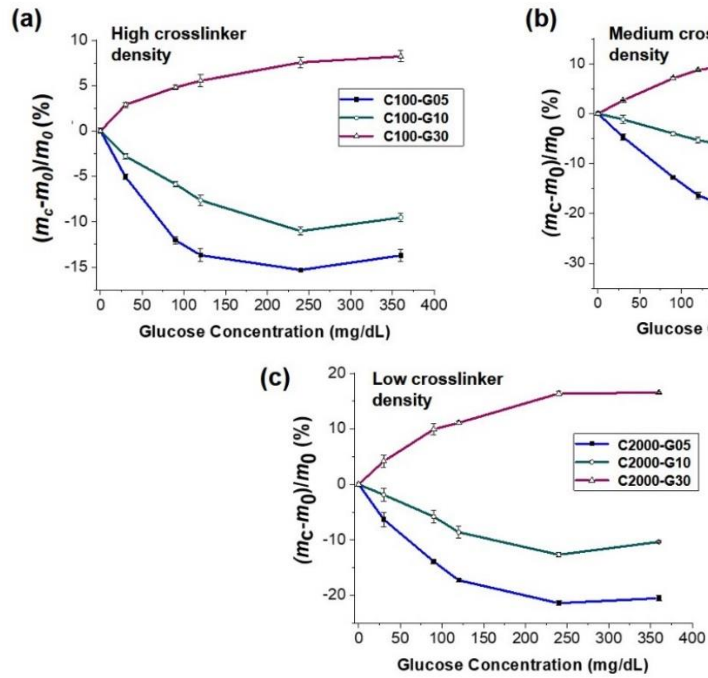

Figure 3.4: Characterization of mass changes induced by increasing glucose concentrations for PAAPBA-*ran*-PHEAA hydrogels with varying compositions: (a) Hydrogels with a fixed TEGDA-HEAA molar ratio of 1/100 (high crosslinker density), (b) Hydrogels with a fixed TEGDA-HEAA molar ratio of 1/1000 (medium crosslinker density), and (c) Hydrogels with a fixed TEGDA-HEAA molar ratio of 1/2000 (low crosslinker density).

3.3.2 Responses of Hydrogel-Integrated Microsensors

Microsensor devices were integrated with a thin layer of hydrogel (~ 5 μm) and tested for a glucose-induced impedimetric response. Hydrogels made with a TEGDA-HEAA molar ratio of 1/2000, due to their loosely cross-linked structure from low crosslinker density, did not reliably form a thin layer adhering to the sensor chip surface during testing. Therefore, no further characterization was performed on hydrogels with this molar ratio (i.e., the C2000 group). Similar to the mass-based tests (Section 3.3.1), the highest AAPBA-HEAA molar ratio used was 1/5, as higher AAPBA-HEAA mole ratios tended to render unacceptably high phase separation. Guided by mass-based testing results above, the hydrogel C1000-G05 appeared to offer the optimal tradeoff among the different hydrogel compositions. Thus, we first systematically tested microsensor devices modified with the hydrogel C1000-G05, and then devices modified with other hydrogel compositions to investigate the effects of TEGDA-HEAA and AAPBA-HEAA molar ratios. Specifically, we compared devices incorporating the hydrogel C100-G05 to those modified with C1000-G05 to investigate the effects of the TEGDA-HEAA molar ratio (i.e., crosslinker content). We compared devices incorporating the hydrogel C1000-G10 to those integrating C1000-G05 to investigate the effects of the AAPBA-HEAA molar ratio (i.e., the content of the glucose-binding component).

We characterized the response of the hydrogel-integrated devices to glucose concentration changes from 0 to 360 mg/dL, which covered physiologically relevant glucose concentrations (30-360 mg/dL). For the frequency-dependent impedance test, a frequency range of 1 kHz to 1 MHz was chosen since unwanted parasitic impedance induced by the electrical double layer became dominant at frequencies below 1 kHz[120] while the instrument (Biologic SP-200 impedance analyzer) only allowed measurements up to 1 MHz.

3.3.2.1 Frequency-Domain Device Responses

The frequency-dependent impedance of the microsensor integrated with hydrogel C1000-G05 to glucose concentrations ranging from 0-360 mg/dL was characterized and the results are shown in Figure 3.5 a,b. When the glucose concentration was fixed, both the effective capacitance and the effective resistance of the device decreased with increasing frequency over the entire frequency range tested (1 kHz–1 MHz). The magnitude of the dielectric coefficient depends on the ability of dipole units in the material to orient with the oscillations of an external alternating electric field (i.e., dielectric polarization). Several polarization mechanisms, such as dipole reorientation, counterion diffusion, and interfacial polarization, were expected to contribute to the measured sensor capacitance. The relaxation behavior from the rapid decrease with the frequency of measured capacitance could be mainly attributed to these relaxations. At sufficiently high frequencies (> ~ 100 kHz), the dipoles and induced dipoles in the hydrogel could not keep up with the alternating polarity of the electric field and the effective permittivity of the hydrogel and, hence, the effective capacitance of the device becomes diminishingly small. The drastic reduction of the effective resistance with increasing frequency, on the other hand, reflected the decrease in friction-induced energy dissipation at higher frequencies, as dipoles in the hydrogel increasingly decouple from the electric field and leave the ionic resistivity of the buffer as the sole contributor to the effective resistance[121].

When the frequency was fixed between 1 kHz and 1 MHz, the microsensor was observed to exhibit a monotonic decrease in the effective capacitance and a monotonic increase in the effective resistance in the tested glucose concentration range (0–360 mg/dL). This reflects PBA-glucose binding significantly influencing the dielectric polarization of the hydrogel, which may include changes in the hydrogel's structural conformations, permanent dipole moments, elastic resistance to the dipole rearrangement in the electric field, and electric double layer characteristics. Together these effects, which are complex and require elucidation through further in-depth studies, result in the dependence of the hydrogel's dielectric properties on glucose concentration. Also, the observed variation of the microsensor's effective capacitance and resistance depends on the glucose concentration.

We further compared the relative changes in the effective capacitance (ΔC) and the effective resistance (ΔR) of the microsensor integrated with hydrogel C1000-G05 at four frequencies (1, 3, 10, 30 kHz) (Figure 3.5 c,d**)**. ΔC, ΔR are denoted as $\Delta C = C - C_0$, and $\Delta R = R - R_0$, where C_0 and R_0 represent the effective capacitance and resistance of the device to buffer without glucose, respectively. We observed that the relative changes in the capacitance and effective resistance were most pronounced at 1 kHz, with the effective capacitance of the microsensor decreasing monotonically by 48 nF and the effective resistance increasing monotonically by 191 Ω as the glucose concentration increased from 0 to 360 mg/dL. PBA-glucose-binding most significantly altered the dielectric relaxation of the hydrogel at 1 kHz. The sensitivity of the microsensors incorporating the hydrogel C1000-G05 to the glucose in the concentration range of 0-240 mg/dL was 0.156 nF/(mg/dL) at 1 kHz. The capacitance measurement resolution of the system was approximately 3.9 pF, allowing a glucose measurements resolution of 25 μg/dL. Thus, 1 kHz was chosen as the operating frequency for the microsensor in the later fixed-frequency studies.

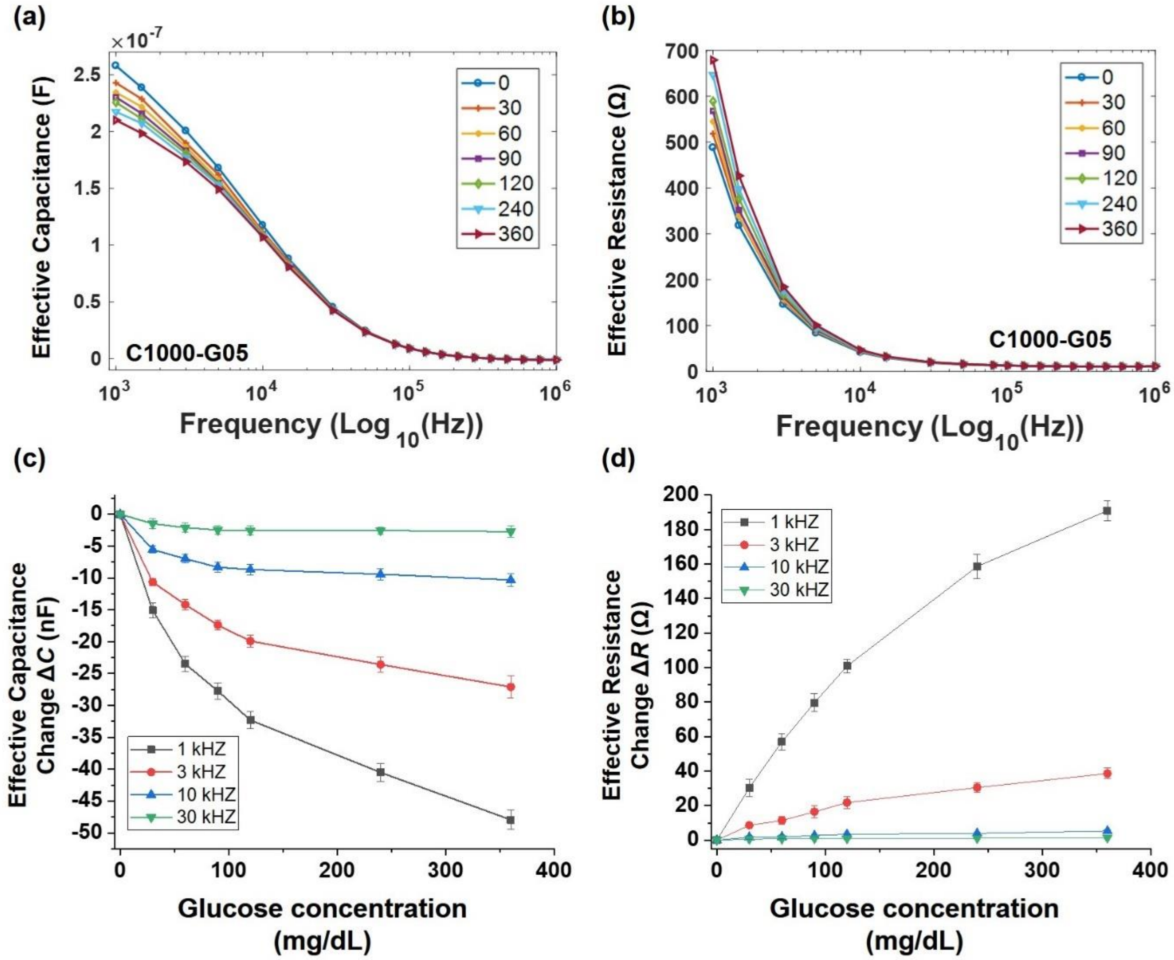

Figure 3.5: Glucose-binding-induced impedance change of the microsensor to physiologically relevant glucose concentrations. The frequency-dependent effective capacitance, and effective resistance of the affinity glucose microsensor integrated with hydrogel C1000-G05: (a) effective capacitance, and (b) effective resistance. Response of the C1000-G05-integrated microsensor as a function of glucose concentrations at fixed frequencies: (c) effective capacitance change (ΔC), and (d) effective resistance change (ΔR).

The glucose-binding-induced impedance change of the microsensor when integrated with the hydrogel C100-G05, which was synthesized with a high crosslinker density but the same AAPBA concentration as the C1000-G05 hydrogel, was characterized to study the effects of crosslinker on the microsensor’s glucose-induced response (Figure 3.6 a,b). Consistent with the mass-based testing results above, glucose-induced effective capacitance and resistance changes were both significantly smaller for the hydrogel C100-G05-based device when compared to the hydrogel C1000-G05-based device. Given that hydrogels C100-G05 and C1000-G05 share the same AAPBA-HEAA molar ratio (1/5), the weaker response of the hydrogel C100-G05-based device is attributed to its greater TEGDA- HEAA molar ratio, causing the hydrogel to be stiffer overall with more resistant changes to deformations generated by PBA-glucose binding.

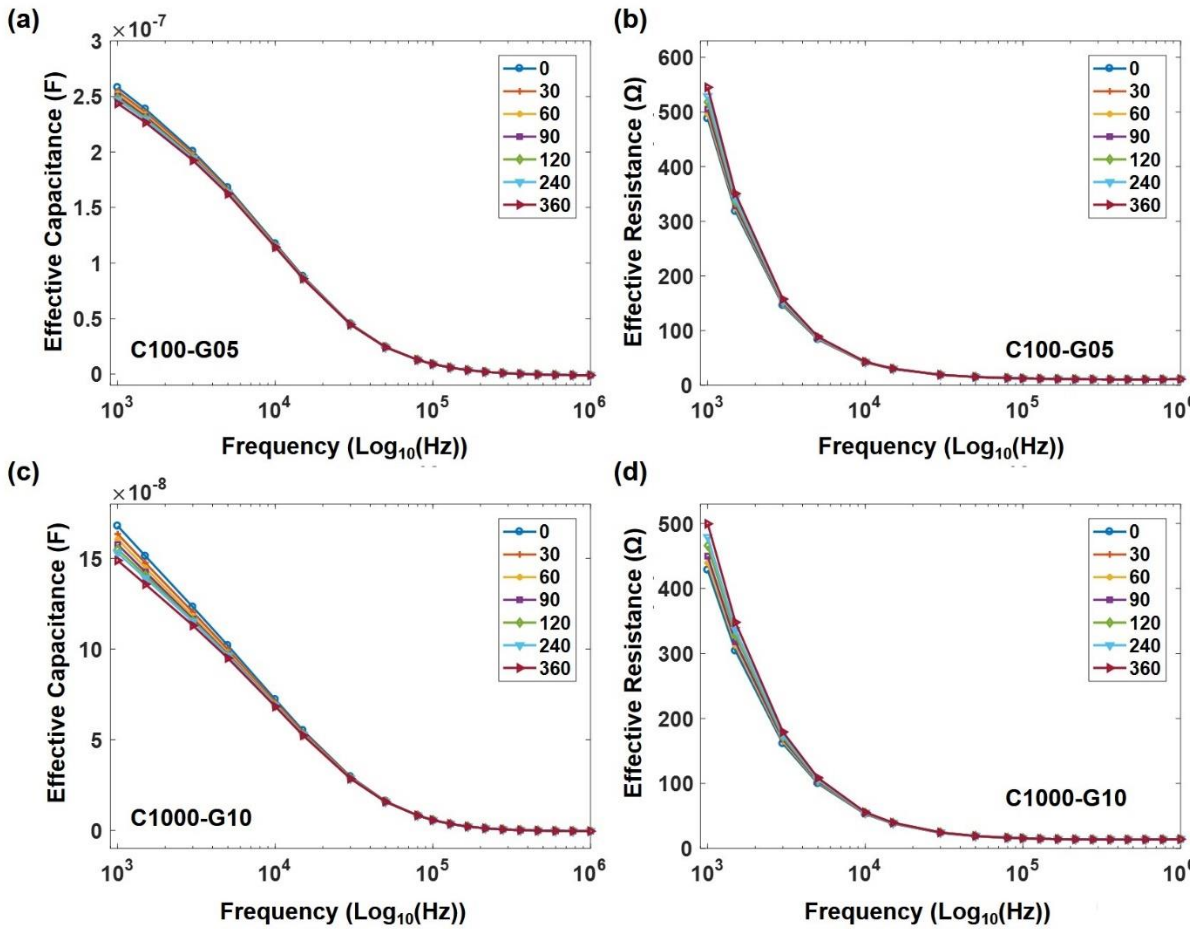

Figure 3.6: The steady-state frequency-dependent effective capacitance and effective resistance of the affinity glucose microsensor integrated with hydrogel C100-G05 and C1000-G10 at varying glucose concentrations. (a) Effective capacitance, and (b) effective resistance of the MEMS transducer functionalized with hydrogel C100-G05. (c) Effective capacitance, and (d) effective resistance of the transducer integrated with hydrogel C1000-G10.

The glucose-binding-induced impedance change of the microsensor when integrated with the hydrogel C1000-G10, synthesized with a lower concentration of glucose-responsive monomer (AAPBA) but the same crosslinker density as the C1000-G05 hydrogel, was characterized to study the effects of AAPBA concentration on the microsensor's glucose-induced response (Figure 3.6 c,d). Glucose-induced changes in the effective capacitance and resistance were also significantly smaller for the hydrogel C100-G10-based device than for the hydrogel C1000-G05-based device. For example, at a frequency of 1 kHz, the effective capacitance and resistance changes of the hydrogel C1000-G10-based microsensor were respectively only 50% and 42% of the changes generated by the hydrogel C1000-G05-based device. This is consistent with the mass-based test results above, reflecting that the AAPBA content of hydrogel C1000-G10 (AAPBA-HEAA molar ratio = 1/10) was only 50% of that of hydrogel C1000-G05 (AAPBA-HEAA molar ratio = 1/5). That is, having 50% fewer PBA groups available to interact with glucose molecules was responsible for the significantly weaker responses of the hydrogel C1000-G10-based device.

For the microsensor to operate reliably in the interstitial fluid, it is important to ensure the device's responses to potential interferents are small compared with those to glucose. In addition to glucose, boronic acid is known to bind other sugars through boronic acid–diol interactions[119]. The main potential interferents present in the blood include fructose, galactose, and lactate. The typical concentrations of these potential interferants are, respectively, below 0.14 mg/dL[122], 0.07 mg/dL[123] and 9 mg/dL[124]. We tested the response of the microsensor with the hydrogel C1000-G05-based microsensor to these potential interferants at 90mg/dL (at 1 kHz). The microsensor's responses to fructose at 0.14 mg/dL and galactose at 0.07 mg/dL were approximately 2.5% and 1.9% of that to glucose at 108 mg/dL[125]. The response of the microsensor to L-lactate at 9 mg/dL was 6.4% of that to glucose at 108 mg/dL. Thus, the microsensor was considered reasonably selective for measurements of glucose in interstitial fluid for CGM applications. To further reduce the response of the affinity glucose microsensor to the potential interferents, improved hydrogel designs could be used in future studies. For example, hydrogels that use 2-acrylamidophenylboronic acid (2-APBA) as a glucose-binding component are minimally responsive to lactate while highly sensitive to glucose[126], thus it could be used to drastically increase the selectivity of the microsensor for glucose relative to lactate.

3.3.2.2 Device Response to Time-Dependent Glucose Concentration Changes

Finally, we tested the microsensor (modified with hydrogel C1000-G05 measured at 1 kHz) in response to dynamically changing glucose concentrations to assess its potential use in monitoring glucose concentration changes in interstitial fluid. The measured capacitance consistently depended on glucose concentration, changing rapidly, regardless of the direction of glucose concentration change (Figure 3.7a). For example, when the glucose concentration was stepped from 0 to 30 mg/dL at 32s, the effective capacitance stabilized at 243.3 nF; when the glucose concentration was stepped from 90 to 30 mg/dl at time 340 s, the capacitance reached 242 nF, showing reversibility of 0.6%. Similarly, the reversibility was 1.2 and 0.8% for the measurement data at glucose concentrations of 90 and 120 mg/dL, respectively. The time response of the device, defined as the time required by the capacitance to reach 90% of the steady-state value [126], was less than < 30 s. The time response of the device when the glucose concentration changed from 120 to 240 mg/dL and from 240 mg/dL to 120 mg/dL was 20 s and 28 s, respectively (Figure 3.7b). These results indicated that our sensor had a fast response and possessed excellent reversibility in response to glucose concentration changes.

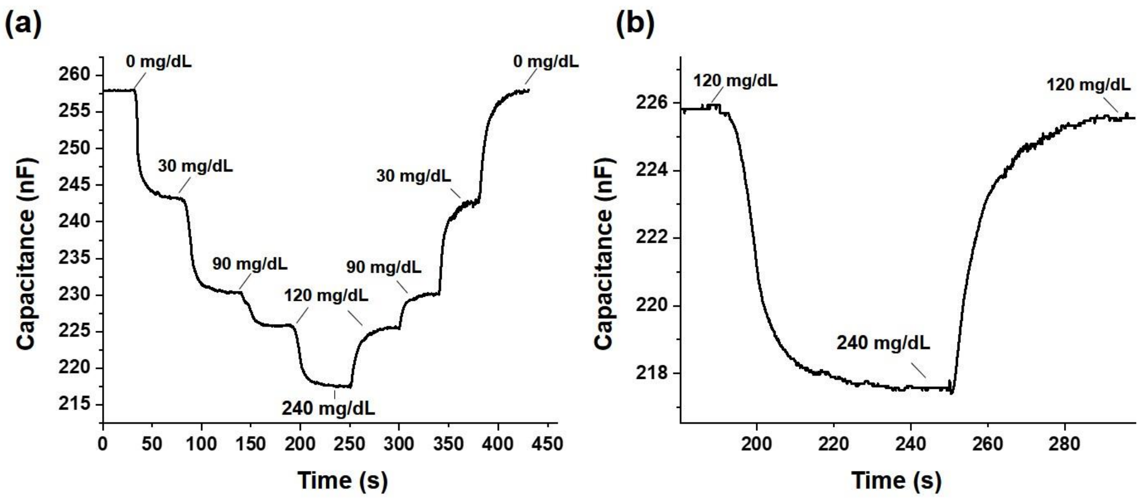

Figure 3.7: Time course of effective capacitance of the microsensor in response to: (a) an increasing sequence of glucose concentrations followed by a decreasing sequence of glucose concentrations, and (b) glucose concentration changes from 120 -240 mg/dL and then reversed back to a glucose concentration of 120 mg/dL. (Hydrogel: C1000-G05, frequency of bias voltage: 1 kHz.)

3.4 Summary

In this chapter, we investigated the effects of hydrogel composition of hydrogel-based affinity glucose microsensors. Each of the microsensors consists of a MEMS transducer in the form of a pair of coplanar electrodes, onto which poly(*N*-hydroxyethyl acrylamide-*ran*-3-acrylamidophenylboronic acid) (PHEAA-*ran*-PAAPBA), a glucose-sensitive hydrogel, is covalently attached. When glucose diffuses into the hydrogel and binds with the boronic acid moiety in AAPBA it induces dielectric property changes in the hydrogel and hence in the impedance between the electrodes, which can be measured to determine the glucose concentration. The coplanar-electrode MEMS transducer is amenable to *in situ* hydrogel preparation while offering ease of fabrication and improved robustness. With a uniform thin layer of hydrogel reliably immobilized onto the coplanar electrodes, the device can sensitively and rapidly respond to glucose concentration changes. By systematically investigating the effects of the hydrogel composition on glucose-induced changes in the hydrogel before and after its integration with the MEMS transducer, the optimal hydrogel composition is identified to allow the microsensor to sensitively and rapidly respond to changes in glucose concentration.

We investigated the hydrogel composition effects using both standalone hydrogel specimens and integrated microsensor devices incorporating the hydrogels. Hydrogel specimens with varying TEGDA-HEAA (i.e., crosslinker to hydrophilic monomer) and AAPBA-HEAA (i.e., glucose-sensitive monomer to hydrophilic monomer) molar ratios were tested, and the hydrogel C1000-G05 hydrogel, with a TEGDA-HEAA and AAPBA-HEAA molar ratios of 1/1000 and 1/5, respectively, showed the highest glucose-binding-induced mass changes. Integrated microsensor devices with ~5 μm thick hydrogels exhibited a repeatable and reversible response to a glucose concentration range of 0–360 mg/dL. Consistent with the mass-based testing results, the C1000-G05 hydrogel allowed reliable attachment to device surfaces, and the associated device was highly responsive to glucose concentration changes. As the glucose concentration was varied from 0 to 360 mg/dL, the effective capacitance measured at 1 kHz decreased from 258 nF to 210 nF and its effective resistance at 1 kHz increased from 488 Ω to 679 Ω. Additionally, the device exhibited a highly reversible response to time-varying glucose concentration changes with a response time of less than 30 s and a measurement resolution of 25 μg/dL. The C1000-G05 hydrogel composition was optimal for the microsensor, this can potentially offer reliable and accurate continuous measurement of glucose in subcutaneous fluid for continuous glucose monitoring applications.

Chapter 4: A Subcutaneously Implantable Hydrogel-Based Differential Microsensor for Continuous Glucose Monitoring

4.1 Introduction

In this chapter, we build on the results from the previous two chapters, and present a differential hydrogel-based microsensor, which has the capability to reject environmental disturbances (such as variations in the temperature and pH) that can compromise the reliability and accuracy of glucose concentration measurements. Our group has previously reported differential affinity microsensors that use a solution of the Poly(*N*-hydroxyethyl acrylamide-*ran*-3-acrylamidophenylboronic acid) (PHEAA-*ran*-PAAPBA) polymer[58,127]. However, solution-based sensors require the use of a semipermeable membrane, which leads to relatively slow time responses, and are also cumbersome and difficult to deploy subcutaneously. These limitations are addressed here with the hydrogel-based differential microsensor.

The microsensor consists of two dielectric measurements units. One of the units (sensing unit) is integrated with a thin layer of a (sensing) hydrogel that binds glucose, while the other (reference unit) is integrated with a thin layer of (reference) hydrogel that does not bind glucose. As glucose diffuses through the sensing hydrogel and binds to the PBA moieties therein, the dielectric properties of the sensing-hydrogel change due to glucose-PBA interaction, while those of the reference hydrogel only change as a result of contemporaneous non-glucose related signals. Measurement of the differences between signals from the two units permits an accurate determination of local glucose concentration by minimizing nonspecific disturbances. The covalent immobilization of a uniform thin layer of hydrogel onto the coplanar electrodes, confers excellent temporal stability and rapid response to glucose concentration changes as required in clinical CGM applications. This differential dielectric sensing mechanism can provide a general measurement method for implantable sensors to accurately quantify analytes in complex *in vivo* environments. *In vitro* and *in vivo* testing demonstrates that the sensor can accurately measure glucose concentrations ranging from 30 to 360 mg/dL reversibly and rapidly (with a time constant < 21 s) with a sensitivity of 7.5 pF/(mg/dL), resolution of 0.1 mg/dL and drift of 0.13%/h.

4.2 Methods

4.2.1 Differential Microsensor Design and Fabrication

4.2.1.1 Microsensor Design

Details of the hydrogel design and synthesis have been described elsewhere[128]. Briefly, the glucose-sensing unit uses a synthetic Poly(*N*-hydroxyethylacrylamide-*ran*-3-acrylamidophenylboronic acid) (PHEAA-*ran*-PAAPBA) hydrogel, which consists of *N*-3-acrylamidophenylboronic acid (AAPBA) as the glucose-sensing component, acryl *N*-hydroxyethyl acrylamide (HEAA), as the hydrophilic component, tetraethyleneglycol diacrylate (TEGDA) as the cross-linker and 2,2'-azobis(2-methylpropionamidine) dihydrochloride (AAPH) as the polymerization initiator (Figure 4.1c). Phenylboronic acid (PBA) in the PAAPBA segments can bind reversibly to glucose to form a cyclic boronic ester (Figure 4.1d) that shrinks the hydrogel volume, concurrently inducing a change in its dielectric properties, this change can be measured to determine the glucose concentration. The reference hydrogel, Poly(*N*-hydroxyethylacrylamide) (PHEAA) hydrogel, containing no AAPBA monomer, does not bind to glucose and has glucose-independent dielectric properties[128].

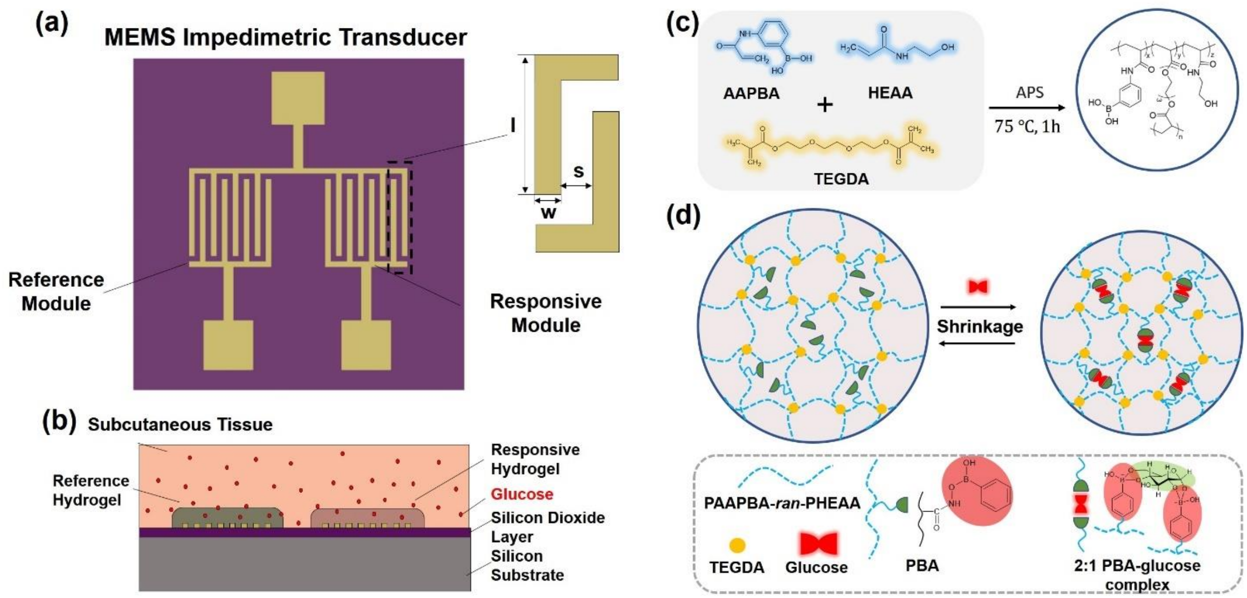

Figure 4.1: Design and principle of the hydrogel-based microsensor: (a) overall schematic, and (b) side view. (c) Components for *in situ* synthesis of the PHEAA-*ran*-PAAPBA hydrogel on gold thin film electrodes: HEAA and AAPBA are monomers and TEGDA is the crosslinker. (d) Binding between phenylboronic acid and glucose.

The MEMS differential dielectric glucose microsensor contains two hydrogel-measurement units that are placed in close proximity (Figure 4.1a). Each measurement unit consists of a coplanar impedimetric transducer that is integrated with a thin layer of hydrogel. The coplanar impedimetric transducer contains a pair of interdigitated electrodes, whose geometries are based on three designs. Each design contains a varying total number (n) of 2-mm long (l) fingers with width (w) and spacing (s) ranging from 10 to 100 µm. One measurement unit (sensing unit) is integrated with a thin layer of glucose-affinity hydrogel (PHEAA-*ran*-PAAPBA hydrogel), while the other measurement unit (reference unit) is integrated with a thin layer of glucose-insensitive hydrogel (PHEAA hydrogel) (Figure 4.1b). A microfluidics-aided approach was used to isolate the integration process for the responsive and reference hydrogels while controlling their thickness and pattern, thereby enabling uniform thin layers of responsive and reference hydrogel integrated with the sensing and reference unit. This method is the key to the construction of a differential microsensor and allows the rapid diffusive exchange of glucose into the hydrogel. As glucose binds to the hydrogel, the dielectric properties (e.g., complex permittivity) of the sensing hydrogel, while those of the reference hydrogel are glucose-independent and only change with environmental disturbances. Therefore, the measurement of the difference between the dielectric properties of sensing and reference hydrogels, defined as differential dielectric properties, can potentially filter the effects of environmental disturbances, compared to a sole measurement of the dielectric property of the sensing hydrogel. Thus, the measurement of the difference between the impedance of the sensing and reference units can potentially allow accurate determination of the glucose concentrations with alleviated environmental disturbances.

The complex permittivity (ε^*) of the hydrogel is represented by $\varepsilon^* = \varepsilon' - j\varepsilon''$, where the real part ε' characterizes the ability of the material to store electric energy, and the imaginary part ε'' accounts for the dissipation of electromagnetic energy[129]. An equivalent circuit model containing a resistor and a capacitor connected in parallel is used to calculate the equivalent resistance and equivalent capacitance of the glucose sensor. While either effective capacitance or resistance can be used as the sensor output, we choose to focus on the effective capacitance as wireless implanted sensor implementation of this measurement was simpler[95]. Denoted C_x, the effective capacitance is reflected by the real part of the complex permittivity by

$$C_x = \frac{\varepsilon'}{K_{\text{cell}}} \tag{2}$$

where K_{cell} is the cell constant of the coplanar electrode transducer, which is dependent on the configuration of the electrodes[130].

4.2.1.2 Microsensor Fabrication and Surface Functionalization

The MEMS transducer was fabricated using standard photolithography described in detail elsewhere[45]. Briefly, a thin layer of metal (Ti/Au 10/100 nm) was deposited by E-Beam evaporation on a silicon wafer coated with a 300-nm thermally grown insulating silicon dioxide layer and patterned using a lift-off process to form coplanar electrodes (Figure 4.2b).

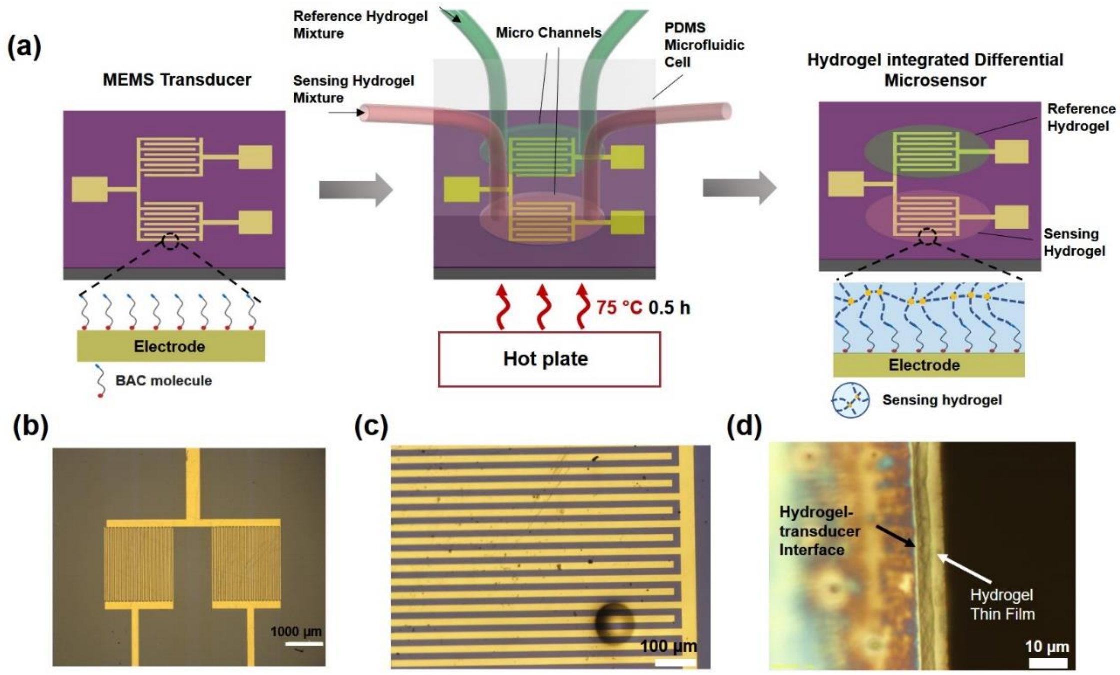

Figure 4.2: Fabrication of the differential glucose microsensor. (a) *In situ* integration of the hydrogel onto the surface of a mems transducer. (b) Microscopic photo of a MEMS transducer. (c) Microscopic photo of a MEMS transducer with a uniform thin layer of hydrogel. (d) Characterization of the hydrogel thin film thickness using a microscope

To allow covalent attachment of hydrogel layers, the surface of the transducer was chemically modified with an *N*,*N*'-bis(acryloyl)cystamine (BAC) self-assembled monolayer (SAM) following the procedures detailed elsewhere[131] to endow the surface with acryloyl groups, which can be copolymerized with hydrogel to form covalent bonds. Responsive and reference hydrogels were integrated *in situ* with the differential MEMS transducer following the procedures below. First, a mixture containing the components for each hydrogel was prepared following the recipe detailed in the material section (section 4.2.2). Reference mixture was injected (10 µl) into a polydimethylsiloxane (PDMS) flow cell clamped to the transducer, consisting of a 10-µm tall elliptic microfluidic channel, used as a mold for patterning the hydrogel thin films (Figure 4.2a) for reference hydrogel integration. The adjacent microfluidic channel was injected with a 10 µl mixture of the responsive hydrogel for integration of the sensing hydrogel. The transducer-microfluidics assembly was then heated in an oven set to 75 °C for 0.5 h to form the hydrogel and covalently link the hydrogel to the electrode surface through *in situ* free-radical copolymerization (Figure 4.2c). The film thickness was ~ 5 µm when fully hydrated (Figure 4.2d), allowing rapid diffusion of glucose into the hydrogel.

4.2.2 Materials

Chemicals and reagents used in the experiments include PHEAA-*ran*-PAAPBA (glucose-responsive) and PHEAA (reference) hydrogel, which are synthesized using previously described methods[45,128]. A mixture for the responsive hydrogel is prepared by dissolving AAPBA (0.06 mM), HEAA (0.3 mM), TEGDA (0.003 mM), and AAPH (0.03 mM) in 1 mL water/DMSO solution (v: v, 1:1) (AAPBA-TEGDA-AAPH-HEAA molar ratio: 20:0.1:1:100). A mixture for reference hydrogel contains 0.3 mM HEAA, 0.003 mM TEGDA and 0.05 mM AAPH dissolved in 1 mL water (TEGDA-AAPH-HEAA molar ratio: 0.1:1:100). Previously, we have empirically found that this formulation gave an optimal glucose response[131] and we have used this formulation for all syntheses of the responsive hydrogels. Phosphate-buffered saline solution (PBS, pH 7.4, ionic strength 0.15 M) and D-(+)-glucose were purchased from Thermo Fisher Scientific (Waltham, MA). *N*,*N*'-bis(acryloyl)cystamine (BAC) were purchased from Sigma-

Aldrich (St. Louis, MO). All chemicals were used as received. Stock solutions (1800 mg/dL) of glucose were prepared by dissolving glucose powder (0.9 g) into 50 mL PBS buffer. Glucose solutions at varying concentrations (30, 60, 90, 120, 240, and 360 mg/dL) were prepared by diluting the stock solution with the appropriate volume of PBS buffer (0.15 M).

4.2.3 Testing Instrumentation and Procedures

Two experimental configurations were used to characterize the sensors. One of the configurations uses an impedance analyzer (SP-200, Biologic) that allows frequency-dependent impedance measurement at a frequency range of 1 kHz to 1 MHz; the other makes time-dependent impedance measurements using a lock-in amplifier (SR830, Stanford Research) with a fixed frequency sinusoidal excitation signal. To measure the glucose-induced time-resolved impedance of a single-sensing unit, we used an impedance/voltage converter (described elsewhere with details)[128]. Time-dependent differential capacitance was measured by interfacing the differential device with a custom-built circuit (Figure 4.3).

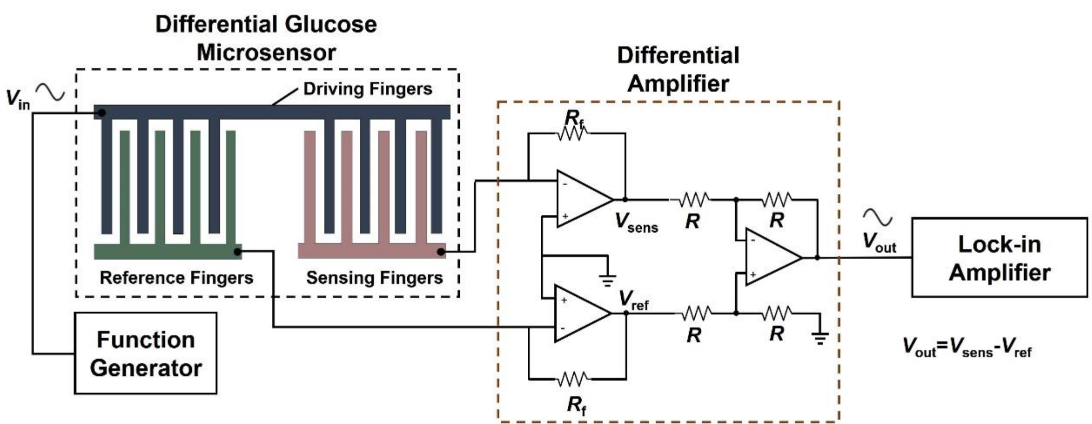

Figure 4.3: Readout circuitry for the hydrogel-based glucose microsensor.

Preliminary *in vivo* testing of the device was conducted at the Columbia University Medical Center using 10-week-old C57BL/6J laboratory mice with a protocol approved by the

Columbia University Institutional Animal Care and Use Committee. The sensor was subcutaneously implanted in the interscapular region of a mouse sedated and stabilized with isoflurane inhalation for 30 minutes before the start of continuous glucose measurements. An excitation voltage of 10 mV AC was imposed on the driving fingers and the two signal output ports, i.e., sensing and reference fingers, were interfaced to a differential amplifier circuit (Figure 4.3). The voltage output was detected with a lock-in amplifier and continuously recorded using the LabVIEW program. Reference blood glucose concentrations were measured with an AlphaTrack2 glucose meter every 10 minutes from the tail vein.

4.3 Results and Discussion

Results presented are 1) testing single sensing units with varying geometries. 2) characterization of the differential microsensor's ability to reject disturbances and reliably measure time-dependent changes in glucose concentration. 3) *in vivo* application of the differential microsensor in laboratory mice.

4.3.1 Characterization of Single Sensing Units

We investigated three MEMS transducer designs, which are referred to as Designs 1, 2, and 3 below (Table 2). Designs 1, 2, and 3-based transducers were fabricated and integrated with a thin sensing hydrogel layer to form single sensing units. The frequency-dependent capacitance of the microsensors was characterized using an impedance analyzer.

Table 2: Geometric parameters of transducer Designs 1, 2, and 3.

Transducer	l (μm)	w (μm)	n
Design 1	1997 ± 4	9.4 ± 0.7	98
Design 2	2001 ± 3	48.5 ± 1.5	20
Design 3	2002 ± 4	97.4 ± 2.5	10

Design 1-based transducers were integrated with a thin film of the responsive hydrogel and reference hydrogel to form a sensing unit and reference unit, respectively. Glucose concentrations were varied from 30 to 360 mg/dl and frequency-dependent effective capacitance changes were measured (Figure 4.4). Error bars reflect standard errors from triplicates of measurements. As shown in Figure 4.4 a,b, the effective capacitance of both Design 1-based sensing and reference units decreased with increasing frequency over the entire frequency range tested (1 kHz–1 MHz) at a fixed glucose concentration. According to Eq. (2), the decrease in the effective capacitance reflected a decrease in the permittivity of the hydrogel, which is associated with the ability of dipole units in the hydrogel to orient with the oscillations of an external alternating electric field (i.e., dielectric polarization). The decrease in the effective capacitance at low frequencies could be due to several dielectric relaxation mechanisms, such as electrode polarization and Maxwell-Wagner-Sillars polarization[114]. At frequencies above 100 kHz, the dipoles and induced dipoles in the hydrogel did not respond to the alternating electric field, resulting in a decrease in the effective permittivity of the hydrogel manifesting as diminished effective capacitance.

The effective capacitance of the Design 1-based sensing unit monotonically decreased over the glucose concentration range tested (30–360 mg/dL) at frequencies ranging between 1 kHz and 1 MHz. This reflects that PBA-glucose binding significantly influenced the dielectric polarization of the hydrogel, which may include changes in the hydrogel's structural conformations, permanent dipole moments, elastic resistance to the dipole rearrangement in the electric field, and electric double layer characteristics. These synergetic effects result in the glucose-dependent effective capacitance of the sensing unit, which requires further detailed study for elucidation of the sensing mechanism.

The Design 1-based reference unit exhibited negligible changes in effective capacitance in response to glucose concentration changes as expected, confirming that the changes in effective capacitance of the sensing unit were caused by binding between PBA groups and glucose.

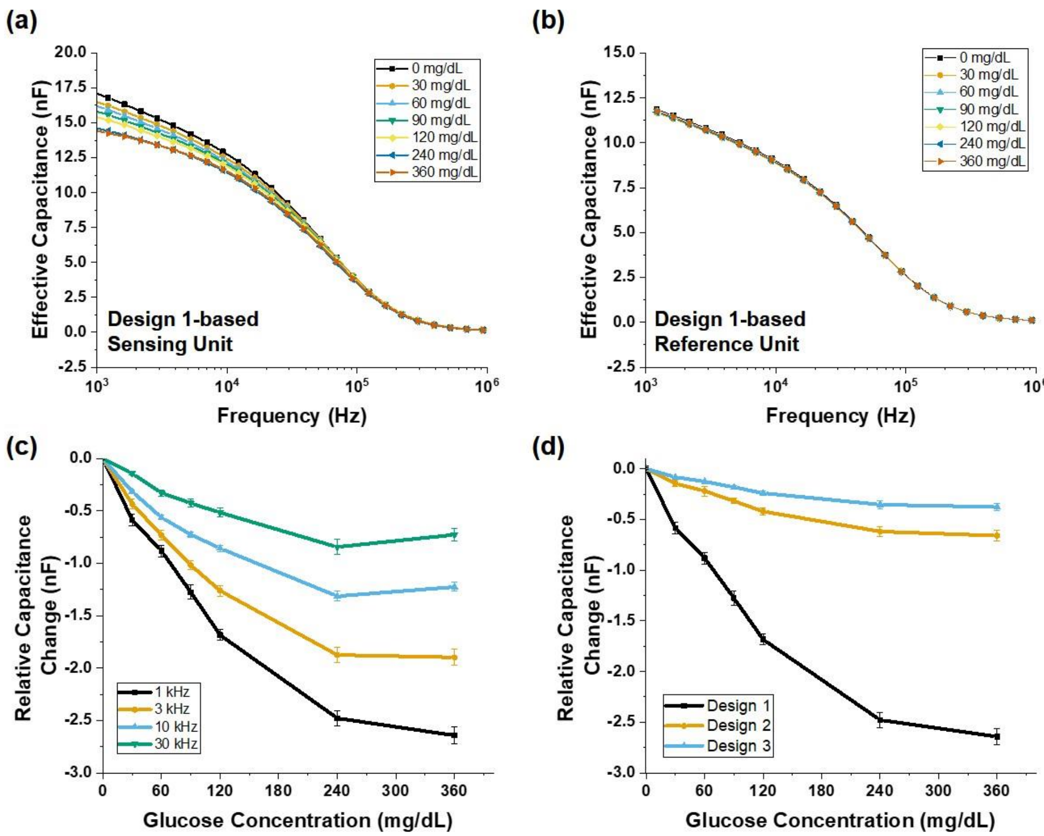

Figure 4.4: Glucose-binding-induced effective capacitance change of microsensors. Frequency-dependent response of Design 1-based (a) sensing unit, and (b) reference unit. (c) Response of the Design 1-based sensing unit as a function of glucose concentration at fixed frequencies (1, 3, 10, 30 kHz). (d) Glucose-induced relative changes in effective capacitance at 1 kHz of Design 1, 2, and 3-based sensing units in response to glucose concentrations.

The relative changes in the effective capacitance of the Design 1-based sensing unit with respect to the effective capacitance at zero glucose concentration were most pronounced at 1 kHz with effective capacitance decreasing monotonically by 2.6 nF as the glucose concentration varied from 30 to 360 mg/dL (Figure 4.4c). The sensitivity of the device to glucose diminished at sufficiently high frequencies (>~ 100 kHz), reflecting that PBA-glucose-binding most significantly altered the dielectric relaxation of the hydrogel at 1 kHz, the optimum operating frequency in use for subsequent fixed-frequency studies (section 4.3.2 and 4.3.3).

We then performed characterization of the glucose-binding-induced changes in frequency-dependent effective capacitances of Designs 1 and 2-based sensing units. The glucose-induced relative changes in the effective capacitance of all three sensing units at the optimum working frequency (1 kHz) were plotted against glucose concentrations, as shown in Figure 4.4d. The effective capacitance of the Design 1-based sensing unit showed the highest change (-2.6 nF) with glucose concentrations increasing from 30 mg/dL to 360 mg/dL, which is 4 times and 7 times the effective capacitance changes produced by Designs 2 and 3-based sensing units, respectively. Hence, Design 1 was adopted to form a differential microsensor for sensitive measurement of glucose in the physiologically relevant glucose concentration range (30-360 mg/dL).

4.3.2 Reduction of Drift by Differential Sensing

When implanted in subcutaneous tissue, the dynamically changing pH, body temperature, and ion concentrations of the interstitial fluid (ISF) could affect the effective capacitance of the single sensing unit and interfere with the sensor signal compromising the *in vivo* accuracy of the glucose sensor. The stability of the differential microsensor’s signal was evaluated by monitoring signal change over an extended period in buffer with glucose concentration fixed at 90 mg/dL and the sensor temperature freely fluctuating under room temperature. The capacitance of a Design 1-based single sensing unit was simultaneously recorded under the same condition for comparison. Over a measurement period of 3 hours, the differential capacitance of the sensor averaged 1.3 nF with a significantly reduced drift level of 0.13%h^{-1}, compared with 1.28%h^{-1} drift of the single sensing unit. The results indicate that the differential microsensor provided effective compensation for environmental variations with excellent stability. The relatively larger drift of the single sensing unit might be caused by changing pH, concentration of ions in solution, and DC voltage drift in the impedance-voltage converter circuit[132,133]. A potential future refinement for the differential microsensor is to alter the interfacing circuits to include an automated drift-compensating system to minimize the residual drift[133].

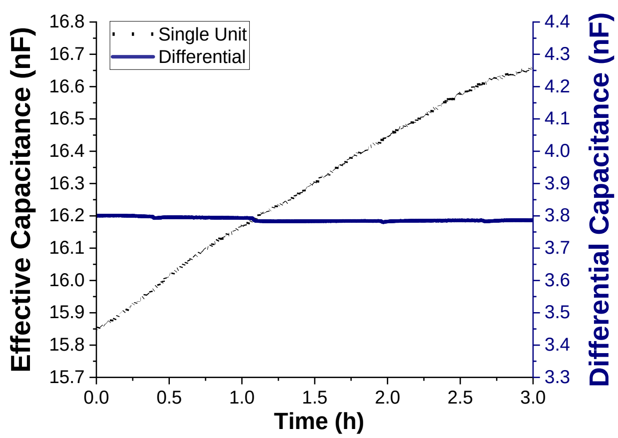

Figure 4.5: Reduction of drift by differential measurements. Capacitance changes of a single-unit device over 3 hours and differential capacitance changes of a differential device over 3 hours.

4.3.3 Time-Dependent Response of the Differential Microsensor

We tested the differential microsensor based on Design 1 in response to time-dependent glucose concentration changes to assess its potential use to track glucose concentration changes in interstitial fluid. A typical microsensor response measured at 1 kHz is shown in Figure 4.6a, in which equilibrium glucose concentration in the test cell was cycled between 60 mg/dL and 90 mg/dL. The effective capacitance at 60 mg/dL over the three time periods (from 0 to 1 min, from

3 to 4.3 min, and 6.2 to 6.9 min) was respectively 4.18 nF, 4.2 nF, and 4.22 nF, agreeing within 0.5%. Similarly, the reversibility was within 0.6% for the measurement data at glucose concentrations of 90 mg/dL. These findings indicate that the microsensor possesses excellent reversibility in response to glucose concentration changes as glucose molecules reversibly bind with the boronic acid moieties in the hydrogel.

The sensor response to varying glucose concentrations in a physiologically relevant range was next investigated. As the glucose concentration changed from 0 to 360 mg/dL, the differential capacitance of the sensor decreased steadily from 5.1 to 2.4 nF, indicating a decrease in the permittivity due to glucose binding with responsive hydrogel (Figure 4.6b). The sensitivity of the sensor was approximately 7.5 pF/(mg/dL) with a noise level of 1 pF, constituting a glucose measurement resolution of 0.1 mg/dL. The time constant of the device, defined as the time required by the capacitance to reach 63% of the 6.2 to 6.9 min steady value, was less than < 21 s. For example, the response time of the device for glucose concentrations from 0 to 30 mg/dL and 120 mg/dL to 180 mg/dL was 20.9 s and 10.5 s, respectively. These results indicated that our sensor displayed rapid response to changes in glucose concentration in the physiological range.

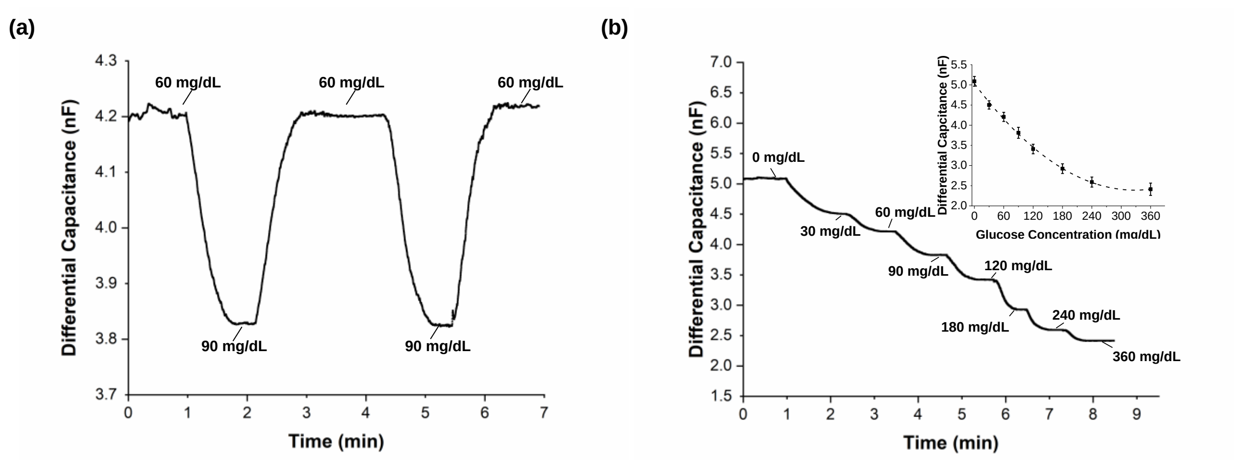

Figure 4.6: Differential capacitance of the microsensor in response to dynamically changing glucose concentrations. (Frequency of bias voltage: 1 kHz.) (a) Time course of the differential capacitance at 1 kHz exposed to glucose concentrations cycled between 60 mg/dL and 90 mg/dL.

(b) Real-time differential capacitance of the device underwent increasing glucose concentration changes from 0–360 mg/dL.

4.3.4 *In vivo* Testing

The differential glucose microsensor was implanted in the interscapular subcutaneous tissue of 10-week-old sedated mice and continuously measured glucose concentrations in the mouse ISF (Figure 4.7a). A commercial glucose meter (AlphaTrack2 glucose meter) measured capillary blood reference glucose concentrations sampled from the mouse's tail at 10-minute intervals.

The initial capillary blood glucose concentration of the mouse (fasted overnight) was 94 mg/dL. Throughout the experiment, the mouse was anesthetized with isoflurane to allow for implantation of the glucose microsensor and continuous glucose measurement. As previously reported, induction of anesthesia with isoflurane induces mild hyperglycemia[134], therefore, the capillary blood glucose concentration increased from 94 mg/dL at baseline to ~200-250 mg/dL after sedating with isoflurane. Following 30 min of microsensor equilibration, glucose was continuously measured for 1.5h followed by intraperitoneal (i.p.) insulin (1.5 units per gram of body weight) administration. Blood glucose declined gradually to 133 mg/dL in about one hour. At this point, another dose of 1.5 U/g insulin was injected i.p. and blood glucose further decreased to 60 mg/dL in ~30 min. When the mouse's capillary glucose concentration declined below 60 mg/dL, i.p. glucose (4 µg per g of body weight) was injected, raising the glucose concentrations to >700 mg/dL in 20 minutes after which the 4-hour experiment was stopped. The recorded output signal from the differential microsensor (Figure 4.7b) followed the trend of the changes of the reference blood glucose concentrations over the entire experiment. From 0 to 140 minutes, the signal of the sensor continuously dropped from 0.54 mV to 0.25 mV, following closely the trend of the decrease of the glucose concentration caused by insulin administration. Rapid response and a wide measurement range of the differential microsensor were demonstrated by the prompt increase of the signal in response to a rapid increase of capillary glucose concentration from 100 mg/dL to 700 mg/dL between 130-160 minutes. Overall, the device response lagged the reference blood glucose concentration change by approximately 10 minutes. Since the time response of the microsensor was < 20 s, this observed time lag can be attributed to the physiological delay of ISF glucose concentration in relation to that in blood, previously reported to range from 5 to 15 minutes[135].

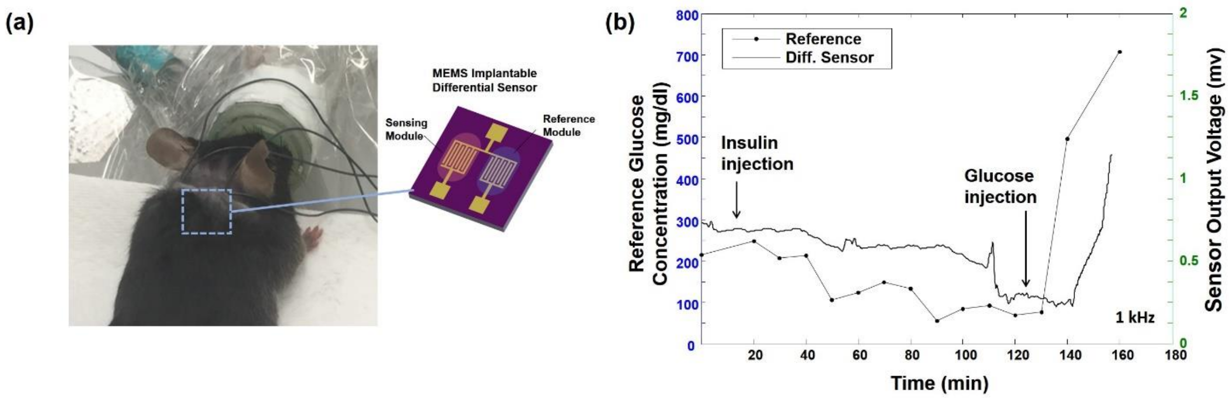

Figure 4.7: *In vivo* testing of the microsensor. (a) Photograph of a sedated mouse with isoflurane via an inhalational anesthetic delivery system. The MEMS differential microsensor was implanted in its back, in the interscapular region. (b) Time-dependent response of the MEMS device compared with blood glucose concentration sampled using a commercial glucose meter.

4.4 Summary

We have presented a hydrogel-based differential dielectric affinity microsensor that allows accurate, rapid, and stable measurement of glucose concentrations. The differential microsensor consists of two measurement units placed in close proximity. The sensing unit contains a coplanar impedimetric transducer functionalized via covalent attachment with a thin layer of PHEAA-*ran*-PAAPBA hydrogel that recognizes glucose by affinity binding. The reference unit is covalently immobilized with a thin layer of glucose insensitive hydrogel (PHEAA hydrogel). Measurement of the differences between signals from the two units allows accurate determination of glucose concentration while minimizing nonspecific excursions. Device geometries were systematically investigated to achieve optimal sensitivity and accuracy. Reliable integration of thin hydrogel layers (~ 5 μm) with the transducer by *in situ* polymerization in a microfluidic channel resulted in a rapid and repeatable response of the differential microsensor. *In vitro* characterization of the differential microsensor demonstrated that the differential capacitance of the device decreased consistently with glucose concentration from 30 to 360 mg/dL with a sensitivity of 7.5 pF/(mg/dL) and a resolution of 0.1 mg/dL. The time constant of the device was less than 21 s, reflecting a rapid response that is highly desirable for CGM. The differential microsensor also showed significantly reduced drift (e.g., 0.13%/h at 90 mg/dL glucose concentration) compared with a non-differential microsensor (1.28%/h). In preliminary *in vivo* testing of the device implanted in a laboratory mouse, the differential microsensor was able to accurately track the trend of capillary blood glucose concentrations. These *in vitro* and *in vivo* experimental results demonstrate that the differential microsensor can potentially enable rapid, accurate, reliable, and stable measurements of glucose concentrations in subcutaneous tissue in CGM applications.

Chapter 5: A Graphene-Based Affinity Glucose Nanosensor: Preliminary Investigation

5.1 Introduction

The hydrogel-based microsensors presented in the preceding chapters are intended to be subcutaneously implanted. While these minimally invasive CGM sensors are capable of monitor glucose concentrations in interstitial fluid (ISF), the procedures for implanting, operating, and replacing such devices are associated with discomfort and inconvenience, and are also significantly susceptible to biofouling effects[19,136]. In contrast, non-invasive glucose in other physiological fluids such as saliva, sweat, and urine, offer painless, less intrusive alternatives to implantation-based continuous monitoring of glucose[137–139]. In particular, tears are highly appealing media for continuous glucose monitoring as they are easily accessible, appropriately reflect blood glucose concentration[140–142], and offer relative insensitivity to interference from activities such as food intake and exercise.

There have been attempts to integrate enzyme-based glucose sensors with a contact lens to monitor the glucose concentration in tears wirelessly[141,143], although they are susceptible to interference of electroactive compounds and are associated with accuracy issues from the irreversible, consumptive nature of the underlying electrochemical reactions. Equilibrium-binding-based affinity detection method using boronic acid can be an alternative approach for CGM applications. In previous chapters, we have presented boronic acid-containing hydrogel-based CGM sensors to monitor glucose concentrations in ISF[45,128,131]. While sensitive to glucose concentrations ranging from 30 to 360 mg/dL, the sensitivity and the resolution of the sensors are not adequate to accurately determine the significantly lower glucose concentrations in tears (as low as 0.5 mg/dL)[140,142]. Thus, new boronic acid-based sensing materials that can recognize the glucose in the submillimolar range with improved resolution and low limit of detection are highly demanded by non-invasive CGM applications.

To address the limitations, affinity sensors using nanomaterial-based transduction are highly attractive because they offer the potential for improved sensitivity and scalability over conventional silicon-based materials[99–102]. Graphene, a monoatomic layer of carbon atoms distributed in honeycomb lattices[103], possesses extraordinary material properties including high surface-to-volume ratio, excellent electronic properties, and optical transparency, which are attractive in constructing field-effect transistor (FET) sensors. Aromatic boronic acid derivatives can adsorb on the surface of the graphene-based FETs through noncovalent π-π stacking to enable specific measurement of glucose.

This chapter describes a preliminary development of graphene-based affinity nanosensors for the measurement of glucose at lower concentrations. We first study the mechanisms of glucose sensing using nanosensors modified with aromatic boronic acid groups via pH-based measurements, and then apply the GFET nanosensors to perform a preliminary demonstration of affinity-based measurements of glucose.

5.2 Methods

5.2.1 Nanosensor Design

The studies in this chapter were based on a nanosensor configured as an electrolyte-gated GFET. The GFET includes three electrodes (Figure 5.1). The source electrode and drain electrode are situated on a silicon/silicon dioxide substrate and graphene is bridged between the two electrodes serving as a conducting channel. A silver/silver chloride (Ag/AgCl) probe was inserted into the electrolyte to serve as the gate electrode. When functionalized with a biorecognition element, such as aptamers or antibodies, GFET nanosensors for specific detection of the target can be formed. The signal transduction of the binding activity to a detectable electrical signal using a GFET biosensor relies on the extreme sensitivity of graphene's electrical property to the change in the charge distribution on its surface. In an affinity glucose nanosensor, glucose binds with the aromatic boronic acids adsorbed on the graphene surface to form a glucose–boronated ester complex, altering the Fermi level and conductivity of the graphene, which are measured to determine the glucose concentration.

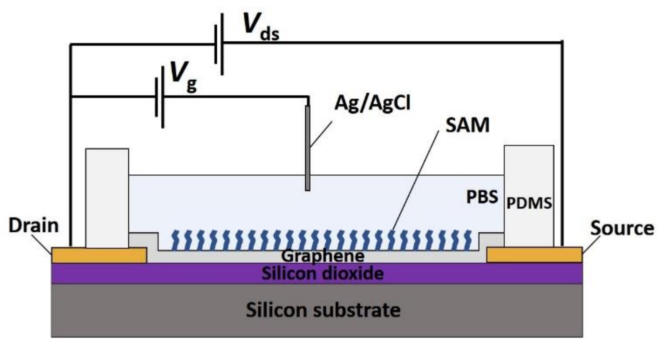

Figure 5.1: Schematic diagram of an electrolyte-gated GFET nanosensor.

5.2.2 Fabrication and Surface Modification

The graphene nanosensor was fabricated with a standard lithography process, as follows. A Ti/Au layer (10 nm/50 nm) was patterned through a standard lift-off process to form the source and drain electrodes process. The graphene was then transferred to form the conduction channel between source and drain electrodes following a wet transfer method[144]. After the transfer, the PMMA protection layer was removed by an acetone bath at 60 °C for 4 h, followed by washing with fresh acetone/isopropanol solution. The fabricated device was stored in a vacuum overnight to enhance the adhesion of the graphene onto the surface of the sensor.

To functionalize the graphene surface with aromatic boronic acid, the nanosensors were immersed in ethanol containing 5 mM aromatic boronic acid to be functionalized for 24 hours. Then a washing step with ethanol was allowed to remove the excess molecules from the surface. The nanosensors were then blow-dried with compressed nitrogen gas for use.

5.2.3 Materials

All aromatic compounds used in the study, including 1-naphthalenemethanol, naphthalene-1-boronic acid (NAPH-1-BA), 4-nitrophenylboronic acid (4-NPBA), 8-quinolinylboronic acid (8-QBA), 3-quinolinylboronic acid (3-QBA), and chemicals to prepare the pH solutions, including sodium hydroxide (NaOH), sodium chloride (NaCl), and hydrochloric acid (HCl), were purchased from Sigma-Aldrich. Phosphate-buffered saline solution (PBS, pH 7.4, ionic strength 0.15 M) and D-(+)-glucose were purchased from Thermo Fisher Scientific (Waltham, MA). Each pH solution was prepared by adjusting sodium chloride (NaCl) solution (0.15 M) with NaOH or HCl to pH values ranging from 4.88 to 13.18, measured by a pH meter (Oakton PH 550, IL, US). Glucose solutions at varying concentrations were prepared by diluting the stock solution with the appropriate volume of PBS buffer (0.15 M).

5.2.4 Testing Instrumentation and Procedures

To test the nanosensors, testing solutions were introduced into the polydimethylsiloxane (PDMS) well bonded to the nanosensor. An Ag/AgCl probe used as a gate electrode was immersed in the testing electrolyte solution to adjust the electrical potential of graphene (Figure 5.2). Two source meters (Keithley 2400, OH, US) were used, one was used to apply a gate voltage V_g and the other apply a voltage V_{ds} between source and drain electrodes while measuring the corresponding current I_{ds}. To characterize the nanosensor's electrical properties, transfer characteristic curves (i.e., the drain-source current I_{ds} as a function of the gate voltage V_g) were measured. For each testing solution, the V_g-I_{ds} curve was obtained every 4 min until the system equilibrated. To allow statistical analysis, characterizations were repeated with the same procedures using three nanosensors. In time-dependent measurements, the sensor's gate voltage was fixed at a specific voltage and the current I_{ds} was monitored.

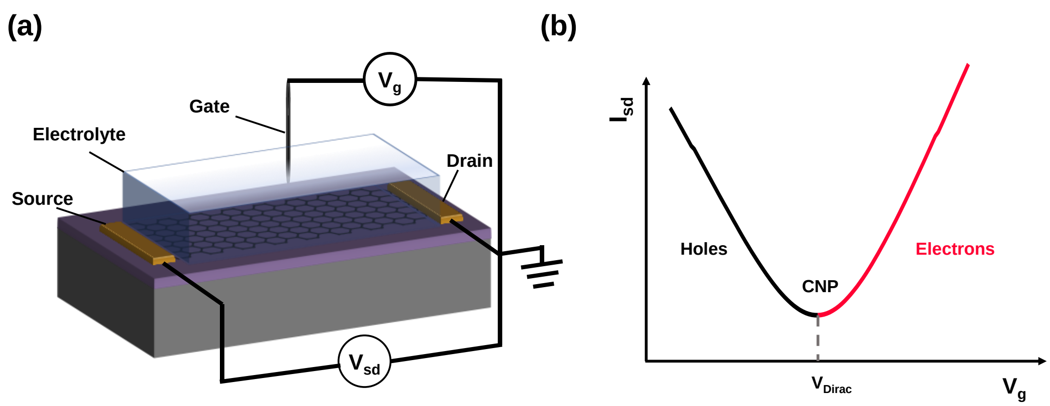

Figure 5.2: Operation of the GFET nanosensor. (a) Schematic of electrolyte-gated GFET sensor with reference Ag/AgCl electrode serving as a gate electrode. (b) Typical transport characteristic curve for GFET device. CNP: charge neutrality point

5.3 Characterization of Graphene Functionalization Process

Before surface modification, pristine graphene was confirmed by characterization using Raman spectroscopy. From the Raman spectra acquired from different locations of a bare nanosensor (Figure 5.3a), the ratio of the intensity of the two-dimensional (2D) band to that of the G band (I_{2D}/I_G) was calculated as 5.18 ± 0.2, and the full width at half maximum of the 2D band was approximately 27 with Lorentz fitting (Figure 5.3b); both findings confirm the evidence from single-layer graphene[145]. In addition, the D′ peak located at 1620 cm^{-1}, an indicator of scattering centers in graphene, was not present in any of the Raman spectra inspected, indicating graphene was free of surface defects[145,146].

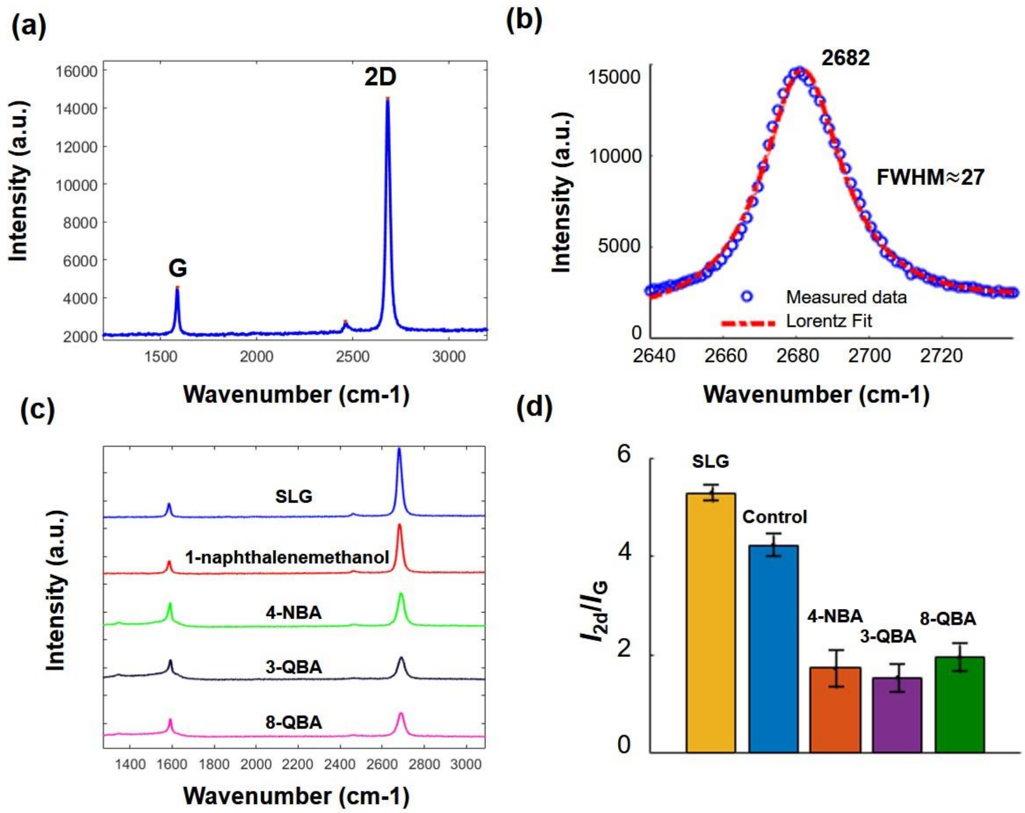

Figure 5.3: Raman spectrum of pristine and functionalized single-layer graphene: (a) G peak and 2D peak identified from Raman spectrum of pristine graphene. (b) Lorentzian fit of the 2D peak for pristine graphene. (c) Raman spectra for pristine graphene and graphene functionalized with 1-naphthalenemethanol, 4-NPBA, 3-QBA and 8-QBA. (d) Ratio of the 2D peak (I_{2D}) to the G peak (I_G).

Raman spectra of pristine graphene and graphene functionalized with 1-naphthalenemethanol, 4-NPBA, 8-QBA, and 3-QBA were evaluated (Figure 5.3c). The decrease in the ratio between the intensity of the 2D band and that of the G band (I_{2D}/I_G) after chemical functionalization indicated the successful functionalization of the molecules (Figure 5.3d)[147].[148]

The successful functionalization of the nanosensor was verified by analyzing the measured transfer characteristic curves, i.e., plots of the drain-source current (I_{ds}) versus the gate voltage (V_g). Here, one example characterization result is presented in Figure 5.4. transfer characteristic curves (I_{sd}-V_g) of pristine graphene and graphene functionalized with 1-

naphthalenemethanol in PBS buffer were both characterized. The Dirac point (V_{Dirac}), which is the value of V_g at which I_{ds} reaches its minimum, was observed to increase from -10 to 70 mV after modification with 1-naphthalenemethanol. The right shift of the transfer characteristic curves indicates p-type doping in the graphene. Electrons were transferred from the graphene to the electron-deficient boron group to induce an electron depletion layer in the graphene and the p-type doping.

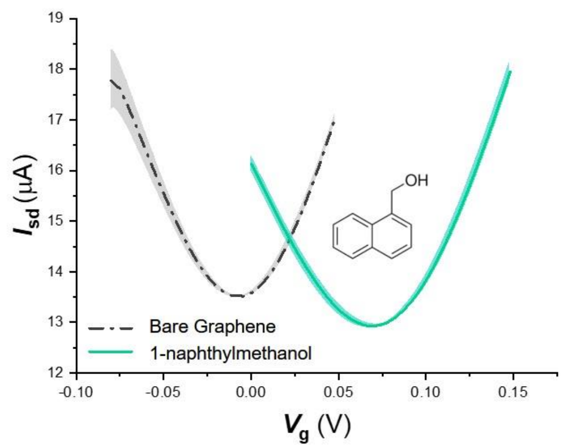

Figure 5.4: Transfer characteristic curves of pristine graphene and graphene functionalized with 1-naphthalenemethanol.

5.4 Characterization of Nanosensor Behavior via pH-Based Measurements

Understanding the interaction between aromatic boronic acids and glucose is critical for the design of the affinity glucose nanosensor. Glucose can bind with boronic acid to form a negatively charged glucose-boronic acid ester complex. The binding is strongly influenced by the solution pH; in general, a basic pH facilitates the binding. Characterization of aromatic boronic acid-functionalized nanosensors via pH measurements without and with the presence of glucose can give insights into the boronic acid-glucose interaction at varying pH and how this interaction alters the charge distribution of the graphene and the signal of the affinity nanosensors, especially at physiological pH.

We examine a series of aromatic boronic acids, including naphthalene-1-boronic acid (NAPH-1-BA), 4-nitrophenylboronic acid (4-NPBA), 8-quinolinylboronic acid (8-QBA) and 3-quinolinylboronic acid (3-QBA). These aromatic boronic acids differ in structure and substitution group, which can influence their interaction with glucose at a given pH (e.g., pH 7.4 for tears). The investigation informs the glucose-sensing mechanism of the nanosensors and provides insights into the design and optimization of affinity glucose sensors.

5.4.1 Validation of pH-Based Characterization of Functionalized Graphene Surfaces

We first test if the characteristics of the nanosensor reflect the charge state of the adsorbed aromatic boronic acid by measuring the response of bare nanosensors and nanosensors that are modified with a neutral molecule to changes in the pH of the measured media.

Transfer characteristic curves of the bare nanosensors at solution pH ranging from 4.88 to 13.17 were characterized. The relative change of the V_{Dirac} ($\Delta V_{\mathrm{Dirac}}$) of the bare nanosensors with varying solution pH is displayed in Figure 5.5b. $\Delta V_{\mathrm{Dirac}}$ is denoted as $\Delta V_{\mathrm{Dirac}} = V_{\mathrm{Dirac}}$-$V_{\mathrm{Dirac,4.88}}$, where $V_{\mathrm{Dirac,4.88}}$ is the Dirac point corresponding to the solution pH at 4.88. The Dirac point increased linearly with the solution pH. The slope of the line is 29.7 mV/pH from a linear fit, which is within the reported range (10 to 60 mV/pH)[149]. The increase in the Dirac point of the graphene was attributed to the electrostatic gating effect. The adsorbed protons (H^+) on the graphene surface at low pH cause accumulation of the electrons in the graphene and induce n-type doping, while the adsorbed hydroxide ions (OH^-) at high pH depletes the electrons and induce p-type doping, thus increasing the V_{Dirac} consistently with an increase in pH.

We then studied the effect of pH on nanosensors functionalized with 1-naphthalenemethanol. The transfer characteristic curves of the nanosensor measured at varying solution pH are shown in Figure 5.5a and the Dirac point of 1-naphthalenemethanol modified nanosensors with varying solution pH is shown in Figure 5.5b. The Dirac point of the device was independent of solution pH with a mean value of -75 mV and a standard deviation of 3 mV. The result is as expected since 1-naphthalenemethanol is a neutral molecule at all pH that does not induce change in the charge distribution at the graphene surface.

The experimental results validate that the characteristics of the nanosensors truly reflect the charge state of the aromatic molecules adsorbed on the graphene surface at a given pH value.

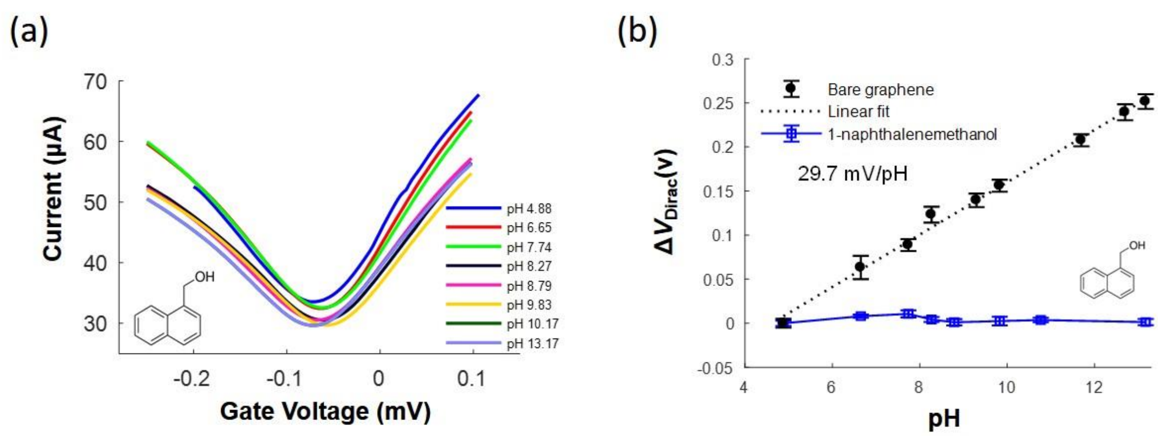

Figure 5.5: Effect of pH on nanosensors without and with 1-naphthalenemethanol modification. (a) Transfer characteristic curves of a nanosensor modified with 1-naphthalenemethanol at varying pH. (b) pH-induced shift in the Dirac point of nanosensors without and with 1-naphthalenemethanol modification.

5.4.2 Characterization of Aromatic Boronic Acids on Graphene

Following the validation of pH-based characterization of nanosensors, we apply this method to investigate the charge state of graphene nanosensors that are modified with NAPH-1-BA or 8-QBA in the absence and presence of glucose, respectively (Figure 5.6).

Figure 5.5a shows the effect of the pH of the testing media on the Dirac point of nanosensors functionalized with NAPH-1-BA. The Dirac point of the nanosensors did not change below pH 6.7 and then decreased gradually with an increase in solution pH. At pH 11.7, the Dirac point reached the minimum value, indicating a saturated sensor response. The plot can be used to determine the pK_a, the negative log of the acid dissociation constant indicating the strength of an acid, of the naphthalene-1-boronic acid adsorbed on the graphene through fitting with Henderson–Hasselbach eqution[150]: $pH = pK_a + \log_{10}(((V_{Dirac} - V_{HA}))/((V_{A-} - V_{Dirac})))$, where V_{HA} and V_{A-} correspond to the Dirac point where all aromatic acids are neutral or charged, respectively. The pK_a of the NAPH-1-BA-functionalized on graphene was determined to be 8.75, which is comparable to its bulk pK_a of 9.

The charge state of NAPH-1-BA at varying pH can be determined by the shift in Dirac point at pH below 6.7, the NAPH-1-BA was neutral. With an increase in solution pH, neutral NAPH-1-BA can be hydrolyzed to become negatively charged, inducing electrons transferred to the graphene and doping graphene with electrons thus decreasing the Dirac point of the nanosensors.

We next studied the boronic acid-glucose binding induced response of the nanosensor at varying pH by characterizing the device in pH solutions with a glucose concentration of 180 mg/dL (Figure 5.6). The normalized Dirac point shift of the device in response to pH solution with and without the presence of glucose is displayed in Figure 5.6b. With the presence of glucose, the Dirac point did not change below pH 6.7 and showed a more decrease at pH ranging from pH 6.7 to 9.8 than without glucose molecules. The findings indicate that there is no detectable binding between boronic acid and glucose at a solution pH below 6.7. When solution pH is above 6.7, glucose-boronic acid interaction induced more decrease in the Dirac point, indicating the formation of the negatively charged boronic acid-glucose ester complex.

Nanosensors functionalized with 8-QBA displayed a more complicated pH-induced response (Figure 5.6c). The Dirac point first increased with pH between pH 4 and 7 and then began to decrease above pH 6.65. The decrease in Dirac point after pH 7 was similar to the observations in NAPH-1-BA, which could be attributed to the increased amount of the negative charged boronic acid. The increase in Dirac point between pH 4 to pH 6.65 was likely a result of the deprotonation of quinolinium ions[151]. Two p*K*a values, 5 and 8.7, were estimated for 8-QBA adsorbed on graphene. pK_a 8.7 could be associated with boronic acid and pK_a 5 was assumed to associate with the nitrogen atom[151]. The values are different with their bulk pK_a, 4 and 10, respectively, determined from a fluorescence-based study[152]. The deviations in the surface pK_a and bulk pK_a values may result from the surface effect, for example, the charge transfer between the 8-QBA and graphene.

The glucose-binding induced Dirac point shift of the 8-QBA functionalized nanosensor is shown in Figure 5.6d. Despite a more complex change in pH, glucose-8QBA interaction-induced changes in Dirac point were similar to the glucose- NAPH-1-BA interaction. For GEFT functionalized with other aromatic boronic acids, including 4-NBA and 3-QBA, their binding with glucose should induce a similar change in the Dirac point at basic pH.

The results above indicate that, at the physiological pH of 7.4 (at which glucose measurements generally occur), the charge state of graphene-immobilized NAPH-1-BA or 8-

QBA is changed when the aromatic boronic acids bind to glucose. Both of the aromatic boronic acids were only insignificantly charged in the absence of glucose. When binding with glucose, these aromatic boronic acids showed an appreciable increase in negative charge, as reflected by relative Dirac point shifts of 2% and 5% respectively for NAPH-1-BA and 8-QBA. Thus, nanosensors in which graphene is modified with such aromatic boronic acids that become more negatively charged when binding to glucose, can be used to enable measurement of glucose concentrations. This is explored in the next section.

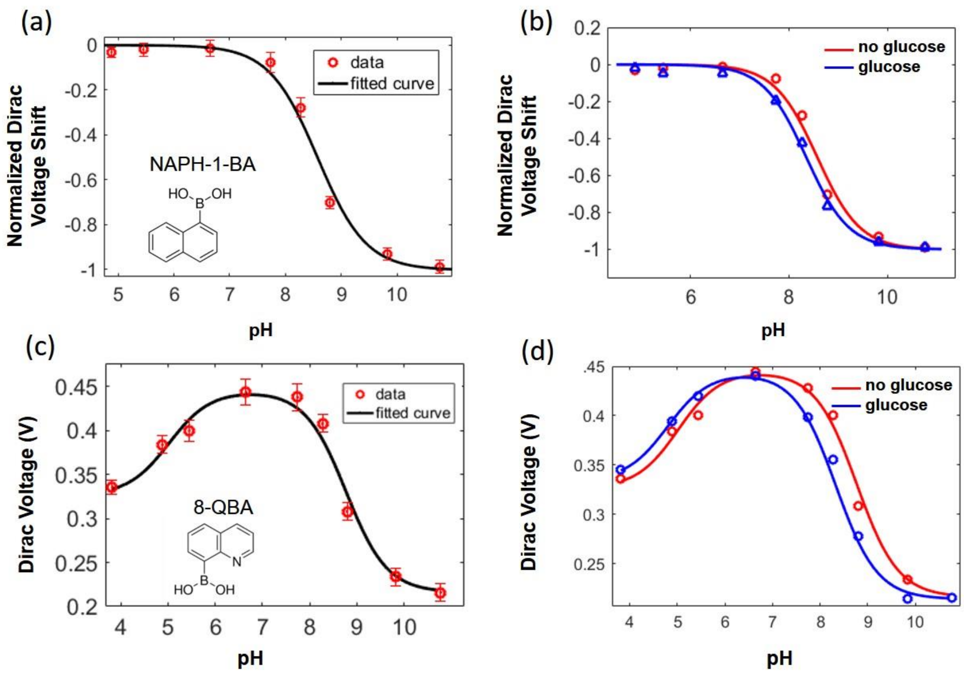

Figure 5.6: Effect of pH on the Dirac point of nanosensors functionalized with NAPH-1-BA or 8-QBA. (a) The pH profiles of V_{Dirac} of nanosensors functionalized with naphthalene-1-boronic acid. (b) Comparison of the pH profiles of V_{Dirac} of a nanosensor functionalized with NAPH-1-BA in the absence and presence of 180 mg/dL glucose. (c) The pH profiles of V_{Dirac} of the nanosensors functionalized with 8-QBA. (d) Comparison of the pH profiles of V_{Dirac} in the absence and presence of 180 mg/dL glucose.

5.5 Graphene-Based Glucose Measurements

Based on insights from pH-based measurements in the preceding section, we apply modification of GFET nanosensors with aromatic boronic acids to measure glucose concentration changes at pH 7.4 and evaluate their sensitivity and dynamic range for the potential utility of such sensors in continuous glucose monitoring in physiological media such as tears. Four aromatic boronic acids have been investigated, including naphthalene-1-boronic acid (NAPH-1-BA), 4-nitrophenylboronic acid (4-NPBA), 8-quinolinylboronic acid (8-QBA), and 3-quinolinylboronic acid (3-QBA). We expect that binding with glucose will cause these surface-immobilized boronic acid groups to become more negatively charged and donate electrons to the graphene, leading to a decrease in the Dirac point V_{Dirac} of the nanosensors. Measuring this Dirac point shift will allow the determination of the glucose concentration.

We measured the response to changes in glucose concentrations in PBS of graphene nanosensors that were functionalized with NAPH-1-BA, 8-QBA, 4-NPBA, or 3-QBA (Figure 5.7). A consistent decrease in the V_{Dirac} with an increase in glucose concentrations was observed for all aromatic boronic acid-functionalized nanosensors, resulting from the negatively charged glucose-boronic acid ester complex. The Langmuir adsorption equation[153] provides a good fit to the experimental data (Figure 5.7). All nanosensors' V_{Dirac} showed a linear dependence at low glucose concentrations with varying linear ranges. The sensitivity of the nanosensor in the linear range was obtained from a linear fit to the data. Sensor characteristics, including the sensing range, linear range, limit of detection, and sensitivity in the linear range to glucose, for each aromatic boronic acid-functionalized nanosensor are summarized in Table 3.

Table 3: Characteristics of the aromatic boronic acid-functionalized nanosensors for glucose measurement.

	NAPH-1-BA	8-QBA	4-NPBA	3-QBA
Sensing Range (mg/dL)	0.18- 36	0.18-180	0.18- 45	0.18-18
Linear Range (mg/dL)	0.18-0.9	0.18-0.9	0.18 – 1.8	0.18 -1.8
Sensitivity (mV/(mg/dL))	16	32	16	27
Limit of Detection (μg/dL)	88	38	112	67

Among the four molecules, the devices functionalized with 8-QBA showed the largest dynamic range, highest sensitivity, and lowest limit of detection. This is consistent with the observation that 8-QBA exhibited a higher relative Dirac point shift than NAPH-1-BA at pH 7.4 (Section 5.4.2). The sensing range completely covers the glucose concentration in tears (0.5 – 60-90 mg/dL[140,142]). Thus, 8-QBA functionalized nanosensors can provide an optimum response to glucose at physiological pH and satisfy the requirement for monitoring glucose concentrations in tears. Next, we will focus on studying the time-dependent response of the 8-QBA functionalized nanosensors.

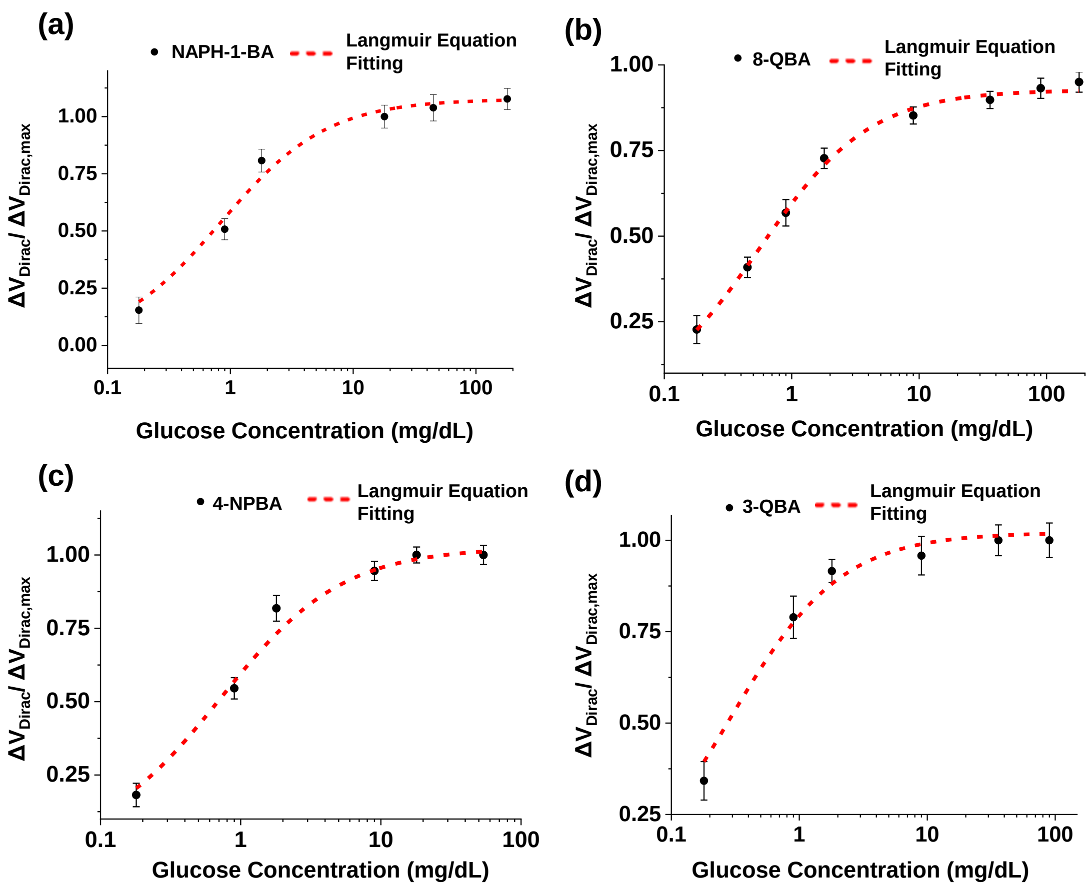

Figure 5.7: Glucose-dependent characteristics of affinity nanosensors. Normalized shift in Dirac point of nanosensors in response to glucose concentrations functionalized with (a) NAPH-1-BA ,(b) 8-QBA ,(c) 4-NPBA, and (d) 3-QBA.

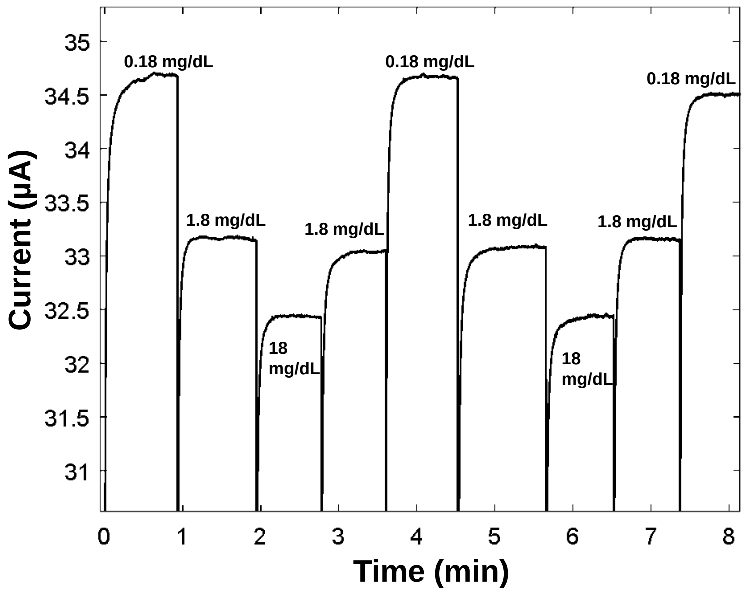

Figure 5.8: Time-dependent measurement of a nanosensor modified with 8-QBA in response to glucose concentrations.

Time-resolved response of 8-QBA-functionalized nanosensor. The time-resolved response of the 8-QBA functionalized graphene affinity nanosensor was then tested with the gate grounded (V_g = 0). The sensor was tested with varying glucose concentrations to test its repeatability and reversibility in glucose measurement. The glucose concentrations were introduced into the PDMS well. Once the glucose-induced current change of the sensor reached equilibration, the glucose concentration was removed and the next glucose concentration was introduced, which instantaneously changed the glucose concentration to which the sensor was exposed. The nanosensors showed fast and reversible responses to glucose, and representative time-dependent data are shown in which the sensor reached 90% of the equilibrated response within 15 s (Figure 5.8) and showed a highly repeatable response.

Response to potential interferents. For the microsensor to operate reliably in the interstitial fluid, it is important to evaluate the device's responses to potential interferents.

Boronic acid is known to bind with compounds that contain diol moieties through reversible boronate formation[154,155]. The main potential interferents present in the blood include fructose, galactose, and lactate, whose concentrations of these interfering sugars (below 0.14 mg/dL[122] for fructose, 0.07 mg/dL[123] for galactose, and 9 mg/dL[156] for lactate) are all considerably lower than glucose concentrations (54 mg/dL in the hypoglycemic limit). The concentrations of these interferents in other physiological fluids are less established. For example, no reports of the concentrations of fructose and galactose in tears have been identified in the literature, although there are reports of the lactate concentrations ranging from 3.6 to 21.6 mg/dL in tear[157,158]. The lactate concentration is comparable to glucose concentrations in the tear. From preliminary tests at 90 mg/dL in PBS buffer, nanosensors modified with 4-NPBA, 3-QBA, and 8-QBA all demonstrated a response to lactate that was approximately 15%-20% of that to glucose, a response to galactose that was comparable to that to glucose, and a response to fructose that exceeded that to glucose by approximately 150%-300%. While this is expected because it is known that boronic acid derivatives bind with diol moieties and may in particular display preferential binding to fructose[109,154], the nanosensors must be made more specific for them to be applicable to continuous monitoring applications. This could be achieved using PBA derivatives that are more selective to glucose over the interfering sugars, as will be discussed in Section 6.2.

5.6 Summary

We have presented a preliminary study on graphene-based affinity nanosensors for non-invasive monitoring of glucose concentrations in physiological media such as tears. The sensing mechanism of the affinity nanosensor has been explored through pH-based measurements, indicating that the glucose-boronic acid complex can donate electrons to graphene and thus increase the electron density of graphene, resulting in a decrease in the Dirac point of the nanosensor. Glucose can bind with aromatic boronic acids at physiological pH and the resulted decrease in the Dirac point can indicate glucose concentrations. Measurements of the glucose-induced response of nanosensors functionalized with naphthalene-1-boronic acid, 8-QBA, 4-NBA, and 3-QBA at physiological pH demonstrate the affinity nanosensors can sensitively measure glucose concentrations. Nanosensors modified with 8-QBA displayed a rapid (<15 s) and reversible response to glucose with the widest sensing range (0.18-180 mg/dL), highest sensitivity (32 mV/(mg/dL)), and low limit of detection (38 μg/dL), which satisfies the requirement for monitoring glucose concentration in tears. The study provides insights into the design and optimization of the graphene-based nanosensors to meet the challenges in building a non-invasive affinity glucose nanosensors for clinical applications.

Chapter 6: Conclusions and Perspectives

6.1 Summary of This Thesis

In this thesis, affinity micro and nanosensors have been investigated to address the needs in CGM applications for stable and accurate measurements of glucose concentrations in physiological media. Commercially available enzyme-based CGM sensors lack long-term stability and accuracy because of the irreversible, consumptive nature of the underlying electrochemical reactions. Affinity sensors, which use equilibrium affinity binding of glucose to a specific receptor, avoid glucose consumption and can offer improved stability and accuracy for long-term CGM applications. Recognizing this opportunity, we have investigated hydrogel-based implantable affinity dielectric microsensors for measuring glucose concentrations in interstitial fluid (ISF), and explored graphene affinity nanosensors for non-invasive monitoring of glucose in physiological media such as tears.

In Chapter 2, we first made an initial demonstration of a MEMS affinity glucose microsensor that measured glucose concentrations via measurement of the changes in the dielectric properties of a PAAPBA-*ran*-PHEAA hydrogel film. The sensor consisted of a coplanar impedimetric transducer coated with a thin layer of hydrogel, serving as the sensing layer to specifically recognize glucose and a biocompatible body-sensor interface that is tolerant to biofouling when implanted. The coplanar impedimetric transducer reduces the fabrication cost and eliminates the fragile structures used in micro parallel-plate capacitors. Testing results showed that the microsensor exhibited a repeatable and reversible response to glucose concentrations in a range of 40-500 mg/dL with a resolution down to 0.27 mg/dL, holding promise for implantable CGM applications.

In Chapter 3, a systematic investigation was made to understand the effects of the compositional parameters, including the glucose-responsive monomer, hydrophilic monomer, and crosslinker, on the glucose-induced changes in swelling and dielectric properties of the hydrogel. The study identified a hydrogel recipe that offered an optimum trade-off between sensitivity to glucose and reliable hydrogel-transducer integration. The integrated coplanar-electrode-based microsensor exhibited a highly repeatable and reversible response to clinically relevant glucose concentrations (30-360 mg/dL) with a high resolution (25 µg/dL) and a fast time response (< 30 s). The microsensor can potentially offer a reliable and accurate measurement of glucose in the subcutaneous fluid.

In Chapter 4, a differential dielectric sensor was presented for *in vivo* glucose measurement. The sensor addressed the susceptibility of the single-sensing unit to environmental fluctuation and nonspecific adsorption by implementing a differential measurement scheme. A differential microsensor relies on the differential measurement of a sensing unit and a reference unit, integrated with a thin layer of either glucose-responsive hydrogel or glucose-insensitive hydrogel, to alleviate environmental disturbances. Preliminary *In vitro* and *in vivo* testing demonstrated that the sensor can accurately measure glucose concentrations ranging from 30 to 360 mg/dL reversibly and rapidly (with a time constant < 21 s) with a sensitivity of 7.5 pF/(mg/dL), resolution of 0.1 mg/dL and drift of 0.13%/h.

Chapter 5, a preliminary investigation was performed on graphene affinity nanosensors for non-invasive monitoring of glucose concentrations in physiological media such as tears. The nanosensor consists of aromatic boronic acid-functionalized graphene in an electrolyte-gated field-effect configuration. The sensing mechanism of the affinity nanosensor has been explored through pH-based measurement, indicating that the glucose-boronic acid complex can donate electrons to graphene, resulting in a decrease in the Dirac point. Measurements of the glucose-induced response of nanosensors functionalized with multiple aromatic boronic acids at physiological pH demonstrate the affinity nanosensor can sensitively measure glucose concentration via measurement of change in Dirac point. Nanosensors modified with 8-QBA exhibited a rapid (<15 s) and reversible response to glucose with the highest sensing range (0.18-180 mg/dL), sensitivity (32 mV/(mg/dL)), and low limit of detection of 38 μg/dL, which satisfies the requirement for monitoring glucose concentration in tears. The study provides insights into the design and optimization of the nanosensors to meet the challenges in building a non-invasive affinity glucose nanosensors for clinical applications.

6.2 Directions for Future Research

There are several possible directions to be pursued for future research. These include improvements in the design of hydrogel-based microsensors to achieve highly reliable measurement of ISF glucose, evaluation of the microsensor performance through further *in vivo* studies in ambulatory mice and rats, and enhancement of the specificity of the graphene affinity nanosensors to allow accurate non-invasive monitoring of glucose.

6.2.1 Improved Hydrogel-Based Microsensor Design

Improvement in specificity. We have demonstrated a microsensor that measures glucose concentrations by detecting glucose-phenylboronic acid-induced dielectric property change in the hydrogel. While sensitive to glucose, the microsensor was also responsive to other potential interferents presented in ISF, including fructose, galactose, and lactate. In future work, we will investigate improving the selectivity of the hydrogel by modifying the components of the hydrogel. For example, hydrogels that use 2-acrylamidophenylboronic acid (2-APBA) as a glucose-responsive monomer are minimally responsive to lactate while highly sensitive to glucose[159], thus it could be used to drastically increase the selectivity of the microsensor for glucose relative to lactate. On the other hand, the addition of a cationic monomer, dimethylaminopropyl acrylamide (DMAPAA), into hydrogel synthesis, may significantly enhance the selectivity of the hydrogel to glucose over fructose[160], which helps minimize the response of the microsensor to fructose.

Wireless telemetry. We will investigate the integration of hydrogel-based microsensors with wireless telemetry for the practical deployment of hydrogel-based sensors for glucose monitoring. A passive telemetry approach would be highly desired for a subcutaneously implanted microsensor. This may be achieved with radio frequency (RF) interrogation of the implanted microsensor using a passive resonant RLC tank circuit formed by an integrated inductor coil with the microsensor[95,161]. Glucose-induced impedance changes of the microsensor would result in a shift in the resonant frequency of the RLC circuit, which may be measured wirelessly by an external inductor coil to determine the glucose concentration. This approach would require the implanted and external inductor coils to be placed in close proximity. If the limited spatial range of this wireless interrogation proves to be an issue, active wireless telemetry approaches could be explored[162,163].

Other improvements in design. Other improvements in the microsensor design include reducing the footprint of the sensor with a more compact sensor layout, fabricating the microsensor on flexible substrates, and packaging the microsensor within a biocompatible synthetic hydrogel, which all contribute to enhancing the compatibility of the microsensor to subcutaneous tissue and alleviating adverse device-tissue interactions.

6.2.2 *In vivo* Testing of Hydrogel-Based Microsensors

***In vivo* study in ambulatory rats.** A 4-hour *in vivo* test has been performed using a hydrogel-based sensor to monitor the ISF glucose of a sedated mouse. In the future, the microsensor performance in glucose monitoring will be characterized through an extended *in vivo* study in ambulatory mice and rats (e.g., up to 7 days). Initially, the device could be electrically connected to readout instruments outside the animal cage via wires. In the later stages of animal testing, the device measurement readout may be made via wireless telemetry to eliminate wire tangling issues. The signal processing circuitry may be attached to the microsensor to process and transmit the measurement data via a radio frequency link to a cage-mounted receiver. Measurement results from the microsensors will be correlated to blood glucose concentrations and the accuracy of the correlations will be examined using the Clarke error grid[164].

6.2.3 Further Investigation of Graphene Affinity Nanosensors

Improvement in specificity. The preliminary *in vitro* study presented in Chapter 5 has shown great potential possessed by the graphene nanosensors to monitor glucose concentrations in tears. Further improvement in the selectivity of nanosensors to glucose is desired for the practical application of devices to determine glucose concentrations in physiological media. We will explore the functionalization of graphene with aromatic boronic acid derivatives which are more selective to glucose over interfering sugars. Since monoboronic acid derivatives are known to display higher sensitivity and selectivity for fructose over glucose[109], divalent boronic acid groups may be explored to design a more glucose-selective receptor[109]. For example, diboronic acid derivatives could be exploited to selectively recognize glucose, thereby enabling nanosensors with enhanced specificity to allow accurate non-invasive monitoring of glucose.

Other improvements in design. Other improvements in the nanosensor design may be explored to make the sensor applicable to continuous monitoring applications. Nanosensors with a back-gated GFET design, where a gate electrode is buried beneath a solid dielectric layer, such as a nanometer-thick layer of hexagonal boron nitride (h-BN) or Hafnium oxide (HfO_2)[165,166], may be investigated to eliminate the bulky Ag/AgCl probe required to apply gate voltage in electrolyte-gated GFET sensors, allowing desired integration and miniaturization of the sensor footprint. Also, similar to our differential hydrogel-based microsensors, differential graphene nanosnesors, which use two graphene sensing elements placed in close proximity to achieve effective common-mode cancellation of noise and environmental disturbances[167], can be explored to improve the measurement accuracy and stability in glucose concentration measurements.

References

1. Centers for Disease Control and Prevention. Prevent Diabetes Complications. https://www.cdc.gov/diabetes/managing/problems.html.

2. National Institute of Diabetes and Digestive and Kidney Diseases. Diabetes, Heart Disease, & Stroke. https://www.niddk.nih.gov/health-information/diabetes/overview/preventing-problems/heart-disease-stroke.

3. Centers for Disease Control and Prevention. National Diabetes Statistics Report. https://www.cdc.gov/diabetes/data/statistics-report/index.html (2020).

4. Olansky, L. & Kennedy, L. Finger-Stick Glucose Monitoring. Diabetes Care 33, 948–949 (2010).

5. Rodbard, D. Continuous Glucose Monitoring: A Review of Recent Studies Demonstrating Improved Glycemic Outcomes. Diabetes Technology & Therapeutics 19, S-25-S-37 (2017).

6. National Institute of Diabetes and Digestive and Kidney Diseases. Continuous Glucose Monitoring. https://www.niddk.nih.gov/health-information/diabetes/overview/managing-diabetes/continuous-glucose-monitoring.

7. Klonoff, D. C., Ahn, D. & Drincic, A. Continuous glucose monitoring: A review of the technology and clinical use. Diabetes Research and Clinical Practice 133, 178–192 (2017).

8. Poolsup, N., Suksomboon, N. & Kyaw, A. M. Systematic review and meta-analysis of the effectiveness of continuous glucose monitoring (CGM) on glucose control in diabetes. Diabetology & Metabolic Syndrome 5, 39 (2013).

9. Juvenile Diabetes Research Foundation Continuous Glucose Monitoring Study Group. Effectiveness of Continuous Glucose Monitoring in a Clinical Care Environment: Evidence from the Juvenile Diabetes Research Foundation Continuous Glucose Monitoring (JDRF-CGM) trial. Diabetes Care 33, 17–22 (2010).

10. Block, C. D., Manuel-y-Keenoy, B. & Van Gaal, L. A Review of Current Evidence with Continuous Glucose Monitoring in Patients with Diabetes. J Diabetes Sci Technol 2, 718–727 (2008).

11. Abbott. FreeStyle Libre 2 System. https://www.freestyle.abbott/us-en/home.html.

12. Dexcom. Dexcom G6 CGM System. https://www.dexcom.com/g6-cgm-system.

13. Medtronic. The Guardian Connect CGM System. https://www.medtronicdiabetes.com/products/guardian-connect-continuous-glucose-monitoring-system.

14. Ricci, F. et al. Novel planar glucose biosensors for continuous monitoring use. Biosensors and Bioelectronics 20, 1993–2000 (2005).

15. Luo, J. et al. A new type of glucose biosensor based on surface acoustic wave resonator using Mn-doped ZnO multilayer structure. Biosensors and Bioelectronics 49, 512–518 (2013).

16. Funtanilla, V. D., Candidate, P., Caliendo, T. & Hilas, O. Continuous Glucose Monitoring: A Review of Available Systems. P T 44, 550–553 (2019).

17. Lee, I., Probst, D., Klonoff, D. & Sode, K. Continuous glucose monitoring systems - Current status and future perspectives of the flagship technologies in biosensor research -. Biosensors and Bioelectronics 181, 113054 (2021).

18. Heller, A. Implanted Electrochemical Glucose Sensors for the Management of Diabetes. Annu. Rev. Biomed. Eng. 1, 153–175 (1999).

19. Klueh, U. et al. Metabolic Biofouling of Glucose Sensors in Vivo : Role of Tissue Microhemorrhages. J Diabetes Sci Technol 5, 583–595 (2011).

20. Gifford, R. et al. Protein interactions with subcutaneously implanted biosensors. Biomaterials 27, 2587–2598 (2006).

21. Fundamental sensing limit of electrochemical glucose sensors. IEEE Conference Publication. IEEE Xplore. https://ieeexplore.ieee.org/document/6091890.

22. Valdes, T. I. & Moussy, F. In vitro and in vivo degradation of glucose oxidase enzyme used for an implantable glucose biosensor. Diabetes Technol Ther 2, 367–376 (2000).

23. Van Enter, B. J. & von Hauff, E. Challenges and perspectives in continuous glucose monitoring. Chem. Commun. 54, 5032–5045 (2018).

24. Schultz, J. S., Mansouri, S. & Goldstein, I. J. Affinity Sensor: A New Technique for Developing Implantable Sensors for Glucose and Other Metabolites. Diabetes Care 5, 245–253 (1982).

25. Ballerstädt, R. & Ehwald, R. Suitability of aqueous dispersions of dextran and Concanavalin A for glucose sensing in different variants of the affinity sensor. Biosensors and Bioelectronics 9, 557–567 (1994).

26. Li, S., Huang, X., Davis, E. N., Lin, Q. & Wang, Q. Development of Novel Glucose Sensing Fluids with Potential Application to Microelectromechanical Systems-Based Continuous Glucose Monitoring. J Diabetes Sci Technol 2, 1066–1074 (2008).

27. Rogers, K. R. Principles of Affinity-Based Biosensors. MB 14, 109–130 (2000).

28. Leech, D. Affinity biosensors. Chem. Soc. Rev. 23, 205 (1994).

29. Chapter 4 Affinity Biosensors. in Techniques and Instrumentation in Analytical Chemistry vol. 11 253–290 (Elsevier, 1992).

30. Zhao, Y. et al. A MEMS viscometric sensor for continuous glucose monitoring. J. Micromech. Microeng. 17, 2528–2537 (2007).

31. Ballerstadt, R. & Schultz, J. S. A Fluorescence Affinity Hollow Fiber Sensor for Continuous Transdermal Glucose Monitoring. Anal. Chem. 72, 4185–4192 (2000).

32. Mansouri, S. & Schultz, J. S. A Miniature Optical Glucose Sensor Based on Affinity Binding. Bio/Technology 2, 885–890 (1984).

33. Alexeev, V. L., Das, S., Finegold, D. N. & Asher, S. A. Photonic Crystal Glucose-Sensing Material for Noninvasive Monitoring of Glucose in Tear Fluid. Clinical Chemistry 50, 2353–2360 (2004).

34. Badugu, R., Reece, E. A. & Lakowicz, J. R. Glucose-sensitive silicone hydrogel contact lens toward tear glucose monitoring. J. Biomed. Opt. 23, 1 (2018).

35. Egawa, Y., Gotoh, R., Niina, S. & Anzai, J. Ortho-azo substituted phenylboronic acids for colorimetric sugar sensors. Bioorganic & Medicinal Chemistry Letters 17, 3789–3792 (2007).

36. Dou, Q. et al. Ultrasensitive Poly(boric acid) Hydrogel-Coated Quartz Crystal Microbalance Sensor by Using UV Pressing-Assisted Polymerization for Saliva Glucose Monitoring. ACS Appl. Mater. Interfaces 12, 34190–34197 (2020).

37. Orthner, M. P., Buetefisch, S., Magda, J., Rieth, L. W. & Solzbacher, F. Development, fabrication, and characterization of hydrogel based piezoresistive pressure sensors with perforated diaphragms. Sensors and Actuators A: Physical 161, 29–38 (2010).

38. Wang, H.-C. et al. A bis-boronic acid modified electrode for the sensitive and selective determination of glucose concentrations. Analyst 138, 7146 (2013).

39. Li, J., Liu, L., Wang, P., Yang, Y. & Zheng, J. Amplified detection of saccharide based on redox-poly(phenol-co-3-hydroxyphenylboronic acid) coupling with a redox cycling. Sensors and Actuators B: Chemical 198, 219–224 (2014).

40. Li, J., Wang, P., Zhang, N., Yang, Y. & Zheng, J. Enhanced detection of saccharide using redox capacitor as an electrochemical indicator via a redox-cycling and its molecular logic behavior. Electrochimica Acta 166, 253–260 (2015).

41. Wang, Q. et al. Sensitive sugar detection using 4-aminophenylboronic acid modified graphene. Biosensors and Bioelectronics 50, 331–337 (2013).

42. Shang, J. et al. A hydrogel-based glucose affinity microsensor. Sensors and Actuators B: Chemical 237, 992–998 (2016).

43. Zhu, Y. et al. A graphene-based affinity nanosensor for detection of low-charge and low-molecular-weight molecules. Nanoscale 8, 5815–5819 (2016).

44. Lerner, M. B. et al. Scalable, non-invasive glucose sensor based on boronic acid functionalized carbon nanotube transistors. Appl. Phys. Lett. 102, 183113 (2013).

45. Zhang, Z. et al. A dielectric affinity glucose microsensor using hydrogel-functionalized coplanar electrodes. Microfluid Nanofluid 21, 93 (2017).

46. Ballerstadt, R., Evans, C., Gowda, A. & McNichols, R. Fiber-coupled fluorescence affinity sensor for 3-day in vivo glucose sensing. J Diabetes Sci Technol 1, 384–393 (2007).

47. James, T. D., Sandanayake, K. R. A. S. & Shinkai, S. Saccharide Sensing with Molecular Receptors Based on Boronic Acid. Angew. Chem. Int. Ed. Engl. 35, 1910–1922 (1996).

48. Sawayama, J., Okitsu, T., Nakamata, A., Kawahara, Y. & Takeuchi, S. Hydrogel Glucose Sensor with In Vivo Stable Fluorescence Intensity Relying on Antioxidant Enzymes for Continuous Glucose Monitoring. iScience 23, 101243 (2020).

49. Ben-Moshe, M., Alexeev, V. L. & Asher, S. A. Fast Responsive Crystalline Colloidal Array Photonic Crystal Glucose Sensors. Anal. Chem. 78, 5149–5157 (2006).

50. Zhang, C., Cano, G. G. & Braun, P. V. Linear and Fast Hydrogel Glucose Sensor Materials Enabled by Volume Resetting Agents. Adv. Mater. 26, 5678–5683 (2014).

51. Pan, X., Yang, X. & Lowe, C. R. Evidence for a cross‐linking mechanism underlying glucose‐induced contraction of phenylboronate hydrogel. J. Mol. Recognit. 21, 205–209 (2008).

52. Yetisen, A. K. et al. Glucose-Sensitive Hydrogel Optical Fibers Functionalized with Phenylboronic Acid. Adv. Mater. 11 (2017).

53. Elsherif, M., Hassan, M. U., Yetisen, A. K. & Butt, H. Hydrogel optical fibers for continuous glucose monitoring. Biosensors and Bioelectronics 137, 25–32 (2019).

54. Tokuda, T. et al. CMOS image sensor-based implantable glucose sensor using glucose-responsive fluorescent hydrogel. Biomed. Opt. Express 5, 3859 (2014).

55. Dou, Q. et al. High performance boronic acid-containing hydrogel for biocompatible continuous glucose monitoring. RSC Adv. 7, 41384–41390 (2017).

56. Lin, G. et al. Osmotic swelling pressure response of smart hydrogels suitable for chronically implantable glucose sensors. Sensors and Actuators B: Chemical 144, 332–336 (2010).

57. Boss, C., Meurville, E., Sallese, J.-M. & Ryser, P. A viscosity-dependent affinity sensor for continuous monitoring of glucose in biological fluids. Biosensors and Bioelectronics 30, 223–228 (2011).

58. Huang, X. et al. A MEMS differential viscometric sensor for affinity glucose detection in continuous glucose monitoring. J. Micromech. Microeng. 23, 055020 (2013).

59. Huang, X., Li, S., Schultz, J. S., Wang, Q. & Lin, Q. A MEMS affinity glucose sensor using a biocompatible glucose-responsive polymer. Sensors and Actuators B: Chemical 140, 603–609 (2009).

60. Anzai, J. Recent progress in electrochemical biosensors based on phenylboronic acid and derivatives. Materials Science and Engineering: C 67, 737–746 (2016).

61. Lacina, K. & Skládal, P. Ferroceneboronic acid for the electrochemical probing of interactions involving sugars. Electrochimica Acta 56, 10246–10252 (2011).

62. Lacina, K. et al. Combining ferrocene, thiophene and a boronic acid: a hybrid ligand for reagentless electrochemical sensing of cis-diols. Tetrahedron Letters 55, 3235–3238 (2014).

63. Chen, M., Cao, X., Chang, K., Xiang, H. & Wang, R. A novel electrochemical non-enzymatic glucose sensor based on Au nanoparticle-modified indium tin oxide electrode and boronate affinity. Electrochimica Acta 368, 137603 (2021).

64. Sugnaux, C. & Klok, H.-A. Glucose-Sensitive QCM-Sensors Via Direct Surface RAFT Polymerization. Macromol. Rapid Commun. 35, 1402–1407 (2014).

65. Chen, D. et al. A wireless-electrodeless quartz crystal microbalance method for non-enzymatic glucose monitoring. Sensors and Actuators B: Chemical 287, 35–41 (2019).

66. Toghill, K. & Compton, R. Electrochemical Non-Enzymatic Glucose Sensors: A Perspective and an Evaluation. Int. J. Electrochem. Sci. International Journal 5, 1246–1301 (2010).

67. Bahadır, E. B. & Sezgintürk, M. K. A review on impedimetric biosensors. Artificial Cells, Nanomedicine, and Biotechnology 44, 248–262 (2016).

68. Impedance spectroscopy: theory, experiment, and applications. (Wiley, 2018).

69. Huang, X., Li, S., Schultz, J. S., Wang, Q. & Lin, Q. A dielectric affinity microbiosensor. Appl. Phys. Lett. 96, 033701 (2010).

70. Zou, Z., Kai, J., Rust, M. J., Han, J. & Ahn, C. H. Functionalized nano interdigitated electrodes arrays on polymer with integrated microfluidics for direct bio-affinity sensing using impedimetric measurement. Sensors and Actuators A: Physical 136, 518 – 526 (2007).

71. Xu, M. & Yadavalli, V. K. Flexible Biosensors for the Impedimetric Detection of Protein Targets Using Silk-Conductive Polymer Biocomposites. ACS Sens. 4, 1040–1047 (2019).

72. Pandey, C. M., Sumana, G. & Malhotra, B. D. Microstructured Cystine Dendrites-Based Impedimetric Sensor for Nucleic Acid Detection. Biomacromolecules 12, 2925–2932 (2011).

73. Barton, A. C. et al. Labeless AC impedimetric antibody-based sensors with pgml−1 sensitivities for point-of-care biomedical applications. Biosensors and Bioelectronics 24, 1090–1095 (2009).

74. Bergveld, P. Development of an Ion-Sensitive Solid-State Device for Neurophysiological Measurements. IEEE Trans. Biomed. Eng. BME-17, 70–71 (1970).

75. Syu, Y.-C., Hsu, W.-E. & Lin, C.-T. Review—Field-Effect Transistor Biosensing: Devices and Clinical Applications. ECS J. Solid State Sci. Technol. 7, Q3196–Q3207 (2018).

76. Lowe, B. M., Sun, K., Zeimpekis, I., Skylaris, C.-K. & Green, N. G. Field-effect sensors – from pH sensing to biosensing: sensitivity enhancement using streptavidin–biotin as a model system. Analyst 142, 4173–4200 (2017).

77. Schöning, M. J. & Poghossian, A. Recent advances in biologically sensitive field-effect transistors (BioFETs). Analyst 127, 1137–1151 (2002).

78. Hao, Z. et al. An Intelligent Graphene ‐ Based Biosensing Device for Cytokine Storm Syndrome Biomarkers Detection in Human Biofluids. Small 17, 2101508 (2021).

79. Kang, H. et al. Ultrasensitive Detection of SARS-CoV-2 Antibody by Graphene Field-Effect Transistors. Nano Lett. 21, 7897–7904 (2021).

80. Hao, Z. et al. Real-Time Monitoring of Insulin Using a Graphene Field-Effect Transistor Aptameric Nanosensor. ACS Appl. Mater. Interfaces 9, 27504–27511 (2017).

81. Schäfer, S. et al. Time-dependent observation of individual cellular binding events to field-effect transistors. Biosensors and Bioelectronics 24, 1201–1208 (2009).

82. Gu, Y. et al. Three-dimensional transistor arrays for intra- and inter-cellular recording. Nat. Nanotechnol. (2021) doi:10.1038/s41565-021-01040-w.

83. Cummins, B. M., Garza, J. T. & Coté, G. L. Optimization of a Concanavalin A-Based Glucose Sensor Using Fluorescence Anisotropy. Anal. Chem. 85, 5397–5404 (2013).

84. Beyer, U., Ehwald, R. & Fleischer, L.-G. Post-Stress Thickening of Dextran/Concanavalin A Solutions Used as Sensitive Fluids in a Viscosimetric Affinity Assay for Glucose. Biotechnol. Prog. 13, 722–726 (1997).

85. Ballerstadt, R., Evans, C., McNichols, R. & Gowda, A. Concanavalin A for in vivo glucose sensing: A biotoxicity review. Biosensors and Bioelectronics 22, 275–284 (2006).

86. Yang, W., Gao, X. & Wang, B. Boronic acid compounds as potential pharmaceutical agents. Med. Res. Rev. 23, 346–368 (2003).

87. Li, S., Davis, E. N., Anderson, J., Lin, Q. & Wang, Q. Development of Boronic Acid Grafted Random Copolymer Sensing Fluid for Continuous Glucose Monitoring. Biomacromolecules 10, 113–118 (2009).

88. Locke, A. K., Cummins, B. M., Abraham, A. A. & Coté, G. L. PEGylation of Concanavalin A to Improve Its Stability for an In Vivo Glucose Sensing Assay. Anal. Chem. 86, 9091–9097 (2014).

89. Nichols, S. P., Koh, A., Storm, W. L., Shin, J. H. & Schoenfisch, M. H. Biocompatible Materials for Continuous Glucose Monitoring Devices. Chem. Rev. 113, 2528–2549 (2013).

90. Yu, B. et al. Use of hydrogel coating to improve the performance of implanted glucose sensors. Biosensors and Bioelectronics 23, 1278–1284 (2008).

91. Dhanjai et al. Polymer hydrogel interfaces in electrochemical sensing strategies: A review. TrAC Trends in Analytical Chemistry 118, 488–501 (2019).

92. Sun, X. & James, T. D. Glucose Sensing in Supramolecular Chemistry. Chemical Reviews 37.

93. Holtz, J. H. & Asher, S. A. Polymerized colloidal crystal hydrogel films as intelligent chemical sensing materials. 389, 4 (1997).

94. Wang, X., Liu, X. & Wang, X. Hydrogel diffraction grating as sensor: A tool for studying volume phase transition of thermo-responsive hydrogel. Sensors and Actuators B: Chemical 204, 611–616 (2014).

95. Lei, M., Baldi, A., Nuxoll, E., Siegel, R. A. & Ziaie, B. A Hydrogel-Based Implantable Micromachined Transponder for Wireless Glucose Measurement. Diabetes Technology & Therapeutics 8, 112–122 (2006).

96. Arnold, F. H., Zheng, W. & Michaels, A. S. A membrane-moderated, conductimetric sensor for the detection and measurement of specific organic solutes in aqueous solutions. Journal of Membrane Science 167, 227–239 (2000).

97. Kajisa, T. & Sakata, T. Glucose-responsive hydrogel electrode for biocompatible glucose transistor. Science and Technology of Advanced Materials 18, 26–33 (2017).

98. Dautta, M., Alshetaiwi, M., Escobar, J. & Tseng, P. Passive and wireless, implantable glucose sensing with phenylboronic acid hydrogel-interlayer RF resonators. Biosensors and Bioelectronics 151, 112004 (2020).

99. Dankerl, M. et al. Graphene Solution-Gated Field-Effect Transistor Array for Sensing Applications. Adv. Funct. Mater. 20, 3117–3124 (2010).

100. Tran, T.-T. & Mulchandani, A. Carbon nanotubes and graphene nano field-effect transistor-based biosensors. TrAC Trends in Analytical Chemistry 79, 222–232 (2016).

101. Gruner, G. Carbon nanotube transistors for biosensing applications. Anal Bioanal Chem 384, 322–335 (2005).

102. Vu & Chen. Field-Effect Transistor Biosensors for Biomedical Applications: Recent Advances and Future Prospects. Sensors 19, 4214 (2019).

103. Wong, H.-S. P. & Akinwande, D. Carbon Nanotube and Graphene Device Physics. (Cambridge University Press, 2010). doi:10.1017/CBO9780511778124.

104. Broadband Dielectric Spectroscopy. (Springer Berlin Heidelberg, 2003). doi:10.1007/978-3-642-56120-7.

105. Oh, S., Lee, J. S., Jeong, K. H. & Lee, L. P. Minimization of electrode polarization effect by nanogap electrodes for biosensor applications. in The Sixteenth Annual International Conference on Micro Electro Mechanical Systems, 2003. MEMS-03 Kyoto. IEEE 52–55 (IEEE, 2003). doi:10.1109/MEMSYS.2003.1189685.

106. Woo, H. J., Majid, S. R. & Arof, A. K. Dielectric properties and morphology of polymer electrolyte based on poly(ε-caprolactone) and ammonium thiocyanate. Materials Chemistry and Physics 134, 755–761 (2012).

107. Keenan, D. B., Mastrototaro, J. J., Voskanyan, G. & Steil, G. M. Delays in Minimally Invasive Continuous Glucose Monitoring Devices: A Review of Current Technology. J Diabetes Sci Technol 3, 1207–1214 (2009).

108. Ni, N. et al. Probing the general time scale question of boronic acid binding with sugars in aqueous solution at physiological pH. Bioorganic & Medicinal Chemistry 20, 2957–2961 (2012).

109. Wu, X. et al. Selective sensing of saccharides using simple boronic acids and their aggregates. Chem. Soc. Rev. 42, 8032 (2013).

110. Krogstad, A. L., Jansson, P. A., Gisslén, P. & Lönnroth, P. Microdialysis methodology for the measurement of dermal interstitial fluid in humans. Br J Dermatol 134, 1005–1012 (1996).

111. Kern W & Puotinen D A. Cleaning solutions based on hydrogen peroxide for use in silicon semiconductor technology. RCA Rev. 31:187-206, 1970. 1.

112. Briones, N., Choong, V.-E. & Johnson, W. T. Method for adhesion of polymers to metal-coated substrates. (2002).

113. Shur, M. et al. Soft Printable Electrode Coating for Neural Interfaces. ACS Appl. Bio Mater. 3, 4388–4397 (2020).

114. Mohanty, P. S. et al. Dielectric spectroscopy of ionic microgel suspensions. Soft Matter 12, 9705–9727 (2016).

115. Schwan, H. P. Electrode Polarization Impedance and Measurements in Biological Materials. Annals of the New York Academy of Sciences 148, 191–209 (1968).

116. Zhang, C., Losego, M. D. & Braun, P. V. Hydrogel-Based Glucose Sensors: Effects of Phenylboronic Acid Chemical Structure on Response. Chem. Mater. 25, 3239–3250 (2013).

117. Alexeev, V. L. et al. High Ionic Strength Glucose-Sensing Photonic Crystal. Anal. Chem. 75, 2316–2323 (2003).

118. Yang, X., Pan, X., Blyth, J. & Lowe, C. R. Towards the real-time monitoring of glucose in tear fluid: Holographic glucose sensors with reduced interference from lactate and pH. Biosensors and Bioelectronics 7 (2008).

119. Kabilan, S. et al. Holographic glucose sensors. Biosensors and Bioelectronics 9 (2005).

120. S. Oh, J. S. Lee, K. H. Jeong, & L. P. Lee. Minimization of electrode polarization effect by nanogap electrodes for biosensor applications. in The Sixteenth Annual International Conference on Micro Electro Mechanical Systems, 2003. MEMS-03 Kyoto. IEEE 52–55 (2003). doi:10.1109/MEMSYS.2003.1189685.

121. Dielectric relaxation in biological systems: physical principles, methods, and applications. (Oxford University Press, 2015).

122. Kawasaki, T., Akanuma, H. & Yamanouchi, T. Increased Fructose Concentrations in Blood and Urine in Patients With Diabetes. Diabetes Care 25, 353–357 (2002).

123. Ning, C. & Segal, S. Plasma galactose and galactitol concentration in patients with galactose-1-phosphate uridyltransferase deficiency galactosemia: Determination by gas chromatography/mass spectrometry. Metabolism 49, 1460–1466 (2000).

124. Aduen, J. et al. The Use and Clinical Importance of a Substrate-Specific Electrode for Rapid Determination of Blood Lactate Concentrations. JAMA 272, 1678–1685 (1994).

125. Rodriguez-Segade, S. et al. Continuous glucose monitoring is more sensitive than HbA1c and fasting glucose in detecting dysglycaemia in a Spanish population without diabetes. Diabetes Research and Clinical Practice 142, 100–109 (2018).

126. McDonagh, C., Bowe, P., Mongey, K. & MacCraith, B. D. Characterization of porosity and sensor response times of sol–gel-derived thin films for oxygen sensor applications. Journal of Non-Crystalline Solids 306, 138–148 (2002).

127. Huang, X. et al. A differential dielectric affinity glucose sensor. Lab Chip 14, 294–301 (2014).

128. Shang, J. et al. A hydrogel-based glucose affinity microsensor. Sensors and Actuators B: Chemical 237, 992–998 (2016).

129. Yang, C. et al. An ultra sensitive and selective impedance sensor based on protein-imprinted polymer. Sensors and Actuators B: Chemical 282, 818–823 (2019).

130. Olthuis, W., Streekstra, W. & Bergveld, P. Theoretical and experimental determination of cell constants of planar-interdigitated electrolyte conductivity sensors. Sensors and Actuators B: Chemical 24, 252–256 (1995).

131. Zhang, Z. et al. Effects of Hydrogel Composition on a Hydrogel-Based Affinity Microsensor for Continuous Glucose Monitoring. Manuscript submitted for publication (2022).

132. Morrison, R. Grounding and shielding: circuits and interference. (Wiley, 2016).

133. Kos, T., Rojac, T., Petrovčič, J. & Vrančić, D. Control system for automated drift compensation of the stand-alone charge amplifier used for low-frequency measurement. AIP Advances 9, 035133 (2019).

134. Sano, Y. et al. Effects of different types of anesthesia on hemodynamics, cardiac function, and glucose and lipid metabolism in rats. American Journal of Physiology-Heart and Circulatory Physiology 311, H1360–H1366 (2016).

135. Thennadil, S. N. et al. Comparison of Glucose Concentration in Interstitial Fluid, and Capillary and Venous Blood During Rapid Changes in Blood Glucose Levels. Diabetes Technology & Therapeutics 3, 357–365 (2001).

136. Wisniewski, N., Moussy, F. & Reichert, W. M. Characterization of implantable biosensor membrane biofouling. Fresenius' Journal of Analytical Chemistry 366, 611–621 (2000).

137. Kownacka, A. E. et al. Clinical Evidence for Use of a Noninvasive Biosensor for Tear Glucose as an Alternative to Painful Finger-Prick for Diabetes Management Utilizing a Biopolymer Coating. Biomacromolecules 19, 4504–4511 (2018).

138. Lee, H., Hong, Y. J., Baik, S., Hyeon, T. & Kim, D. Enzyme‐Based Glucose Sensor: From Invasive to Wearable Device. Adv. Healthcare Mater. 7, 1701150 (2018).

139. Sempionatto, J. R., Moon, J.-M. & Wang, J. Touch-Based Fingertip Blood-Free Reliable Glucose Monitoring: Personalized Data Processing for Predicting Blood Glucose Concentrations. ACS Sens. 6, 1875–1883 (2021).

140. Baca, J. T., Finegold, D. N. & Asher, S. A. Tear Glucose Analysis for the Noninvasive Detection and Monitoring of Diabetes Mellitus. The Ocular Surface 5, 280–293 (2007).

141. Y. T. Liao, H. Yao, A. Lingley, B. Parviz, & B. P. Otis. A 3μW CMOS Glucose Sensor for Wireless Contact-Lens Tear Glucose Monitoring. IEEE Journal of Solid-State Circuits 47, 335–344 (2012).

142. Sen, D. K. & Sarin, G. S. Tear glucose levels in normal people and in diabetic patients. British Journal of Ophthalmology 64, 693–695 (1980).

143. Keum, D. H. et al. Wireless smart contact lens for diabetic diagnosis and therapy. Sci. Adv. 6, eaba3252 (2020).

144. Liang, X. et al. Toward Clean and Crackless Transfer of Graphene. ACS Nano 5, 9144–9153 (2011).

145. Ferrari, A. C. & Basko, D. M. Raman spectroscopy as a versatile tool for studying the properties of graphene. Nature Nanotech 8, 235–246 (2013).

146. Wu, J.-B., Lin, M.-L., Cong, X., Liu, H.-N. & Tan, P.-H. Raman spectroscopy of graphene-based materials and its applications in related devices. Chem. Soc. Rev. 47, 1822–1873 (2018).

147. Ferrari, A. C. Raman spectroscopy of graphene and graphite: Disorder, electron–phonon coupling, doping and nonadiabatic effects. Solid State Communications 143, 47–57 (2007).

148. Georgakilas, V. et al. Noncovalent Functionalization of Graphene and Graphene Oxide for Energy Materials, Biosensing, Catalytic, and Biomedical Applications. Chem. Rev. 116, 5464–5519 (2016).

149. Kaisti, M. Detection principles of biological and chemical FET sensors. Biosensors and Bioelectronics 98, 437–448 (2017).

150. Vlandas, A., Kurkina, T., Ahmad, A., Kern, K. & Balasubramanian, K. Enzyme-Free Sugar Sensing in Microfluidic Channels with an Affinity-Based Single-Wall Carbon Nanotube Sensor. Anal. Chem. 82, 6090–6097 (2010).

151. Shen, Q. J. & Jin, W. J. Chemical and photophysical mechanism of fluorescence enhancement of 3-quinolineboronic acid upon change of pH and binding with carbohydrates. Luminescence 26, 494–499 (2011).

152. Yang, W., Yan, J., Springsteen, G., Deeter, S. & Wang, B. A novel type of fluorescent boronic acid that shows large fluorescence intensity changes upon binding with a carbohydrate in aqueous solution at physiological pH. Bioorganic & Medicinal Chemistry Letters 13, 1019–1022 (2003).

153. Huang, C., Hao, Z., Qi, T., Pan, Y. & Zhao, X. An integrated flexible and reusable graphene field effect transistor nanosensor for monitoring glucose. Journal of Materiomics 6, 308–314 (2020).

154. Brooks, W. L. A., Deng, C. C. & Sumerlin, B. S. Structure–Reactivity Relationships in Boronic Acid–Diol Complexation. ACS Omega 3, 17863–17870 (2018).

155. Springsteen, G. & Wang, B. A detailed examination of boronic acid–diol complexation. Tetrahedron 58, 5291–5300 (2002).

156. Aduen, J. The Use and Clinical Importance of a Substrate-Specific Electrode for Rapid Determination of Blood Lactate Concentrations. JAMA 272, 1678 (1994).

157. Van Haeringen, N. J. Clinical biochemistry of tears. Survey of Ophthalmology 26, 84–96 (1981).

158. Palleschi, G., Faridnia, M. H., Lubrano, G. J. & Guilbault, G. G. Determination of lactate in human saliva with an electrochemical enzyme probe. Analytica Chimica Acta 245, 151–157 (1991).

159. Yang, X., Lee, M.-C., Sartain, F., Pan, X. & Lowe, C. R. Designed Boronate Ligands for Glucose-Selective Holographic Sensors. Chem. Eur. J. 12, 8491–8497 (2006).

160. Tierney, S., Volden, S. & Stokke, B. T. Glucose sensors based on a responsive gel incorporated as a Fabry-Perot cavity on a fiber-optic readout platform. Biosensors and Bioelectronics 24, 2034–2039 (2009).

161. DeHennis, A. D. & Wise, K. D. A Fully Integrated Multisite Pressure Sensor for Wireless Arterial Flow Characterization. J. Microelectromech. Syst. 15, 678–685 (2006).

162. Yoo, S. et al. Wireless Power Transfer and Telemetry for Implantable Bioelectronics. Adv. Healthcare Mater. 10, 2100614 (2021).

163. Rezaeiyan, Y., Zamani, M., Shoaei, O. & Serdijn, W. A. Mixed-Signal IC With Pulse Width Modulation Wireless Telemetry for Implantable Cardiac Pacemakers in 0.18-μm CMOS. IEEE Trans. Biomed. Circuits Syst. 1–12 (2018) doi:10.1109/TBCAS.2018.2819021.

164. Clarke, W., Anderson, S. & Kovatchev, B. Evaluating Clinical Accuracy of Continuous Glucose Monitoring Systems: Continuous Glucose – Error Grid Analysis (CG-EGA). CDR 4, 193–199 (2008).

165. Wang, C. et al. High k -Solid-Gate Transistor Configured Graphene Biosensor with Fully Integrated Structure and Enhanced Sensitivity. Adv. Funct. Mater. 26, 7668 – 7678 (2016).

166. Benz, C. et al. Graphene on boron nitride microwave transistors driven by graphene nanoribbon back-gates. Appl. Phys. Lett. 102, 033505 (2013).

167. Li, Y., Zhu, Y., Wang, C., He, M. & Lin, Q. Selective detection of water pollutants using a differential aptamer-based graphene biosensor. Biosensors and Bioelectronics 126, 59–67 (2019).